Novel CO_2 Capture and Conversion into Fuels via Artificial Photosynthesis by Artificial Inorganic Leaves

---

A thesis submitted in fulfilment of the requirements for the

Degree of Doctor of Philosophy in Chemical Engineering

By

Iman Hashemizadeh

Department of Chemical and Process Engineering,

University of Canterbury,

New Zealand

2017

To my beloved mum, for her endless love. I can no longer see her with my eyes, but I will feel her in my heart for ever.

"God made solids, but surfaces were the work of the devil."

Wolfgang Pauli; theoretical physicist (1900-1958)

Abstract

Researches on sustainable processes for efficient converting of solar energy to fuels have recently received enormous efforts. The main issue facing solar-assisted reactions is insufficient light harvesting by photocatalysts in the visible light regions. The objective of this project was photoreduction of CO_2 with water (known as artificial photosynthesis) using visible light. The full architecture of the leaf photosystem was successfully replicated at both the nano and micro levels using biotemplating with TiO_2. Recently, bio-inspired materials have emerged as a potential area of research for developing advanced functional systems. Our multi-step chemical replication method resulted in a unique TiO_2 architecture with highly porous network. This improved biotemplating method could address the issues in controlling the morphology of final product associated with conventional procedures of synthesis of titania platforms. Scanning and transmission electron microscopy images of the final products confirmed that the detailed microscale framework and nanostructures, such as the chloroplast and the thylakoids were well replicated. In our preliminary tests of photocatalytic activity, the biotemplated artificial TiO_2 leaves outperformed well-known P25 TiO_2 in photocatalytic degradation of methylene blue dye under visible light. The artificial titania leaf and P25 achieved 13±1.5% and 7±0.9% of methylene blue conversion, respectively, under blue light (440 nm). Under green light irradiation (515 nm), the methylene blue conversion given by the biotemplated photocatalyst (9±1.2%) is also higher than that achieved by P25 (6.3±0.8%). The enhanced visible light activity of the bio-mimicked titania catalyst could be attributed to several key factors given by the 3-dimensional interconnected nanosheets structure (the thylakoid replicas), including enhance reactant-catalyst contact and high efficiency of the light absorption.

The novel porous TiO_2 architecture was used to catalyse the photoreduction of CO_2 with H_2O. The artificial TiO_2 leaves showed higher selectivity to methane (CH_4) in CO_2 photoreduction compared to non-porous commercial titania catalysts. The CO_2 photoreduction reactions catalysed by artificial TiO_2 leaves and P25, after 20 h under UV light (370 nm), produced 3.8±0.6 and 2.7±0.5 μmol/g-cat. of CH_4, respectively. The chloroplast-like 3-D TiO_2 materials also outperformed the product yields of P25 titania under visible light. The CO (0.5±0.1 μmol/g-cat.) and CH_4 (2.2±0.35 μmol/g-cat.) were yielded by the biotemplated titania photocatalyst, after 30 h under green light (515 nm), compared to the CO (2±0.5 μmol/g-cat.) given by P25. We hypothesised that there is a strong correlation between the morphology of the inorganic artificial leaves made of TiO_2 and their superior photocatalytic performance. Moreover, the advantages of the surface chemical modification of titania photocatalysts with the ruthenium dioxide were demonstrated. The RuO_2/artificial leaf materials possessed a substantially higher efficiency of the CO_2 photoreduction compared to the neat artificial TiO_2 leaves in the case of visible light. The CO_2 photoreduction reactions catalysed by neat and RuO_2/artificial TiO_2 leaves, after 30 h under green light (515 nm), produced 2.2±0.35 and 3.15±0.35 μmol/g-cat. of CH_4, respectively. Finally, two kinetic models for photocatalytic reduction of CO_2 with H_2O, were validated with the products concentration profiles. The experimental data have obtained a very good fit to the kinetic model developed based on Eley-Rideal mechanism. The understanding of the morphological contribution of the photocatalyst provided in this study, could help to augment the efficiency and selectivity of the CO_2 photoreduction.

Deputy Vice-Chancellor's Office
Postgraduate Office

UNIVERSITY OF CANTERBURY
Te Whare Wānanga o Waitaha
CHRISTCHURCH NEW ZEALAND

Co-Authorship Form

This form is to accompany the submission of any thesis that contains research reported in co-authored work that has been published, accepted for publication, or submitted for publication. A copy of this form should be included for each co-authored work that is included in the thesis. Completed forms should be included at the front (after the thesis abstract) of each copy of the thesis submitted for examination and library deposit.

Please indicate the chapter/section/pages of this thesis that are extracted from co-authored work and provide details of the publication or submission from the extract comes:

Chapter 3 – results from this chapter has been submitted to the "RSC Advances" as a full paper entitled "Bio-mimicked TiO_2 Architectures for Enhanced Photocatalytic Activity under UV/Visible Light." Also, partial results from this chapter were presented at the Chemeca 2016, 25-28 September in Adelaide, Australia as a conference paper entitled "Enhanced photocatalytic activity using artificial inorganic leaves made from TiO_2."

Chapter 4 – results from this chapter will be presented at the APCChE2017, 23-27 August in Hong Kong and is invited for publication in "Catalysis Today" as a full paper entitled "The Photocatalytic Reduction of CO_2 with H_2O Using Bio-mimicked TiO_2 Architectures."

Please detail the nature and extent (%) of contribution by the candidate:

Iman Hashemizadeh is the first author of the abovementioned papers. His works in the submitted PhD thesis involve literature search, experimental design, data collection and analysis as well as writing of each chapter. His contribution is about 90%.

Certification by Co-authors:

If there is more than one co-author then a single co-author can sign on behalf of all

The undersigned certifys that:

- The above statement correctly reflects the nature and extent of the PhD candidate's contribution to this co-authored work
- In cases where the candidate was the lead author of the co-authored work he or she wrote the text

Name: *Alex Yip*	Signature: 	Date: *23/06/2017*

Table of Contents

Acknowledgments

Foremost, I would like to express my genuine gratitude to my supervisors, Dr. Alex Yip and Dr. Vladimir Golovko. I would surely never have completed this task without their wonderful supervision. They spent an enormous time and effort on guiding and assisting me throughout my Ph.D. project. My two supervisors have kept me motivated and on-task during good and bad times.

I wish to extend my thanks to the academics and researchers at both chemical engineering and chemistry departments of the University of Canterbury who have helped me throughout my research. Very special thanks go to the Dr. Aaron Marshal group for providing a stream of help regarding gas chromatography analysis. I also must thank the technical staff of the University of Canterbury for their unending support. Next, I would like to express my gratitude to the senior members of the Yip and Golovko groups, for showing me the ropes of organising lab works. I have my warm gratitude to my friends at the University of Canterbury and in Christchurch who make my life in New Zealand colourful.

I am grateful to Royal Society of New Zealand for partially funding this project under the Catalyst: Seeding General grant (16-UOC-002-CSG). Last but definitely not least, my deepest and most heart-felt gratitude to my beloved family for their endless love and support. It is more than just words to show how much I feel indebted to my father, for giving me the opportunity to pursue my dream.

Abbreviations

Å: Angstroms

AChl: Artificial Chloroplast

AL: Artificial Leaf

CEM: Controlled Evaporator Mixer

DLS: Dynamic Light Scattering

DRIFTS: Diffuse Reflection Infrared Spectroscopy

DR UV-vis: Diffuse Reflectance UV-Vis Spectroscopy

EPR: Electron Paramagnetic Resonance

EtOH: Ethanol

GC: Gas Chromatography

GC–FID: Gas Chromatograph equipped with Flame Ionisation Detector

GC–TCD: Gas Chromatography equipped with Thermal Conductivity Detector

ICP–MS: Inductively Coupled Plasma Mass Spectrometry

LED: Light–Emitting Diode

MAL: Micro-Structure Mimicked Artificial Leaf

MNAL: Micro- and Nano-Structure Templated Artificial Leaf

P25: Aeroxide P25 commercially available TiO_2

S.D.: Standard Deviation

SDR: Spin-Dependent Recombination

S.E.: Standard Error

SEM: Scanning Electron Microscopy

TEM: Transmission Electron Microscopy

wt %: Weight per cent

XRD: X–Ray Diffraction

XPS: X-Ray Photoelectron Spectroscopy

List of Tables

List of Figures

List of Schemes

Chapter 1 – Introduction

1.1 The energy challenge

Along with global population growth, global primary energy consumption is projected to increase dramatically by 2050. Thus, shifting energy production toward abundant, clean, secure and renewable sources is one of the key technological challenges facing mankind. A wide range of energy sources, including nuclear power, wind, solar energy, biomass, geothermal energy, hydroelectric power and wave power have been investigated for future use but several issues still need to be addressed, such as, restrictions on plant-based biomass growth in terms of land and climate requirements, slow growth, weather contingencies, pests, and so on (Corma et al., 2011; Huber & Corma, 2007).

In this regard, solar energy is almost infinite, nonpolluting, free, and available on all continents. Sunlight is responsible for life on earth where an hour of solar radiation represents nearly the world's total annual energy consumption and natural photosynthesis is responsible for the survival of nearly all life forms. However, the daily solar cycle limits its direct use when high levels of energy are required during non-daytime hours. If it were easy to capture solar radiation and store the energy efficiently, there would be no global scarcity of renewable and clean energy. Hence, researches on sustainable processes for efficient converting of solar energy to fuels have recently received enormous efforts (Abbott, 2010; Roy et al., 2010; Youngblood et al., 2009).

1.2 The environmental challenge

All energy technologies involve an environmental impact, with the most important environmental concern being the emission of greenhouse gases that contribute to global warming. A persistent greenhouse gas originating from all combusted fuels is carbon dioxide (CO_2) that is not currently being captured or removed from stack emissions. Current reports indicate that there is an excess of approximately 4% CO_2 with respect to the natural "carbon cycle" which the atmosphere may contain by 2100 according to Intergovernmental Panel on Climate Change (IPCC) predictions, causing a rise in the mean global temperature of approximately 2°C accompanied by increased desertification, and species extinction (Maginn, 2010). In this context, the conversion of CO_2 to clean fuels and useful chemicals such as methanol has recently been studied intensely. This attractive solution not only does address the energy crisis issue, but also overcomes concerns on pollutant removal and environmental impact by optimizing the carbon cycle. However, current processes utilizing CO_2 as chemical feedstock needs substantial consumption of energy causing leakage of greenhouse gases back into the environment (Mikkelsen et al., 2010; Yang et al., 2008a).

1.3 Solar-assisted recycling of carbon dioxide to fuels

Based on the foregoing, the process of reducing CO_2 using sunlight is considered to be zero- or even negative-cost sources to supply sustainable alternatives to conventional energy sources. Natural photosynthesis, which plays a fundamental role in the life cycle of nature, provides a promising blueprint for such systems design. A less-explored approach for converting carbon dioxide (CO_2) into fuel and chemicals is the reduction of CO_2 in the presence of water, known as artificial photosynthesis. Natural green leaves capture CO_2 and convert it into chemicals through photosynthesis using solar energy. In chemical terminology, artificial photosynthesis is the conversion of water and CO_2 into carbohydrates and oxygen

under ambient temperature and pressure (Nelson & Ben-Shem, 2004). The overall reaction of the artificial photosynthesis is illustrated in Figure 1-1.

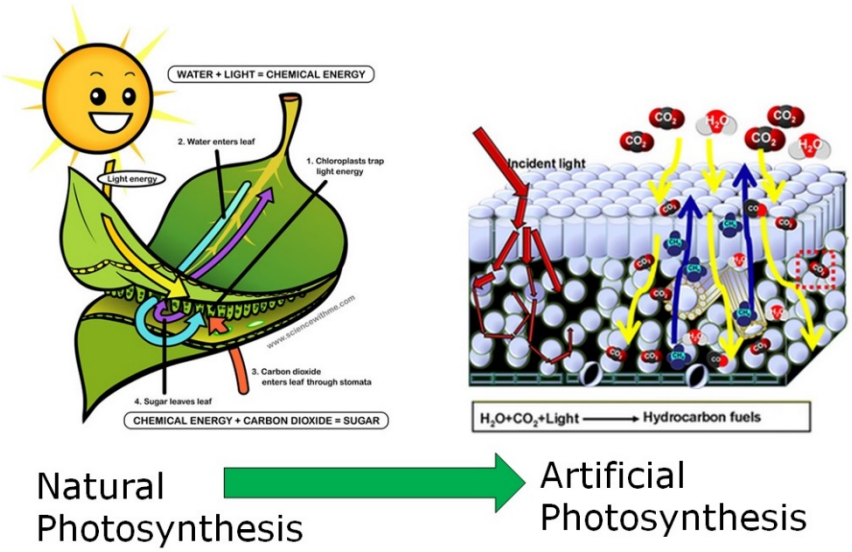

Figure 1-1. Analogy of photosynthesis using solar energy by natural leaves (Zhou et al., 2011).

The indirect application of solar energy by generation of electricity for the reduction of carbon dioxide has been reviewed over the past few decades. Many studies have been conducted on the electrochemical reduction of CO_2. While the details of the reaction mechanism is still a matter of debate, the main products reported are CO, H_2, formic acid, and methane, as well as trace amounts of C_2 hydrocarbons. However, the main issue confronting the use of an aqueous solution is the low solubility of carbon dioxide in water at room temperature and pressure, which results in there being very small amounts of CO_2 available at the surface of the electrode enabling the reaction to proceed. Rapid deactivation also often occurs in this approach (Centi & Perathoner, 2009; Corma & Garcia, 2013).

Photocatalytic reaction is an alternative method that is feasible for CO_2 reduction. The ultimate goal of it is to combine the water splitting and CO_2-reduction reactions into a single step, using the hydrogen atoms and electrons released during the water splitting to drive the CO_2 reduction and thereby produce fuels. The reaction can be catalyzed by the semiconductors with a band structure which splits water by using solar light. Semiconductors possess a band structure in which the conduction band is separated from the valence band by a band gap with a suitable width for the absorption of photons. When the energy from incident light is greater than that of the band gap, electron-hole pairs are formed (Abbott, 2010; Corma & Garcia, 2013; Roy et al., 2010; Stechel & Miller, 2013). The initial step of the process involves the absorption of photons and excitation of the semiconductor so that the latter becomes photocatalytically active. Subsequently, water molecules are oxidized by the holes (h+) at valence bands to produce O_2 and reduced by the electrons at conduction bands to generate H_2. During the final stage, yielded hydrogen cations could utilize CO_2 and produce hydrocarbons (Figure 1-2). The efficiency of this artificial photosynthesis process requires a catalyst structure that is able to harvest solar light effectively. The current issue facing this approach is that there is insufficient light harvesting in the visible light regions and inefficient charge transfer in the photocatalyst (Dey, 2007; Indrakanti et al., 2009).

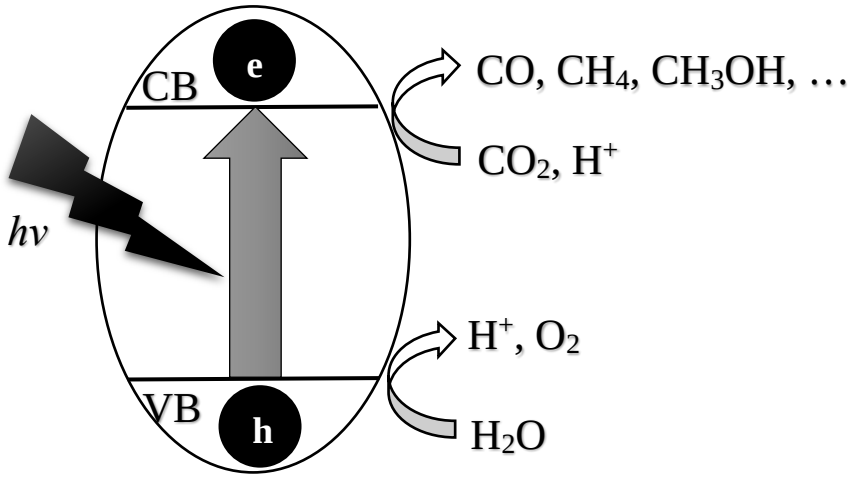

Figure 1-2. Reaction scheme for the photocatalytic reduction of carbon dioxide with water.

In this project, we aimed to develop a novel TiO_2 photocatalyst with enhanced visible light activity. Our main objective was to capture CO_2 and convert it into fuels using visible (solar) light. This dissertation is constructed with six chapters, the descriptions of the chapters are;

Chapter 1: A brief introduction of the motivations of this study, the general backgrounds, and the overview of the whole dissertation were explained in this chapter.

Chapter 2: The background knowledge of photocatalytic reduction of carbon dioxide with water, the development progress of the titanium dioxide (TiO_2) photocatalysts, and the application of bio-mimicked materials for sustainability**.**

Chapter 3: The synthesis methods and characterization results of various biotemplated photocatalysts were described in this chapter. After considering the photocatalytic performance of the synthesized materials in degradation of methylene blue dye, the artificial TiO_2 leaves were selected to catalyse the photo-reduction of CO_2. The results of this chapter has been

submitted as a full paper to the “RSC Advances” journal (IF: 3.108). Also, this chapter was partially presented as a conference paper in Chemeca2016 25-28 September in Adelaide, Australia.

Chapter 4: The performance of the artificial TiO_2 leaves for the photocatalytic reduction of CO_2 with water was demonstrated. The improvements of the efficiency and selectivity of the photoreduction reactions catalysed by biotemplated materials compared to commercial titania photocatalysts were presented. The relationship between the morphology of the photocatalysts and the photocatalytic performance was highlighted. The results from this chapter would be presented as a conference paper to APCChE2017 23-27 August in Hong Kong and is invited for publication as a full paper in “Catalysis Today” journal (IF: 4.636).

Chapter 5: The modification methods to enhance visible light activity of the bio-mimicked catalyst were presented in this chapter. The advantages of the chemical surface modification of titania materials with ruthenium dioxide (RuO_2) were demonstrated.

Chapter 6: The key findings of the present study were concluded. Based on the knowledge obtained from this study, we made the recommendations to the future work on photoreduction of CO_2 and other solar-assisted reactions.

Chapter 2 - Literature review

2.1 Photocatalytic reduction of CO_2 with H_2O

Slurry CO_2 photoreduction systems are stirred batch reactors with a suspension of catalyst. The reaction phases involve the photocatalysis with participation of both gas and liquid phases. The formation of hydrocarbons from CO_2 photocatalytic reduction via irradiation of semiconductors powder suspended solutions was first reported by Fujishima and Honda (Inoue et al., 1979). Halmann summarised the pioneering works about the photoreduction of CO_2 on semiconductors in aqueous suspension (Halmann, 1983). The wavelength and/or intensity of light source, reactor configuration and the reaction media affect the efficiency and selectivity of the reaction. The influence of the reaction variables have been investigated in many studies (Aresta et al., 2016; Habisreutinger et al., 2013; Ni et al., 2007).

The optimization of reaction conditions are significant but the efficiency and selectivity of solar-assisted reactions strongly depend on the performance of the photocatalysts. The free charge carriers in the semiconductors could be formed upon absorption of photons (Figure 1-2). The electron-hole pairs are spatially separated in an illuminated semiconductors. The carriers may migrate to the surface of the photocatalyst leading to desired oxidation and reduction reactions. Alternatively, the carriers may recombine in the bulk of the semiconductor (Furube et al., 1999). The number of carriers collected by acceptor molecules versus those optically induced is defined as quantum yield of the photocatalytic reactions (Krishnan, 2007).

The semiconductor materials tend to return to the equilibrium by recombination of the electron-hole pairs. The de-excitaion may follow different pathways; if the carriers which

recombine are both free, this is called band to band recombination. Alternatively, the carriers may be captured on a localized state. If the captured carrier recombines with an opposite sign carrier on the same capture centre, the annihilation process is called recombination on localized states. If the captured carrier is released into the band, the capture centre is called a trap and the release process is called detrapping (Adachi, 1999). These different situations are illustrated in Figure 2-1.

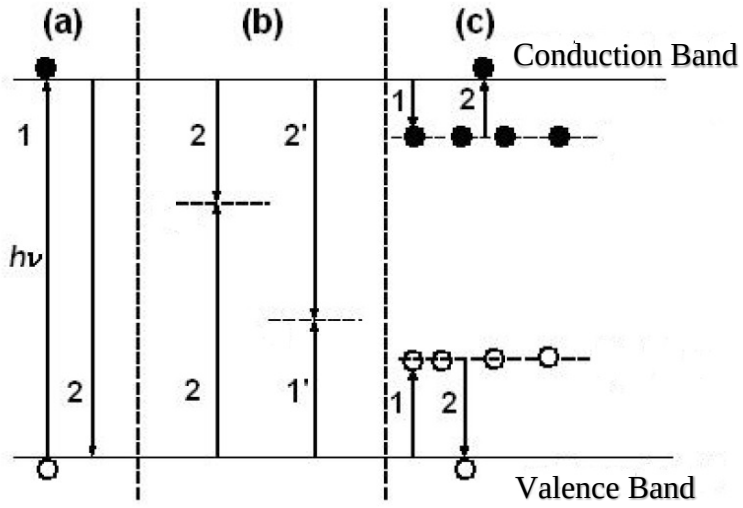

Figure 2-1. The annihilation process of photoinduced electron-hole pairs in bulk semiconductors: a) band to band recombination. b) recombination on localized states. c) detrapping process (Adachi, 1999).

Currently, more than 130 materials and derivatives are known to catalyse hydrogen generation via splitting of water, including simple metal oxides, niobates, tantalates, metal nitrides, metal sulphides and covalent network solids such as C_3N_4 (Corma & Garcia, 2013). The sulphide semiconductors have initially been at the centre of interest for CO_2 photoreduction. Many metal sulphides have a narrow band gap enabling light absorption in the visible region. ZnS and CdS were the most studied sulphides for photocatalytic reduction of CO_2. The major disadvantage is that sulphides are not stable under irradiation in an aqueous dispersion because of oxidation of lattice S^{2-} ions (Dey, 2007; Liu et al., 2010). The ability of

several metal phosphides have also been studied in regard to photochemical CO_2 reduction. The phosphide semiconductors possess a highly reducing conduction band with a reasonably narrow band gap. It has been shown that GaP and InP semiconductors photoreduce CO_2 to methanol more efficiently than other groups of semiconductors. However, the position of valence band in metal phosphides are not suitable for the oxidative water splitting (Dey, 2007; Liu et al., 2010).

The metal oxides are the most used semiconductors to catalyse CO_2 photoreduction. In contrast to sulphides, most of oxides do not suffer from photooxidation under illumination. The photogenerated holes in valence band of metal oxides has a strong oxidizing power and their wide band gap make them thermodynamically capable of CO_2 reduction (Habisreutinger et al., 2013). Conduction band and valence band potentials of various semiconductors relative to the redox potentials involved in CO_2 photoreduction with water are shown in Figure 2-2.

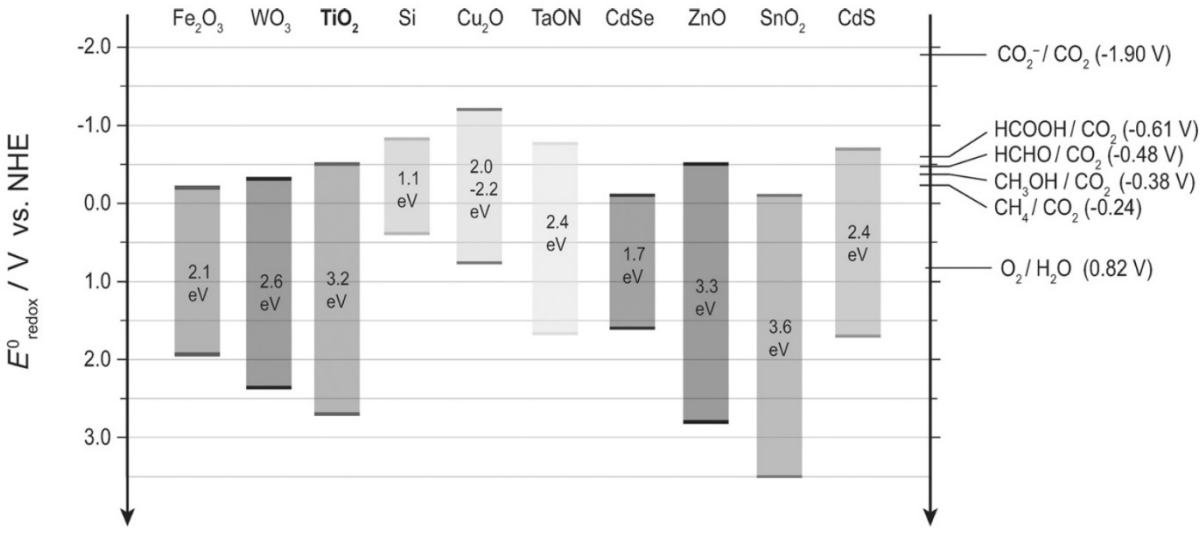

Figure 2-2. Conduction band, valence band potentials, and band gap energies of various semiconductor photocatalysts relative to the redox potentials of compounds involved in CO_2 reduction (Habisreutinger et al., 2013).

Two main groups of metal oxides with closed-shell electronic configurations have received a lot of attention in regard to the photocatalytic CO_2 reduction. The first group contains transition metal ions (Ti^{4+}, Zr^{4+}, Ta^{5+}, W^{6+}, and etc) that have an empty d orbital. The second group contains main metal oxides (Ga, Ge, In, Sn, or Sb) with a fully occupied d orbital (Mori et al., 2012). Among all of these materials, titanium dioxide (TiO_2)-based photocatalysts have been considered as one of the best materials due to their wide availability, low toxicity, good durability, high stability and, most importantly, the energy of photoinduced electron-hole pairs matches the potential of the water oxidation and the CO_2 reduction (Habisreutinger et al., 2013).

The potential of oxidation or reduction is the tendency of the molecular orbital of the reactants to donate or accept electrons, respectively. The ability of the semiconductor to transfer photoinduced electron-hole pairs to adsorbed species is governed by the position of the valence and conduction band edges (Kisch, 2013). For the reduction process, the conduction band edge of TiO_2 photocatalysts is located above the lowest unoccupied molecular orbital of the acceptor molecules. For the water oxidation, the energy level of the highest occupied molecular orbital of the H_2O molecule lies above the valence band edge of titania (Colombo & Bowman, 1996; Mori et al., 2012).

The literature has suggested two possible reaction schemes for the photocatalytic reduction of CO_2 with H_2O on TiO_2 catalysts (Habisreutinger et al., 2013). The different products could be yielded depending on the specific pathway of C — O bonds cleavage and formation of C — H bonds. The pathways differ according to the bonding mode of CO_2 molecules to the surface of the catalyst. The monodentate binding may occur through one of

the oxygen atoms to a titanium atom or the carbon atom to a surface bridging oxygen atom (Gattrell et al., 2006). Alternatively, the carbon dioxide radicals could bond via bidentate binding of both oxygen atoms to two Ti atoms (He et al., 2012).

The early proposed reaction scheme is known as the formaldehyde pathway due to its unique intermediate. The production of methanol before methane formation would be expected in this mechanism (Sasirekha et al., 2006; Subrahmanyam et al., 1999). The early methanol formation has not been verified by products concentration profiles in experimental data (Habisreutinger et al., 2013; Tan et al., 2008). According to the other reaction scheme, called the carbene mechanism, the pathway starts with an immediate cleavage of the oxygen atom and the carbon atom bonds. This results in dissociation of CO_2 and formation of CO. The methanol is a side product, not an intermediate in this pathway, and the formaldehyde is not produced (Anpo et al., 1995). The carbene reaction pathway leads to a common set of products that are reported in many experiments (Ikeue et al., 2002; Ikeue et al., 2001; Varghese et al., 2009). The details of the pathways are illustrated in the Table 2-1.

Table 2-1. Proposed elemental steps in photocatalytic reduction of CO_2 with H_2O: formaldehyde and carbene pathways.

Formaldehyde pathway	$CO_2 \xrightarrow{+e^-} O - C^{\cdot} - O^-$ $O - C^{\cdot} - O^- \xrightarrow{+H^+} HO - C^{\cdot} = O$ $HO - C^{\cdot} = O \xrightarrow{+e^- + H^+} HCOOH$ $HCOOH \xrightarrow{+e^- + H^+} H - C^{\cdot}(OH) - OH$ $H - C^{\cdot}(OH) - OH \xrightarrow{+e^- + H^+} H - CO - H + H_2O$ $H - CO - H \xrightarrow{+e^- + H^+} H - C^{\cdot}(OH) - H$ $H - C^{\cdot}(OH) - H \xrightarrow{+e^- + H^+} CH_3OH$ $CH_3OH \xrightarrow{+e^- + H^+} C^{\cdot}H_3 + H_2O$ $C^{\cdot}H_3 \xrightarrow{+e^- + H^+} CH_4$
Carbene pathway	$CO_2 \xrightarrow{+e^-} O - C^{\cdot} - O^-$ $O - C^{\cdot} - O^- \xrightarrow{+e^- + H^+} CO + OH^-$ $CO \xrightarrow{+e^-} C^{\cdot}O^-$ $C^{\cdot}O^- \xrightarrow{+e^- + H^+} C + OH^-$ $C \xrightarrow{+e^- + H^+} C^{\cdot}H$ $C^{\cdot}H \xrightarrow{+e^- + H^+} CH_2$ $CH_2 \xrightarrow{+e^- + H^+} C^{\cdot}H_3$ $C^{\cdot}H_3 \xrightarrow{+e^- + H^+} CH_4$ $C^{\cdot}H_3 \xrightarrow{+OH^{\cdot}} CH_3OH$

2.2 TiO_2 photocatalysts for reduction of CO_2

Three crystal structures of titanium dioxide (TiO_2) are brookite, anatase, and rutile. The brookite is seldom studied because it is difficult to synthesis (Beltrán et al., 2006). The rutile is the stable phase whereas the anatase is metastable. The Ti — O distances are larger in rutile, while the Ti — Ti distances are shorter than those in anatase. The different lattice structures cause different band structures of the two forms of titania. The band gap of the anatase and rutile TiO_2 are 3.2 and 3 eV, respectively (Hanaor & Sorrell, 2011).

The potential for the application of the TiO_2-based photocatalysts has attracted considerable interest over the last three decades. The photocatalytic effects in titania materials are shown to be applicable in a range of important energy and environment areas, including: electrochemical and photochemical oxidation of water to produce hydrogen, solar cells, water treatment, and self-cleaning coatings (Hanaor & Sorrell, 2011).

The electronic properties of TiO_2 are a function of the local structure of the photocatalyst, particularly the the crystalline phase composition and particle size and shape (Cheng et al., 2014; Schiavello, 1997; Testino et al., 2007). Recent researches have suggested the TiO_2 nanostructures to more efficiently harvest light (Chen & Mao, 2007; Teoh et al., 2012). A vast range of TiO_2 architectures, including nanorods (Lei et al., 2004; Liu et al., 2016), nanosheets (Ohwada et al., 2013; Sasaki et al., 2001), nanowires (Wen et al., 2005a; Zhang et al., 2002), nanotubes (Kar et al., 2016; Yao et al., 2003), aerogels (Fort et al., 2014; Zhao et al., 2009), opal and photonic materials (Cheng et al., 2012; Waterhouse & Waterland, 2007), and etc, have been developed to enhance the activity.

Commonly studied nanoscale TiO_2 materials can be synthesised via a number of different methods, including sol-gel, micellar and solvothermal syntheses, direct oxidation, chemical or physical vapour deposition, electrodeposition, and microwave synthesis (Chen & Mao, 2007). TiO_2 nanostructures can be produced by hydrothermal treatment of peptized precipitates of a titanium precursor with water. The temperature can be elevated above the boiling point of water, reaching the pressure of vapour saturation. The solvothermal method is almost identical to the hydrothermal method except that the solvent used here is nonaqueous. The temperature can be elevated much higher than that in hydrothermal method, since a variety

of organic solvents with high boiling points can be chosen. The hydrothermal and solvothermal methods are widely used in the ceramic industry (Teoh et al., 2012). Titania nanoparticles could also be obtained by direct oxidation of titanium metal using oxidants or under anodization. At high temperature, acetone can be used as a good oxygen source for the preparation of TiO_2 nanomaterials via direct oxidation (Lei et al., 2004; Liu et al., 2016). The promising synthesis of TiO_2 nanowires have been reported using electrodeposition. The substrate to be coated is used as cathode and immersed into a solution which contains a salt of the metal to be deposited. The metallic ions are attracted to the cathode and reduced to metallic form (Chen & Mao, 2007; Teoh et al., 2012).

Recently, vapour deposition processes have been widely explored to fabricate various nanomaterials. Vapour deposition refers to any process in which materials in a vapour state are condensed to form a solid-phase material. They usually take place within a vacuum chamber. If no chemical reaction occurs, this process is called physical vapor deposition (Wen et al., 2005a; Zhang et al., 2002). Microwave radiation is also applied to prepare various TiO_2 nanomaterials. The major advantages of using microwaves for industrial processing are rapid heat transfer, and volumetric and selective heating (Chen & Mao, 2007).

The sol-gel method is widely used to produce small, well-defined particles even at relatively low temperatures. This method also enables the introduction of secondary components (*e.g.*, active metals) into the reaction mixture, which allows the synthesis of application-oriented TiO_2-based materials. Although titanium tetrachloride ($TiCl_4$) was used as a precursor in the initial studies of TiO_2 synthesis, this approach resulted in the formation of chloride ions as impurities in the product. Recent synthetic methods have focused on the use

of titanium alkoxides, $Ti(OR)_4$, where R is an alkyl group, as precursors. The precursor is dissolved in water or in a mixture of solvents and is hydrolysed to give $Ti(OH)_xR_{4-x}$, which subsequently undergoes condensation through either substitution or addition reactions to produce TiO_2 (MacWan et al., 2011).

Both halide and alkoxide compounds of titanium hydrolyse rapidly in the presence of water, causing difficulty in controlling the end product. Thus, post-synthesis modifications are necessary for tuning the properties of the end product. The most common technique is to use a solution containing acids and alcohol, in which the former serve as a catalyst and peptising agent. The use of alcohol as a solvent, on the other hand, can substantially reduce the temperature required in the TiO_2 synthesis process (Chen et al., 2013a; Mutin & Vioux, 2009). However, using structural facilitating agents to control the shape, size and crystallinity of the end product still remains as a challenge. For example, the use of fluoride and other fluorine-containing ions to control the particle shape of TiO_2 often results in surface-bound fluorine in the end product, which negatively influences the photocatalytic properties of TiO_2 (Ruzicka et al., 2014; Yang et al., 2008b).

2.3 Bio-mimicked materials for sustainable energy and environment

Recently, bio-inspired materials have emerged as a potential area of research for developing advanced functional systems with a higher standard of environmental compatibility, recyclability and energy efficiency (Sanchez et al., 2005). Natural materials offer a combination of advantageous properties, such as sophistication, miniaturization, hierarchical organization, hybridization, resistance and adaptability, which have evolved through billions of years of the natural selection processes. The morphologies of the biological structures

ranging from the nanometre to the millimetre scale inspire the design of artificial materials that aim at advanced applications, such as energy capture, storage and conversion (Lu & Schüth, 2006; Xia & Jiang, 2008). Table 2-2 summarizes some typical examples on unique structures and corresponding specific functions of biological systems.

Many bio-mimicking methods have recently been developed, including the following approaches:

a) replication, which involves use of biological templates to replicate the morphology *via* chemical transformations or physical processes**,** such as nanocasting and nanolithography;

b) self-assembly, which relies on using biological systems (usually at the nanoscale) as building blocks for a controllable assembly into complex structures through electrostatic, metal–ligand and inter-biomolecular interactions;

c) encapsulation, whereby biomolecules or living cells are isolated from their superstructures and encapsulated into manmade matrices with complex structures to form bioreactors (Lu & Schüth, 2006; Zhou et al., 2011).

Table 2-2: Typical examples of biological systems with unique structures and corresponding specific functions (Zhou et al., 2011).

	Biology	**Structures**	**Functions**
Biomolecules	DNA	Nanostructures	Miniaturization
Microorganism	Virus, Bacteria, Fungi, Yeats	Nanostructures	Self-assembly, Miniaturization
	Algae	Periodic porous structures / hierarchical micro-nanostructures	Chemical energy conversion, Particular optical functions
Plants	Wood	Hierarchical porous structures	High mechanical strength
	Leaves	Hierarchical structures	Chemical energy conversion, Superhydrophobicity self-cleaning
Animals	Insects	Periodic structures/ hierarchical structures	Structural colour, Superhydrophobicity
	Compound eyes	Periodic structures	Anti-reflection
	Feathers	Periodic structures	Structural colour, Superhydrophobicity
	Seashells, Teeth	Periodic structures	Structural colour, High mechanical strength
	Marine animals	Periodic structures	Particular optical functions
	Gecko feet	Hierarchical structures	Strong adhesive force
	Mosquito`s legs	Hierarchical structures	Water-supporting ability
	Fur and skin of polar bear	Hollow structures	Thermal insulation

Chapter 3 - Bio-mimicked TiO_2 architectures for enhanced photocatalytic activity under UV/visible light

3.1 Introduction

The templating method has recently emerged as an effective approach to overcome the difficulty in controlling the morphology of the end product (Cheng et al., 2012; Li et al., 2005; Waterhouse & Waterland, 2007). The main advantage of this technique is that the final structure can be easily tuned through selection of a template with an appropriate morphology. By contrast, the conventional sol-gel synthesis is strongly affected by the conditions of the synthesis, including the pH of the solution, drying, subsequent thermal treatments *etc*, while controlled assembly of the primary nanoparticulate building blocks into larger-scale structures being a major challenge. In efforts to develop TiO_2-based photocatalysts with improved light-harvesting functions, researches have recently proposed a few bio-templating techniques for reproduction of the natural hierarchical structures (Chen et al., 2013a,b; Li et al., 2009; Ye et al., 2014). However, further research on the details of the bio-templating process and the relationship between the morphology of obtained product and its photocatalytic performance is required.

The photosystem of the green leaves naturally evolved both at the molecular level and the structural level of nanoscale and microscale frameworks, making it overall a superior light-harvesting structure (Niinemets & Sack, 2006; Zhou et al., 2011). The lens-like epidermal cells focus incident light, and cylinder cells of palisade parenchyma serve as channels for the focused light, where the channels are arranged parallel to the incident light direction. The less-regular arrangement of spongy mesophyll leads to light scattering and long effective light path lengths

in the intercellular air spaces of the leaf.(Bone et al., 1985; Poulson & Vogelmann, 1990; Vogelmann et al., 1996; Vogelmann & Martin, 1993) Although such complex porous architectures trap sunlight within the leaves, the main antenna of plants' photosystem is the chloroplast. The thylakoid cylindrical stacks (granum) inside the chloroplast are 3-dimensional constructions made of interconnected nanolayers. These structures harvest the light efficiently by directing the sunlight to the chlorophyll molecules which are the reactive centres of the plant photochemical machine.(Mustárdy, 1996; Ruban et al., 2011; Rumak et al., 2010) The overall structure of the leaf photosystem is illustrated in Figure 3-1.

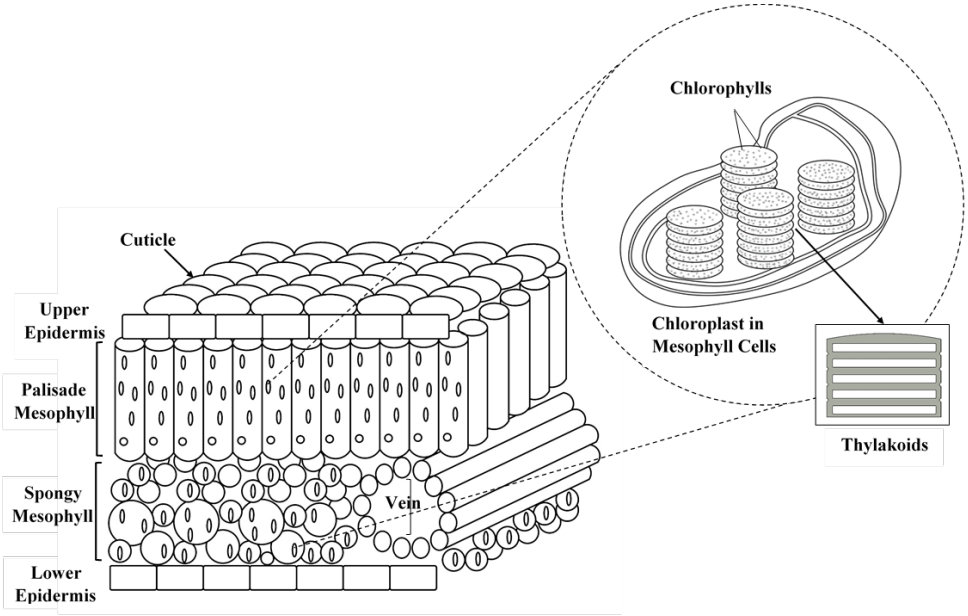

Figure 3-1. The microscale-to-nanoscale structures of leaf photosystem.

In this chapter, the structure of *Camellia sinensis* tree leaves from the family *Theaceae*, belonging to C_4 plants possessing the Kranz anatomy, has been replicated using TiO_2 from the microscale to the nanoscale. The photocatalytic activity of the artificial TiO_2 leaves at different level of biomimicked structures was studied through methylene blue degradation and the photocatalytic oxidation of ethanol under UV and visible light irradiation. The advantages of

possessing structures analogous to the stack-layered nanostructures and mesoporous architecture in natural leaves, offer a unique opportunity for TiO_2 and semiconductors to be used under visible light.

3.2 Methodology

3.2.1 Materials

All reagents were of analytical grade and were purchased from Sigma-Aldrich. Methylene Blue was supplied by Sekolah Tinggi Teknologi Tekstil, Indonesia. All reagents were used as received. All glassware was oven dried and experiments were performed using Schlenk line technique to avoid contact with ambient air when required.

3.2.2 Synthesis procedure of bio-mimicked TiO_2 architectures

The replication of nano- to micro-architectures of leaf photosystem was done by ion-exchange method to mimic the natural chlorophyll breakdown process. Fresh leaves were first washed with MilliQ water, dried and cut into *ca*. 5 by 5 mm pieces. Then, 6 g of cut leaves was acid treated with a 5 v/v% HCl solution under inert atmosphere (Schlenk line technique) with vigorous stirring (250 rpm) using magnetic stirrer at room temperature overnight until the leaves changed the colour to yellow-brown. Ion-exchange was subsequently carried out in a 5 v/v% $TiCl_3$ solution in water with stirring (250 rpm) under inert atmosphere at ambient temperature for 24 hours. The Ti^{3+} exchanged leaves were then coated with titania using a sol-gel approach modified from the previously reported method (He et al., 2013). The treated leaves were collected on the Büchner funnel, washed with MilliQ water (3 x 50 mL) and dried in the vacuum desiccator over P_2O_5. Resulting dry leaves were suspended with stirring (250 rpm) in dry isopropanol (200 mL) and the mixture was stirred for 24 h to ensure soaking/exchange. After water exchange or soaking step, the leaves were filtered off and

quickly cut into smaller pieces (*ca.* 1 x 1 mm) to allow more efficient diffusion of titanium isopropoxide within the leaf structure. Titanium isopropoxide (4 mL, 14.5 mmol) was then added using a syringe to the suspension of dry leaves (stirred at 250 rpm) in dry isopropanol (240 mL) as sol-gel precursor. The mixture was kept stirring at room temperature for another 24 h. Finally, the mixture was refluxed with stirring for 6 h, cooled and the product was filtered off, washed with isopropanol (10 mL), and dried in an aerated oven at 353 K for 12 h. The sample was then heat treated under static air at 773 K for 2 h (ramping rate of 1 K/min to avoid thermal shock damage) to remove all organic components and to crystalize the TiO_2 leaves.

Intact chloroplasts were isolated from *Spinacia oleracea* leaves using the method proposed by Robinson *et al*. (Robinson, 1983) as described in Scheme 3-1. The resulted chloroplast cells were used as biotemplates for the replication of the nanostructure of leaf photosystem using the abovementioned Ti^{3+} exchange method with no cutting of leaves required. The product was filtered off, washed with isopropoxide, dried and heat treated at 773 K for 2 h (ramping rate of 1 K/min) under static air.

3.2.3 Characterizations

The morphology of the TiO_2 architectures synthesized *via* the bio-templating method was imaged using a JEOL 7000F scanning electron microscope (SEM). The samples were sputtered with carbon, and the working distance was varied between 10 mm and 4 mm to give the best image quality; the accelerating voltage was maintained at 10 kV.

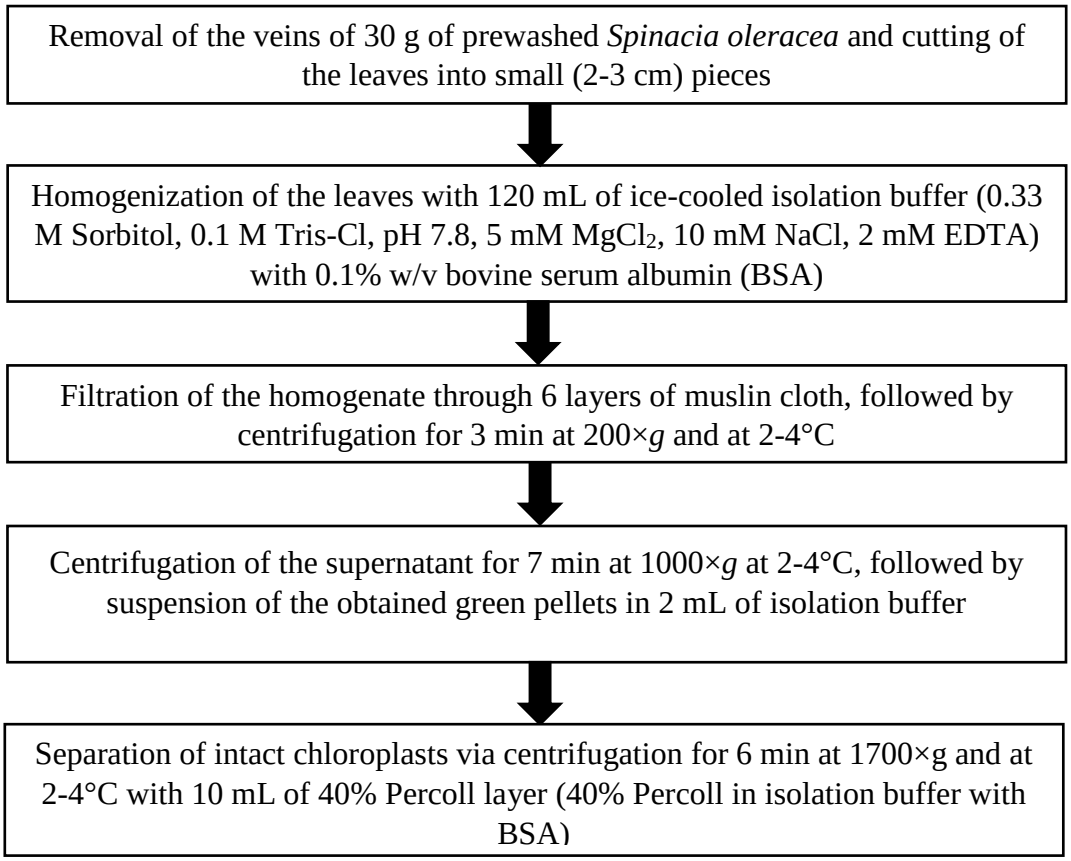

Scheme 3-1. Chloroplast isolation procedure; all steps were performed at 2-4°C.

Transmission electron microscopy (TEM) images were recorded using a Philips CM-200 transmission electron microscope operating at 200 kV. The samples were prepared by sonication in ethanol until fully dispersed followed by drop-casting onto a 150 square mesh copper TEM grid coated with carbon film.

The crystal phase of TiO_2 was identified by X-ray diffraction (XRD) on a Bruker APEXII X-ray diffractometer equipped with a Mo Kα radiation source and a graphite monochromator.

The surface area was estimated by nitrogen adsorption measurements using the BET equation. The measurements were conducted at 77 K using a Micromeritics Gemini VI 2385-C Surface Area Analyser. All of the samples were degassed at 473 K under vacuum overnight before the measurements.

The surface compositions were measured by X-ray photoelectron spectroscopy (XPS) using a Thermo Scientific ESCALAB250Xi probe with monochromated Al Kα radiation ($h\nu$ = 1486.68 eV). The binding energy was calibrated using the C 1s peak at 284.8 eV as reference. Measured spot was defined as a 500 µm square. The survey scans and the high-resolution (HR) XPS spectra were collected at the pass energy of 100 eV and 20 eV, respectively, and the photoelectron take off angle at 90° with respect to the surface plane. The XPS data was analysed using the Avantage software.

Dynamic light scattering (DLS) measurements were performed using a Microtrak Zetatrak DLS instrument. The samples were homogeneously dispersed in Milli-Q water (1 g L^{-1}) via sonication for 15 min followed by 30 min of stirring (same conditions as used in the dye degradation reaction before UV/visible light irradiation) in order to evaluate of the particle size effect on the reaction.

3.2.4 Photocatalytic activity under UV/visible light

UV-Visible spectroscopy is a technique to study electronic transitions that occur in material under ultra-violet (UV) and/or visible light illumination (Skoog et al., 2017). In UV-vis experiment absorption of light as a function of wavelength is measured. UV-Vis measurements are usually performed in either transmission (typically for liquid samples) or

diffuse reflectance configuration (for solids). In transmission configuration, the sample is placed in the path of collimated beam of light, which is partially absorbed at characteristic wavelengths that correspond to electronic transitions of the sample (Figure 3-2). The transmitted light, collected by spectrometer, is referenced to a baseline measurement, which takes into account the absorbance by a sample holder (*e.g.* cuvette or glass slide). The spectra in transmission configuration are plotted in coordinates absorbance $A = -log(I/I_0)$ versus wavelength λ.

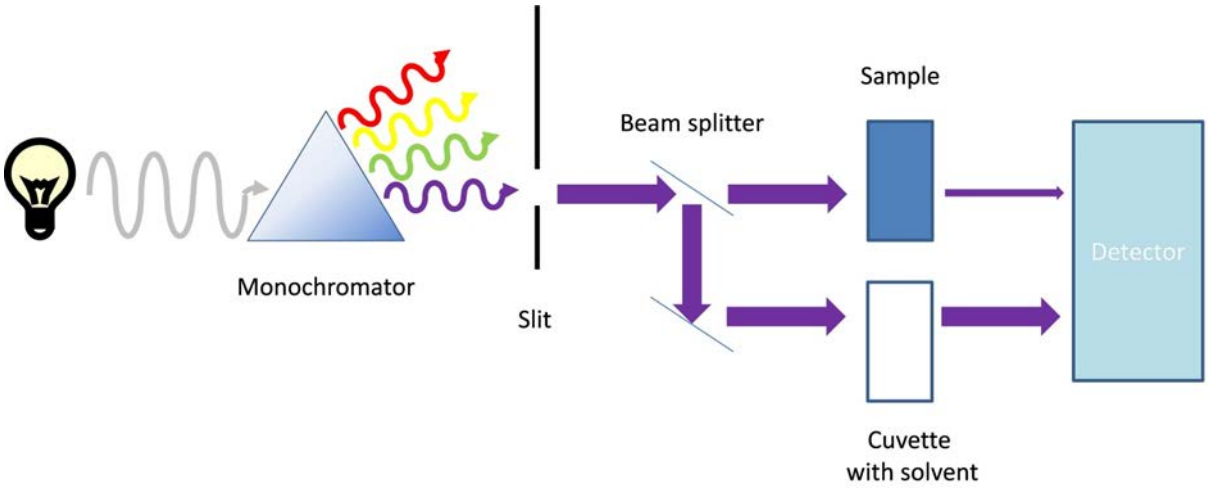

Figure 3-2. Scheme of UV-vis measurement in transmission configuration.

In diffuse reflectance UV-vis spectroscopy (DR UV-vis), the spectrometer measures the diffusely reflected light from the sample. Collection of diffuse reflected light could be performed using mirror optics, fiber optics or integrating spheres. The latter is most widely used and enables to capture photons that are reflected in all directions from the sample (Figure 3-3).

After incident beam reaches the sample, two types of reflections occur: specular and diffuse. In specular reflectance, incident beam reflects at an angle equal to the angle of incidence. Because specularly reflected light does not undergo an absorption process it contains little to no information about electronic states of material and only increases the noise. In diffuse reflection, the incident beam penetrates the sample surface, gets partially absorbed and then reemitted at various non-incident angles. Powders are typically diluted with non-absorbing material, such as $BaSO_4$, which increases diffuse reflectance and minimizes specular reflectance.

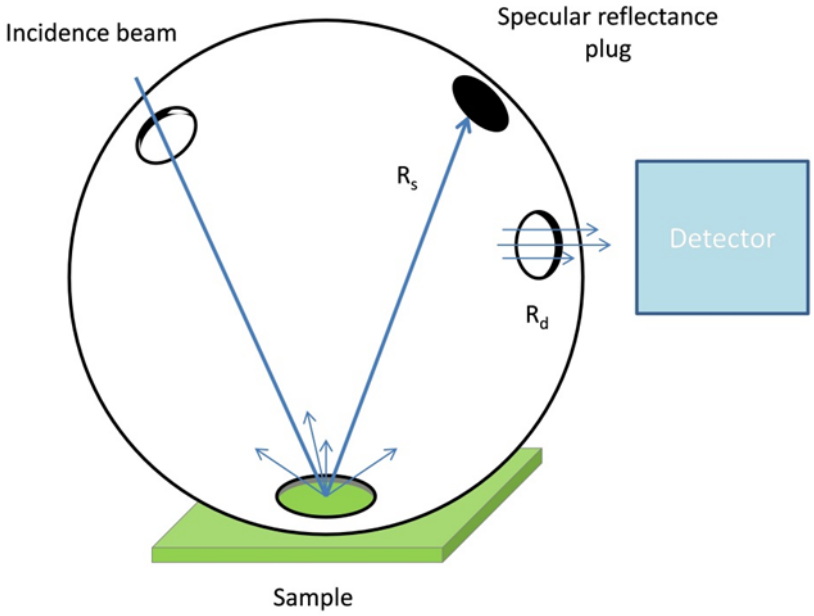

Figure 3-3. Scheme of DR UV-vis configuration using integrating sphere. R_s – specularly reflected light, R_d – diffuse reflected light.

Diffuse-reflectance UV-vis spectra were recorded using a Citra 4040 spectrophotometer equipped with an integrating sphere and operated in reflectance mode. The catalyst samples were diluted with $BaSO_4$, and the resulting mixture was uniformly mixed, ground and loaded into the sample-holder. UV-vis spectra were recorded in reflectance mode,

and the obtained reflectance values (R) were transformed to the Kubelka-Munk function F(R) according to the equation 3-1:

$$F(R) = \frac{(1-R)^2}{2R} \quad (3\text{-}1)$$

The band gap was estimated by creating a Tauc plot of $(hvF(R))^{1\backslash n}$ against hv (where h is Planck's constant, v is the frequency of vibration and n = 1/2 for direct transitions) (Adachi, 1999).

Preliminary, the photocatalytic activity of the bio-mimicked TiO_2 architectures under ultraviolet (UV) and visible light was studied in methylene blue degradation in a batch mode. An enclosed photocatalytic chamber equipped with two 50 W LEDs with maximum intensities at 370 nm (UV), 440 nm (blue) or 515 nm (green) was used in these experiments with remote sampling performed using syringe equipped with a long needle. The light flux was monitored to ensure that it was consistent across all experiments. The experimental conditions were set according to the literature (Abu Bakar et al., 2015; Bae et al., 2014; Tayade et al., 2009; Yao & Wang, 2010). The solution pH was maintained at 7 to exclude the effects of acidity and alkalinity on the photocatalytic activity. The reaction solution was prepared by dispersing 15 mg of catalyst in 100 mL of dye solution (6.5 mg of methylene blue in 1 L deionised water) in a clean, dry quartz tube. The slurry was sonicated for 15 min to ensure that the catalyst was homogeneously dispersed before the reaction. The dye-catalyst slurry in the quartz tube was placed into the sealed photolysis chamber and stirred for 30 min in the dark to reach adsorption equilibrium. A 3-mL initial sample was collected before irradiation started. The reaction was timed immediately after the irradiation began and the temperature of the solution increased only marginally (up to 303 K maximum) during irradiation. Samples were collected at different

reaction time and were centrifuged twice (13,000 rpm, 3 min) and analysed by UV-vis spectroscopy within a wavelength range from 500 to 750 nm. The dye conversion was determined by equation 3-2 on the basis of the maximum absorption.

$$Conversion\% = \frac{(A_0 - A_t)}{A_0} \times 100 \quad (3\text{-}2)$$

where A_0 is the initial absorbance of dye and A_t is the absorbance at time *t*. The rate constants of the decolourization reaction was estimated using a pseudo first-order kinetic (Abu Bakar et al., 2015):

$$-ln\frac{C_t}{C_0} = kt \quad (3\text{-}3)$$

where C_0 is the initial concentration of dye, C_t is the concentration at time *t*, *t* is the irradiation time and *k* is the apparent kinetic constant.

Control experiments without irradiation were performed to make sure that adsorption equilibrium was established after 30 min. The result of the dark experiments are provided in Figure 3-4. Blank reactions were also conducted to ensure that the decomposition of methylene blue was due to the photocatalytic degradation. No significant dye conversion (< 3%) was observed under UV and visible lights in the absence of photocatalyst. The result of blank reactions are included in the dye conversion figures.

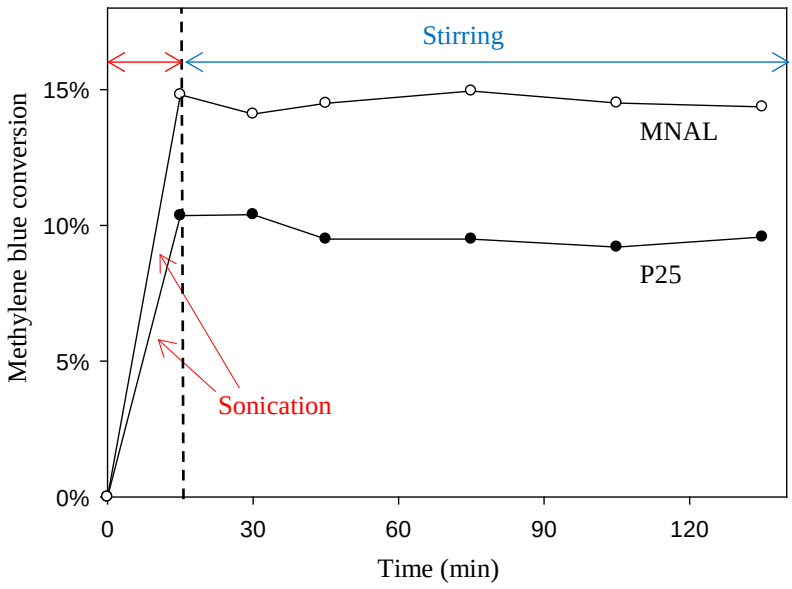

Figure 3-4. Adsorption of methylene blue under dark on the MNAL (biotemplated TiO_2 catalyst) and the reference P25. The experimental conditions are 6.5 ppm dye solution, a catalyst loading of 150 mg cat./L, a pH of 7, 30°C.

The photocatalytic oxidation of ethanol was carried out in a stirred batch annular reactor made from quartz with an internal volume of 150 ml and wall thickness of 0.5 cm. The catalyst powder (50 mg) was suspended in 50 ml of 20 v/v% ethanol solution for typical batches. The reaction slurry was stirred vigorously at 500 rpm for 60 min using magnetic stirrer to ensure homogeneity before the reaction. The reactor was purged with an inert gas using Schlenk line technique and was closed tightly. The reactor was placed inside an enclosed photolysis chamber and the mixture was stirred at 250 rpm to prevent sedimentation of the catalyst. Green LEDs with a maximum intensity at 515 nm were used to irradiate the reactor. The solution temperature and the gas phase pressure were continuously monitored. A gas sample was collected at the end of each reaction using a gas-tight syringe (10 ml). The samples were immediately analysed using a gas chromatograph (SRI Instruments, methanizer FID and TCD detectors, Haysep-D column). The photocatalytic performance in ethanol oxidation was assessed by the CO_2 yield.

3.3 Results and discussion

3.3.1 Improved fabrication of the biotemplated TiO_2 leaf

The templated materials with micro- and nano-architecture of the leaf photosystem are referred to as a "micro- and nano-structure templated artificial leaf" (MNAL). The natural enzymatic reactions of chlorophyll breakdown generally include breakdown of the chlorophyll chains by the chlorophyllase enzyme, followed by the Mg-dechelatase step and then oxidation of pheophorbide (Hörtensteiner & Kräutler, 2011). In this study, the colour change of the acid treated leaves to the yellow-brown indicates the conversion of chlorophyll into pheophorbide (Drzewiecka-Matuszek et al., 2005; Küpper et al., 1998). The ion-exchange procedure was performed under inert atmosphere to prevent Ti^{3+} ions from oxidizing. Energy-dispersive X-ray spectroscopy (EDS) results in Table 3-1 clearly demonstrate that there are no detectable metal contents of Mg^{2+} and other metal ions present in the leaf template. This finding indicates that the acid treatment was effective in extracting such metals during the artificial leaf synthesis process. Trace amount of a vast range of metals including Mg, Zn, Fe, Pb *etc* was observed in the non-treated samples. The extraction of metal ions is significant because the presence of metals may affect the crystal phase formation of the final TiO_2 catalyst. In addition, the presence of metal ion impurities could make the final product composition difficult to control because the leaf contents change over the seasons (Yuan et al., 2015).

In this research, an important improvement of the synthesis method was made by a solvent exchange step using dry isopropanol. This step was introduced to exchange or extract water present within leaves and replace it with isopropanol and also washing out any remaining salts from ion-exchange procedure. Minimizing water content inside the leaves allows titanium isopropoxide to diffuse deep inside the leaves, allowing better replication of the structure. Attempts to perform extraction using Soxhlet technique resulted in visible structural

deterioration of the leaves, most likely due to higher temperature of the process. It is well known that water is critically important for the start of titanium isopropoxide hydrolysis. Therefore, the sol-gel was carried out open to ambient air to allow very gradual diffusion of water into the system which resulted in noticeable hydrolysis and formation of titania. When this step was performed under inert dry atmosphere (Schlenk line) no visible signs of titania sol formation can be detected, thus confirming success of the earlier water extraction step. Noteworthy, the optimum size of leaf cuts accelerate infiltration of titanium ions through the leaf structure. Preliminary experiments using larger sizes of leaf cuts (*ca*. 5 mm by 5 mm) produced material which had titania structures formed only at the periphery of the leaf fragments.

To investigate the relationship between the morphology of the bio-templated product and its photocatalytic performance, Ti^{3+} exchange step was excluded to produce templated materials with only the microstructure of leaf photosystem. According to Li *et al.* (Li et al., 2009), it is hypothesised that the Ti^{3+} ions get trapped within the thylakoids via ion-exchange with the hydrogen in the chlorophylls. During the heat treatment, the titania coat produced from titanium isopropoxide hydrolysis act as seeding sites for crystallization of TiO_2 to form the nano-scale interconnected stacked-sheets structure. Hence, the sample synthesized *via* the sol-gel method alone does not possess the nano-architecture of leaf photosystem and is referred to as a "micro-structure mimicked artificial leaf" (MAL).

In our preliminary experiments, the sol-gel coating step of the Ti^{3+}-exchanged leaves was omitted to replicate the nano-architecture of leaf photosystem alone. The produced templated materials showed no photocatalytic activity for degradation of methylene blue under

UV light which could be attributed to the titania crystalline phase. The XRD pattern of non-coated sample showed that the crystalline phase is mostly rutile. These results show that eliminating of sol-gel step favours the anatase-to-rutile phase transformation during crystallization of the TiO_2 leaves. Therefore, intact chloroplast cells were isolated from *Spinacia oleracea* leaves using the method involving mechanical breaking of the cell wall and the plasma membrane, filtration of cell debris and unbroken leaf tissues, collection of chloroplasts by centrifugation, and separation of the intact chloroplasts from the broken ones. The resulted replicas of isolated chloroplast cells are referred to as "artificial chloroplast" (AChl).

Several samples from different synthesis batches were used to repeat the catalyst characterizations and photocatalytic activity experiments to ensure that the developed replication approach is reproducible. All characterizations were in an acceptable criteria and the photocatalytic activity results obtained from different batch of same catalysts under UV/visible light are within the error bars.

3.3.2 Catalyst characterization

Figure 3-5 a-c shows the scanning electron microscopy images of the final catalysts after calcination. These images demonstrate that the porous microstructures of the photosystem, including the palisade and spongy layers of the mesophylls, are replicated and the removal of the organic components of the leaves was successfully accomplished. The well-replicated layered nanostructures of the thylakoids in the chloroplast are shown in the higher resolution TEM images of the MNAL and AChl samples (Figure 3-5 d-f). The average length of the bio-templated TiO_2 chloroplasts is 1.5-2 µm, which is in a good agreement with the size of natural chloroplast cells (Ellis & Leech, 1985; Rudowska et al., 2012; Shimoni et al., 2005).

The results show that the developed method provides a reliable approach to synthesize TiO_2 hierarchical architectures similar to natural materials. This improved templating method could address the issues in controlling the morphology of final product associated with conventional procedures of synthesis of TiO_2 structures.

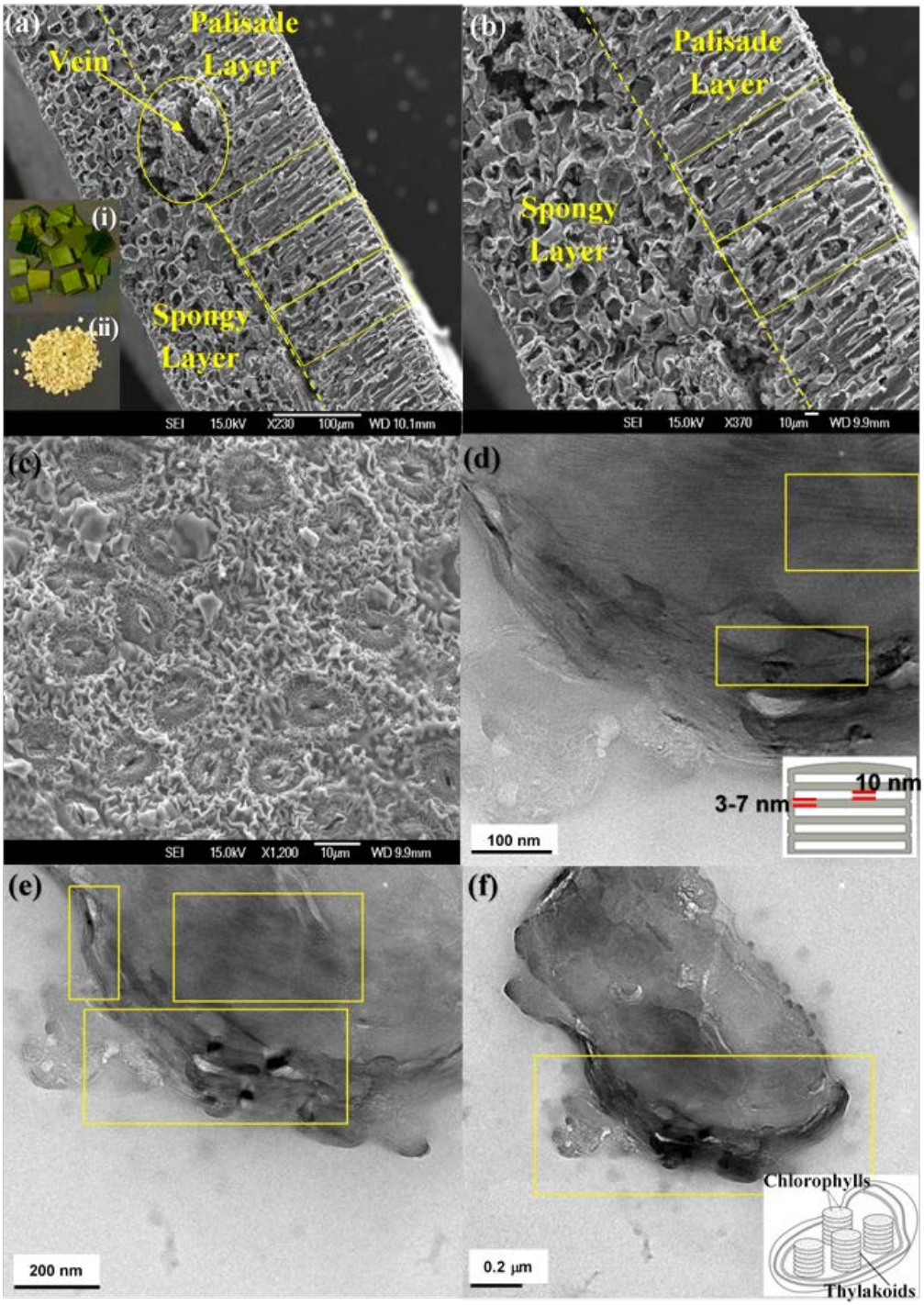

Figure 3-5. a-b) Cross-section SEM images of final catalysts, showing the well-replicated microarchitecture of the leaf photosystem. Inset: (i) photos of natural *camellia sinensis* leaves and (ii) TiO_2 artificial leaves. c) Top-view SEM image of final catalysts, illustrating that the porous structure of the stomata is retained after the removal of the leaves. d-e) TEM images of MNAL samples showing that the stack-layered nanostructures of the thylakoids in the chloroplast are retained after the removal of the leaves. f) TEM images of AChl samples illustrating the well-replicated nano-architecture of the thylakoid membranes.

The results of energy-dispersive X-ray spectroscopy (EDS) measurements summarized in Table 3-1 demonstrate that the templated materials are composed mostly from titanium and oxygen. Given a minimum of 2 wt % nonmetal doping has been reported to be required to influence the efficiency of TiO_2 photocatalysts (Rehman et al., 2009), the trace amounts of other elements (N, P and C) retained within the synthesized catalysts from the biotemplates are considered insufficient to contribute to the photocatalytic performance of these materials. In addition, lack of detectable C within the templated samples based on the EDS analysis confirms the effective removal of the organic template which corroborates the observations made under SEM.

Table 3-1. Energy-dispersive X-ray spectroscopy (EDS) results for the final catalysts.

Content (wt %)	Ti	O	N	P	C†
MNAL	70.8	29.2	---	---	---
MAL	67.3	32.2	0.6	---	---
AChl	72.3	27.2	0.4	0.2	---

†No carbon dopant was detected by EDS for all three bio-templated samples.

Although a mixture of anatase and rutile phases has been commonly reported for the room-temperature sol-gel synthesis of TiO_2 followed by a heat treatment, the phase formation strongly depends on several factors, including the nature and volume of the solution, the reaction atmosphere and time, the presences of impurities, the morphology of the sample, and also the rate and thermal homogeneity of the post-synthesis heat treatment (Sharma et al., 2006; Smirnova et al., 2004; Takahashi & Matsuoka, 1988). The XRD patterns in Figure 3-6 show that the MNAL and MAL consist predominantly of the anatase crystalline phase, whereas the

AChl is a combination of anatase and rutile TiO_2 phases. The results show that our biotemplating method generally favours the formation of a pure anatase phase (the MNAL and MAL) after the samples underwent a heat treatment at 500°C for 2 h under static air. This is consistent with the synthesis of TiO_2 films in which the initial crystalline TiO_2 phase formed is usually anatase (Okada et al., 2001; Shin et al., 2005). On the other hand, mixed phases of anatase and rutile in the AChl could be caused by a high ratio between the organic components from natural cells and TiO_2 during heat treatment. Many researches have attempted to study the effects of impurities on the anatase-to-rutile phase transformation. A high content of organic impurities can change the level of oxygen vacancies in the TiO_2 lattice, thus favouring the anatase to rutile phase transformation (Hanaor & Sorrell, 2011). In addition, the faster phase transformation rate observed in the AChl also suggests that there are more potential nucleation sites available for the anatase-to-rutile transformation at low temperatures compared with the MNAL and MAL. As a result, the AChl is finely crystalline with small crystallite sizes.

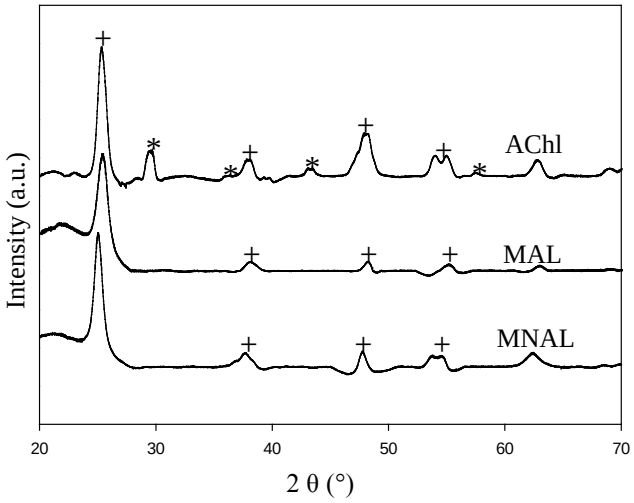

Figure 3-6. XRD patterns of the final catalysts. Corresponding peaks of the anatase phase and the rutile phase TiO_2 are marked by "+" and "*", respectively.

Nitrogen (N_2) physisorption experiments show that the specific surface area of the MAL and the MNAL are 29.9 m^2/g and 66.1 m^2/g, respectively (Figure 3-7). While both samples exhibited mesoporosity in their structures according to the hysteresis observed in the adsorption isotherms, MNAL specifically gave a H3 hysteresis loop indicating possible random pore network and irregular pore shape such as the "ink-bottle" geometry (Sing & Williams, 2004). The stepwise desorption which occurred at the relative pressure of 0.55 suggests the characteristic desorption mechanism *via* cavitation and, thereby, confirms the presence of pore necks that are smaller than the critical size of N_2 (*ca*. 5 - 6 nm) at 77 K. In addition, the amount of N_2 adsorbed (mmol/g) on the MNAL is significantly higher than that adsorbed on the MAL (approximately 2.5 and 2.6 times higher on the MNAL at P/Po of 0.3 and 0.9, respectively, as shown in Figure 3-7), demonstrating that the biotemplated nano-architecture derived from the thylakoid in chloroplasts present within the MNAL gives rise to a larger surface area.

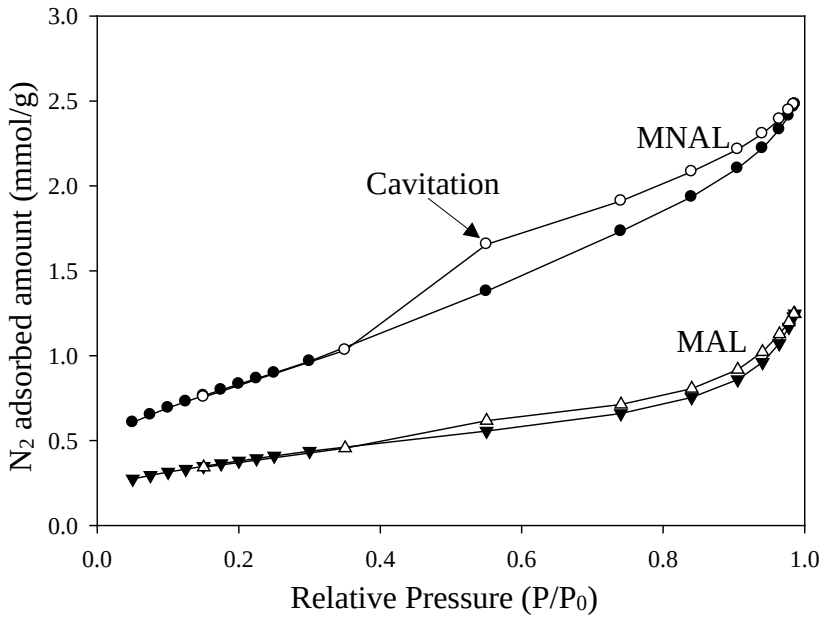

Figure 3-7. Nitrogen adsorption-desorption isotherm of the biotemplated TiO_2 catalysts.

The general XPS spectrum of the MNAL sample is shown in Figure 3-8a. The P and Ca peaks centred at the binding energy (BE) of 133.7 and 347.7 eV could be assigned to the phosphate chemical state (Caporali et al., 2006) and the phosphate/carbonate state (Zhao et al., 2012), respectively. The state of N at BE of 400.1 eV could be attributed to the metal nitrate bonds (Battiston et al., 2000; Cong et al., 2007). The trace amount of phosphorus, calcium and nitrogen detected in the MNAL sample presumably are residues remained from the original biotemplate. The symmetric peak at the BE of 458.9 eV in the Ti 2p high resolution (HR) spectrum (Figure 3-8b) is identified as TiO_2 (Drnovšek et al., 2009; Górska et al., 2008). The BE for the Ti_{2p} peak is expected to decrease if chemical doping occurs, necessitating curve-fitting using peaks corresponding to several complex species (Cong et al., 2007; Paszkiewicz et al., 2016). In the MNAL sample, however, there are no complex peaks of Ti bonds recorded, confirming that doping of other elements (N, C or P) are negligible. The HR spectrum of O 1s was deconvoluted for three peaks (Figure 3-8c). From the reported TiO_2 models (György et al., 2003; Yu et al., 2000), the first peak at the BE of 530.2 eV is related to the TiO_2 crystal lattice, the second at 531.6 eV is referred to the OH group and the third (BE = 532.8 eV) represents Ti−O−N bond formation. The last peak can be also interpreted as the carbonate state.

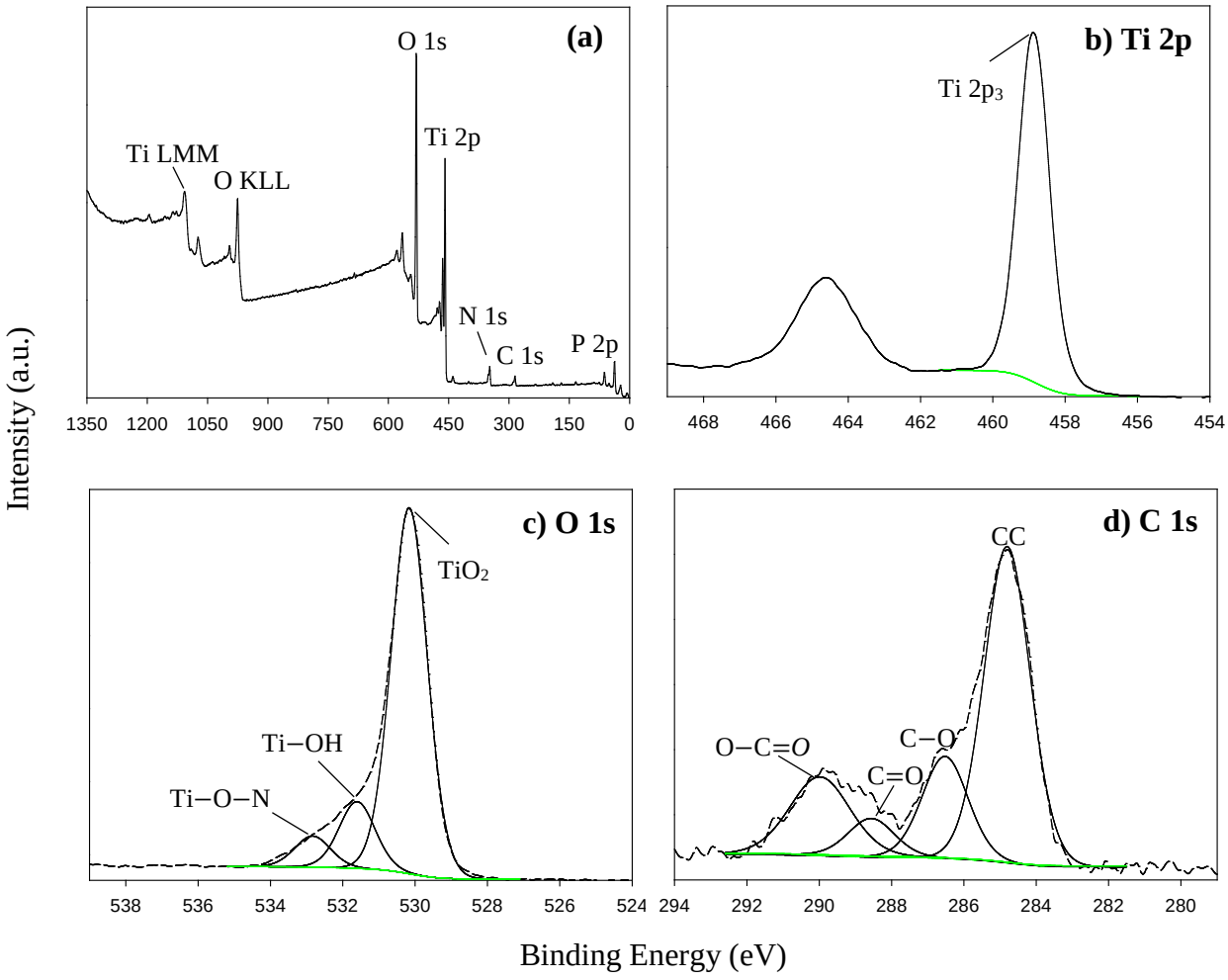

Figure 3-8. a) General XPS spectrum of the MNAL and high resolution deconvoluted XPS spectra of b) Ti 2p, c) O 1s and d) C 1s.

Four carbon states at 284.8 eV (A), 286.5 eV (B), 288.6 eV (C) and 290 eV (D) were separated in the C 1s spectrum (Figure 3-8d). The states “A” and “B” could be assigned to CC (aromatic and aliphatic) and C−O, respectively (Xue et al., 1988). These two states could be attributed to the adventitious carbon contaminants which are commonly reported in samples that have been exposed to the atmosphere (Górska et al., 2008). The peaks “C” and “D” could be characteristics for C=O bond and O−C=O group, respectively (Calliari et al., 2007;

Milczarek et al., 2011). These peaks are also observed in the C 1s spectra reported by Peng *et al.* (Peng et al., 2014) for the activated carbon derived from pomelo peel. The carbon states "C" and "D" are probably related to the remaining carbon from burning the leaf (Chen et al., 2011; Lang et al., 2012). No significant C content was detected in the bulk composition analysis by EDS (Table 3-1), proving that the carbon states were mostly resulted from adventitious carbon contamination. The surface composition of the MNAL was specifically characterized because it exhibited the best photocatalytic performance among the three bio-templated samples under UV (Figure 3-9) and blue (Figure 3-11) wavelengths. The elemental surface composition (atom. %) of the MNAL is summarized in Table 3-2.

Table 3-2. Elemental composition (in atomic %) of the surface of the MNAL sample measured by XPS analysis.

P	Ca	N	O			Ti	C			
(133.7 eV)	(347.7 eV)	(400.1 eV)	(530.2 eV)	(531.6 eV)	(532.8 eV)	(458.9 eV)	(284.8 eV)	(286.5 eV)	(288.6 eV)	(290.0 eV)
1.11 %	2.57 %	0.49 %	49.08 %	8.95 %	4.17 %	24.82%	4.27 %	1.38 %	0.51 %	1.38 %

3.3.3 Superior photocatalytic performance under UV/visible light

The efficiency of a photocatalytic reaction is an overall outcome of various steps: light absorption, the transport of photogenerated charge carriers, the electron/hole recombination rate and mass transfer of the reactant(s) or reactive radical species to/from the catalyst surface. The morphology of the photocatalyst, and particularly the particle size and shape, strongly influences the aforementioned parameters (Cheng et al., 2014; Schiavello, 1997; Testino et al., 2007). Figure 3-9 shows that the MNAL exhibited photocatalytic activity (80±8 %) comparable to that of the commercial P25 catalyst (86±8.5 %) after 60 min of irradiation under UV light (370 nm). The slightly higher conversion given by the commercial P25 (composed by approximately 80 % anatase and 20 % rutile) could be mainly due to the enhanced charge carrier transfer between anatase and rutile (preventing undesirable recombination) caused by the energy difference between the conduction band edges of the two phases (Hurum et al., 2003). On the other hand, nonporous TiO_2 catalysts are not capable of exhibiting favoured excitation behaviour in parallel with a high specific surface area; thereby photogenerated pairs of holes and electrons within the bulk mass of the semiconductor will recombine before being transferred into the surface and collected by the external reactant, causing a low quantum yield (Hao et al., 2002; Jiang et al., 2008; Lin et al., 2006). In contrast to the reference P25, the prolonged residence time of methylene blue through internal interconnected nano-membrane structures and unique hierarchical pore network within the MNAL significantly enhanced the reactant-catalyst. This improved mass transport offsets the theoretically lower photocatalytic activity in the MNAL due to its predominantly pure anatase phase (which is expected to have higher e/h recombination rates compared to P-25). In addition, Howe and Grätzel suggested that photo-induced charge carriers in TiO_2 nanomaterials present at different sites in the bulk defects and on the surface (Howe & Grätzel, 1985,1987). The electron hole recombination rate could be reduced by providing charge traps in defect points located within the TiO_2 hierarchical structures (Krishnan, 2007; Macdonald et al., 2012; Nowotny et al., 2008), it is hypothesized

that a lower recombination rate of the photogenerated electron-hole pairs is possible in the MNAL. The structure that is responsible for the photocatalytic activity of the MNAL is the stacked titania nano-sheets (thylakoid membranes replica) as the micro-architecture (palisade and spongy layers of the mesophylls) of the leaf photosystem tends to disintegrate under stirring. The DLS measurements showed that the synthesized MNAL and MAL catalysts break down to the small particles with an average diameter of 2.3±0.2 μm during the reaction.

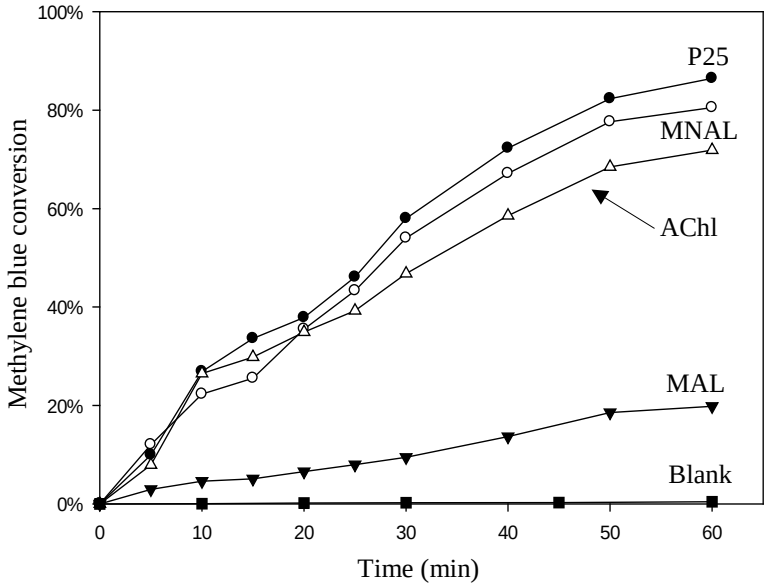

Figure 3-9. Conversion of methylene blue under UV light with a maximum intensity at 370 nm. The experimental conditions are 6.5 ppm dye solution, a catalyst loading of 150 mg-cat/L, a pH of 7, 30°C. The accuracy of all experiments was verified by series of repeated measurements and the relative error of less than 10% was determined.

The AChl structures gave a slightly lower photocatalytic activity (72±7 % methylene blue conversion after 60 min) than the MNAL possibly due to insufficient mesoporous channels for fast adsorption and desorption of the reactants and oxidized products, respectively. This finding indicates that the porous structure, remaining from the broken mesophyll cells replica, could improve the photocatalytic activity. However, the light harvesting by the artificial leaves could not resemble that of the microscale frameworks of leaf photosystem in the slurry reaction

system. Poor photocatalytic performance was observed in the case of using the MAL (only 20±2 % conversion) under UV light irradiation. This low activity in methylene blue degradation probably is resulted from the low surface area of the MAL in which nano-membrane structures (thylakoids replica) are absent and predominantly anatase crystalline phase composition are present. Moreover, the dye degradation measured for MAL (20%) after 120 min is 4 times lower than that measured for MNAL (80%). The difference in dye degradation efficiency is far greater than the 2.5-times factor of their surface area difference. The normalized results of methylene blue degradation are presented in Table 3-3. Both the MNAL and AChl catalysts exhibited photocatalytic dye degradation performance (34.7 and 31.2 mg/g-cat) similar to that of the P25 (37.3 mg/g-cat) with an ordinary particulate form under UV light in contrast to the poor photocatalytic performance of the MAL (8.7 mg/g-cat). Thus, the layered nanostructures replicated from the thylakoid nano-membranes could be considered as the key contributing factor to the photocatalytic performance of the biotemplated materials.

The proposed multi-steps chemical replication method for producing micro- and nano-structure templated artificial leaves (MNAL) is more feasible for large-scale synthesis compared with the intact chloroplast cells isolation procedure which only produces AChl at a very low yield (average yield ~ 40 mg chloroplasts/g *spinach* leaf (Nishimura et al., 1976; Robinson, 1983)). Thus, the AChl was not included in the study of visible light activity.

Table 3-3. Normalized results of methylene blue dye degradation.

Sample name	BET (m^2/g)	under UV (370 nm)		under Blue (440 nm)		under Green (515 nm)	
		mg/g-cat.[(a)]	$mg/m^{2(b)}$	mg/g-cat[(a)]	$mg/m^{2(b)}$	mg/g-cat[(a)]	$mg/m^{2(b)}$
P25	53	37.3	0.700	3.1	0.058	2.7	0.052
MNAL	66	34.7	0.530	5.7	0.086	3.9	0.060
MAL	30	8.7	0.290	0.0	0.000	---	---
AChl	---[(C)]	31.2	---	---	---	---	---

[(a)] Average dye conversion (mg) per gram of catalyst.

[(b)] Average dye conversion (mg) per m^2 of catalyst surface area.

[(C)] The surface area of the AChl was not measured because of the very low yield of the intact chloroplast cells isolation procedure.

The diffuse-reflectance UV-vis spectra shown in Figure 3-10 demonstrate two important features. Firstly, the MNAL exhibits greater absorption in the UV region over a broad UV-vis wavelength (*ca*. 350 - 600 nm) compared to the reference P25 material. We hypothesise that this is due to the improved light trapping and light scattering properties through the layered nano-architectures. Interestingly, this is consistent with the excellent light trapping properties of the parent biotemplating materials (*i.e*. natural chloroplasts) reported in biological science literature (Mustárdy, 1996; Ruban et al., 2011; Rumak et al., 2010), which are capable of maximizing light scattering through the layered structures. Secondly, the absorption efficiency has been improved in the visible light region (particularly between 400-600 nm). Such improvement of the visible light absorbance can be attributed to the presence of localized states within the TiO_2 compact layers in the MNAL. There are two types of trap centres in TiO_2 nanostructures: (1) the lattice defects, such as oxygen vacancies, that can form localized Ti^{3+} centres which may lead to additional electronic states within the TiO_2 band gap, allowing sub-band gap transitions and thus light absorbance in the visible region; (2) the high surface area of such materials (66.1 m^2/g in MNAL) may offer a large number of surface atoms which could act as trap centres (Abayev et al., 2007; Krishnan, 2007). These advanced optical properties of titania nano-architectures have been observed and proved in many reports over the past few years (Chen & Mao, 2007). For instance, Bavykin *et al.*(Bavykin et al., 2005) revealed the improved optical properties in TiO_2 nanotubes; Sato and Sakai *et al.* showed that the effective wavelengthsforlight harvesting red shifted when titania is fabricated in the form of nanosheets (Sakai et al., 2004; Sato et al., 2003).

The observed peak centred at *ca.* 500 nm in the spectrum of the MAL sample could be due to the absorption of light by N content (Asahi et al., 2001; Yang et al., 2007). However, the amount of N is insufficient to contribute to the photocatalytic efficiency of biotemplated

catalyst as discussed earlier. There is no detectable absorption peak associated with N content in the MNAL spectrum, suggesting the nitrogen in the bulk composition of the synthesized catalyst retained from the leaf is negligible (same as the results in Table 3-1). This shows that the extrinsic excitation behaviour of TiO_2 photocatalyst can potentially be augmented by modifying its morphology without changing its composition. The Tauc plot in Figure 3-10 (inset) allows to roughly estimate an energy band gap of 3.2 eV for the NM Art. Leaf, which is lower than that of the reference P25 TiO_2 (E_g = 3.3 eV). Although only a minor reduction of bandgap is evidenced by the Tauc plot, the result is in good agreement with reported band gap narrowing by only 0.2 eV *via* structural modification for TiO_2 nanomaterials (Etacheri et al., 2015).

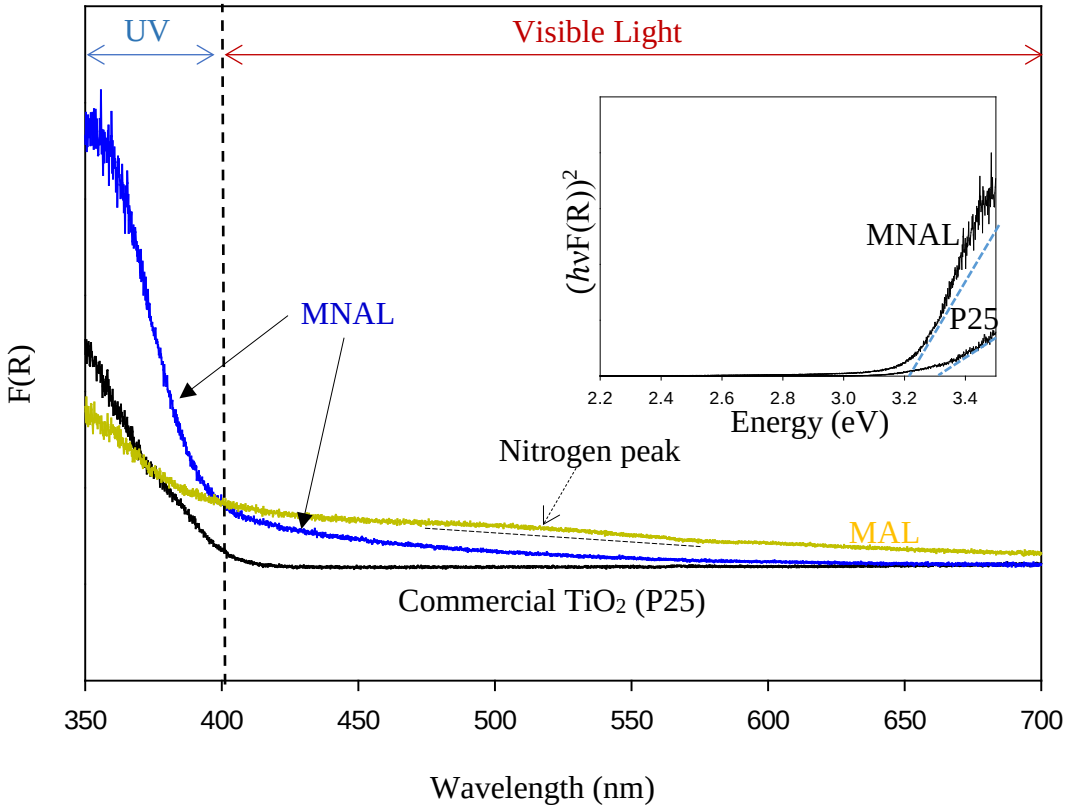

Figure 3-10. Diffuse-reflectance UV-Vis spectra of the MNAL, MAL and the reference P25 (Inset: Tauc plot showing fits used for the estimation of band gap values; The MNAL spectrum was used to estimate the bandgap in order to exclude the effects from the nitrogen peak).

The results of the methylene blue photodegradation in Figures 3-11 and 3-13a show that the MNAL gave a significantly better photocatalytic activity than P25 under both visible blue and green lights. MNAL and P25 achieved 13±1.5% and 7±0.9% of methylene blue conversion, respectively, under blue light at 440 nm which is near the edge of the visible region (Figure 3-11). Under green light irradiation at 515 nm (Figure 3-13a), the methylene blue conversion achieved by MNAL (9±1.2%) is also higher than that achieved by P25 (6.3±0.8%). In addition, the MAL exhibited no apparent photocatalytic activity in methylene blue degradation under blue light, therefore it is not included in the results.

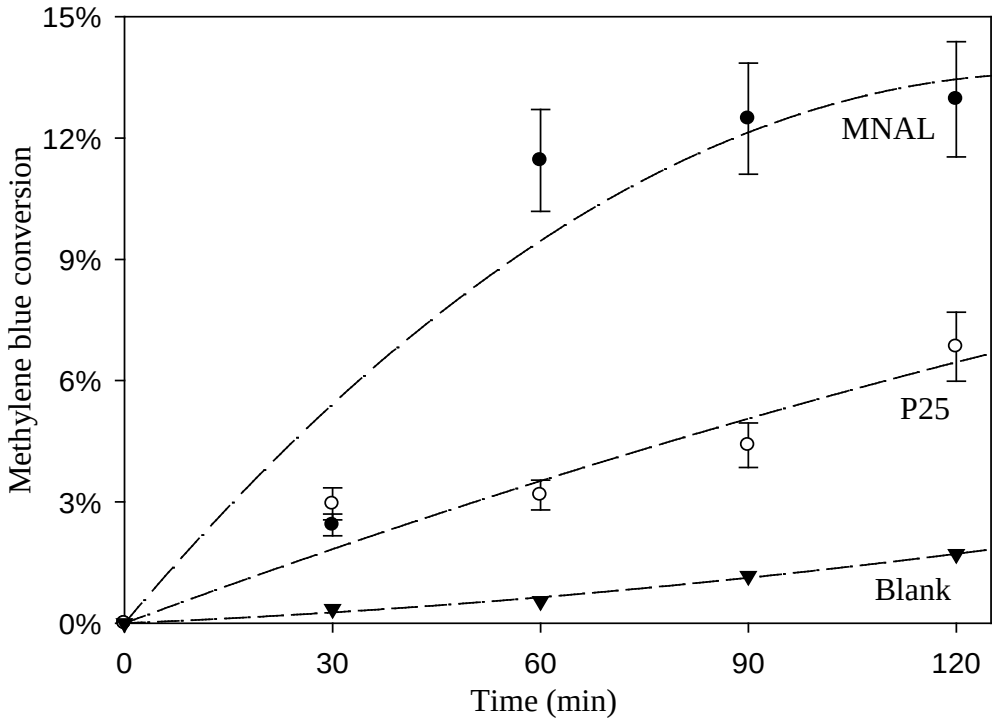

Figure 3-11. Conversion of methylene blue under blue LEDs with a maximum intensity at 440 nm (the edge of the visible light region). The experimental conditions are 6.5 ppm dye solution, a catalyst loading of 150 mg-cat/L, a pH of 7, 30°C. Notes: (i) the MAL exhibited no photocatalytic activity under blue light (result not shown). (ii) a much lower conversion of methylene blue was recorded here due to the use of a lower energy light source; (iii) lines are guide to eyes.

The apparent rate constants are estimated using data reported in Figure 3-12. The MNAL catalyst gave a rate constant approximately 2.4 and 1.3 times higher than those observed in the case of P25 under blue and green light irradiation, respectively (Figure 3-12 b-c). Given that nitrogen species were evidenced by EDS and XPS analysis (Tables 3-1 and 3-2), the estimated rate constants are also compared with the rate constant given by N-doped TiO_2 in the work of Burda et al. (2003). Burda et al. reported that the rate constants of methylene blue photo-degradation by N-doped TiO_2 (8 atomic %) are approximately 3 and 1.5 times higher than those given by the benchmark P25 titania under near blue (390 nm) and green (540 nm) light irradiation, respectively. The superior visible-light photocatalytic activity in heavily N-doped TiO_2 compared with the MNAL could be attributed to the band gap narrowing of titania resulting from substitution of O for N in the TiO_2 lattice. As stated earlier in the discussion of the XPS spectra, the amount of N dopant observed in this work is insufficient to form localized centres by mixing N 1s states with O 1s states in the MNAL. Hence, the trace amount of N dopant is less likely to have influence on the photocatalytic activity of the MNAL.

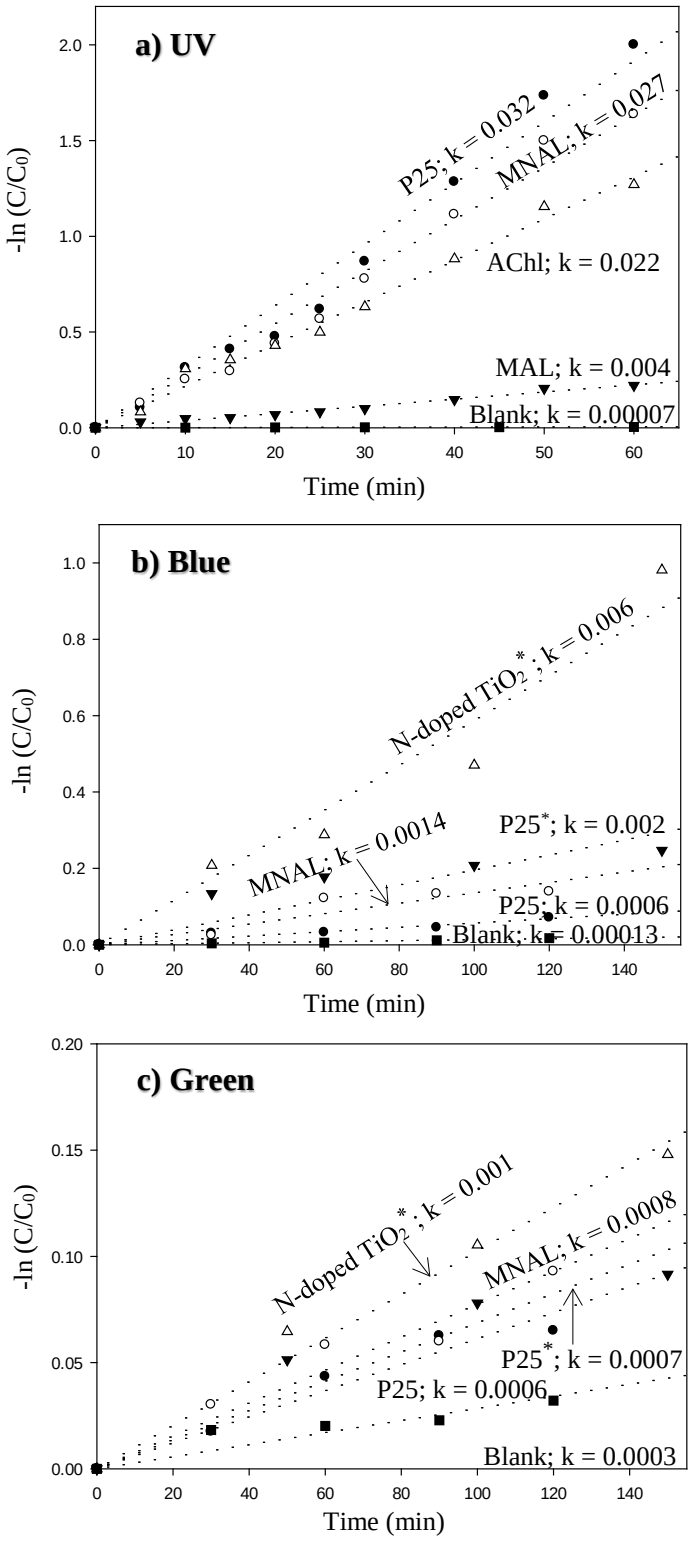

Figure 3-12. Apparent rate constants of methylene blue photodegradation under a) UV LEDs (370 nm), b) blue LEDs (440 nm) and c) green LEDs (515 nm). Notes: (i) The accuracy of all experiments was verified and the relative error was less than 10%. (ii) The experimental data reported by Burda *et al.*[100] were used to estimate the apparent rate constants given by N-doped TiO_2* and P25* TiO_2.

Photocatalytic oxidation of ethanol (Figure 3-13b) was also conducted as an alternative probe reaction to verify the superior photocatalytic activity of MNAL under green light (515 nm). The results show that the yield of CO_2 generated by MNAL (360±25 μmol/g-cat) is almost 1.3 times higher than the yield of CO_2 given by P25 (290±15 μmol/g-cat.) under green light. The MNAL was specifically tested against the reference TiO_2 under green light because it gave the best photocatalytic performance among the three bio-templated samples under UV and blue wavelengths (as shown in Figure 3-9 and 3-11). Anatase is the most photocatalytically active single crystalline phase of titania under wavelengths below 400 nm. However, crystals with a diameter below a critical radius of approximately 10 nm may exhibit an increase of band gap, which causes low efficiency of the system under the visible light region (Gupta & Tripathi, 2011; Kočí et al., 2009). The improved visible-light activity of the MNAL could be attributed to several key factors, including large surface area and high efficiency of light absorption provided by the morphology of the chloroplast-like structures. We hypothesise that the 3D TiO_2 nanocrystalline structure in the MNAL allows rapid injection of charge carriers from bulk into both internal and external surfaces. One of the carriers is then captured on a localized state at the surface while the other one is free for reaction. The net result is that the electron/hole recombination rate is reduced significantly by both the 3D layered structure and the charge trapping phenomena resulted from defect points located within the volume of the MNAL. The 3D construction of the interconnected nanolayers (replicated from thylakoids) in the MNAL also allows efficient trapping of the incident light *via* multiple light scattering. Thus, a longer optical path of light travelling through the MNAL could lead to the greater chance of the eventual photoexcitation events during the photocatalytic reaction. This is consistent with other reported results on the 3D crystalline materials (Paramasivam et al., 2012; Waterhouse et al., 2008; Waterhouse & Waterland, 2007). For example, Cheng *et al.* (Cheng et al., 2012) showed a high photocurrent density of 3D TiO_2 inverse opals under simulated solar-light illumination.

The unique advantages of the layered TiO_2 structure made from biotemplating method are clearly manifested in the two model photocatalytic reactions under visible light. Given that visible light with wavelengths longer than 400 nm makes up more than 95% of the solar spectrum, the novel TiO_2 structure obtained using biotemplating method could be extremely attractive to catalyse the solar-assisted photo-reduction of CO_2.

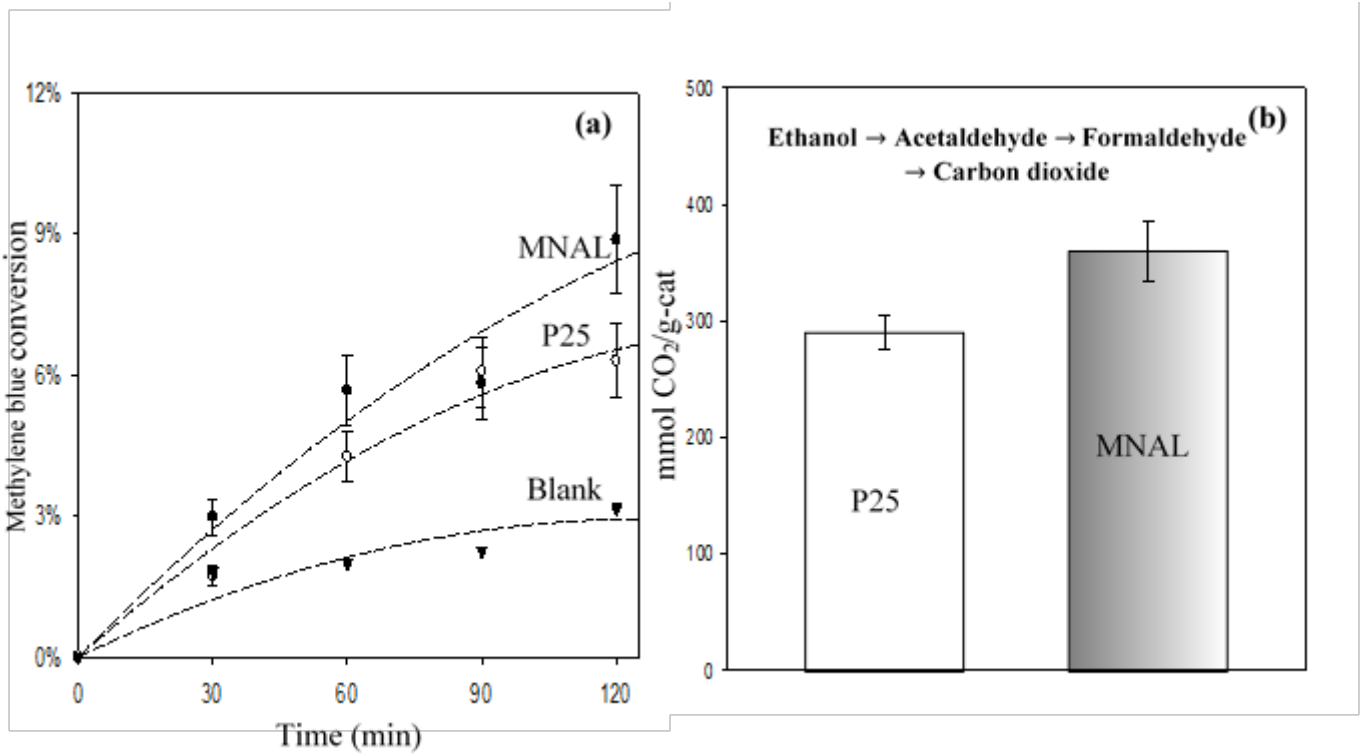

Figure 3-13. a) Conversion of methylene blue under green LEDs with a maximum intensity at 515 nm. The experimental conditions are 6.5 ppm dye solution, a catalyst loading of 150 mg-cat/L, a pH of 7, 30°C (Note: lines are guide to eyes). b) Carbon dioxide yield of photocatalytic oxidation of ethanol under green LEDs with a maximum intensity at 515 nm. The experimental conditions are 20 v/v% ethanol solution, a catalyst loading of 1 g-cat/L, 30°C.

3.4 Conclusions

In this chapter, we developed an improved multi-steps chemical replication method using micro- to nano-architectures of the photosystem of green leaves as templates to prepare an enhanced TiO_2-based photocatalyst. We studied the relationship between its morphology and photocatalytic performance. The new TiO_2 porous architecture produced from biotemplating, referred to as MNAL in this work, exhibited photocatalytic dye degradation performance similar to that of commercial P25 (in particle form) under UV light without a mixed phase (anatase and rutile) composition. A substantially improved photocatalytic activity was further observed with the MNAL under visible (blue and green) lights. The enhanced photocatalytic performance of the MNAL was a result of overall morphological contribution given by the 3D nanostructured light-harvesting system, the extensive pore network and the high surface area resulted from the interconnected titania nanosheets derived from the thylakoid membranes of the natural leaves. This work demonstrated that the extrinsic excitation behaviour of TiO_2 photocatalyst can be potentially augmented by modifying its morphology alone. The reported synthesis method provides a reliable and promising procedure to synthesize TiO_2 hierarchical structures which could overcome the issues in controlling the structure and crystallinity of end product associated with conventional procedures.

Chapter 4 – Enhanced CH_4 yield by photocatalytic reduction of CO_2 with H_2O using bio-mimicked TiO_2 architectures

4.1 Introduction

In spite of intense researches on developing more efficient TiO_2 materials for producing solar fuels, the effects of the morphology of the photocatalyst on the selectivity and yield of CO_2 photoreduction are less studied. The efficiency of the photocatalytic reactions is an overall outcome of various steps: light absorption, the transport of photogenerated charges, the electron hole recombination rate, and mass transfer to the catalyst surface. The local structure of the photocatalyst, particularly the particle size and shape, strongly influences the aforementioned parameters (Cheng et al., 2014; Etacheri et al., 2015; Krishnan, 2007).

Recent researches have revealed the the improved photocatalytic performance of TiO_2 nanostructures. The enhance activity of the TiO_2 3-dimensional nanomaterials is a result of several key factors. These include large surface area, improved excitation behaviour and high efficiency of light absorption. The advantages of TiO_2 nanostructures over conventional TiO_2-based flat platfroms could empower the efforts to address energy and environmental issues (Gupta & Tripathi, 2011). On the other hand, surface chemical modification of TiO_2 materials is a common approach to redshift the effective wavelength for photocurrent generation in the visible light region. Transition metals, such as Cu (Colón et al., 2006; Ganesh et al., 2014), Fe (Deng et al., 2009), Ru (Ohno et al., 1999; Sasirekha et al., 2006), Ag (Suwarnkar et al., 2014; Wen et al., 2005b) and etc, have shown promising results on improving the optical properties of TiO_2 photocatalysts. The well-matched electronic structure of the metals to TiO_2 enhances the charge transfer and results in efficient charge separation.

In this chapter, the morphological contribution of the stack-layered nanostructures of bio-mimicked titania materials towards carbon dioxide photoreduction were studied under UV and visible light irradiation. The advantages of new TiO_2 architecture offer a unique opportunity to enhance CH_4 yield in photocatalytic CO_2 reduction. The strategies to enhance the visible light activity of the TiO_2 catalysts are further studied in chapter 5.

4.2 Methodology

4.2.1 Materials

All reagents were of analytical grade and were purchased from Sigma-Aldrich. All reagents were used as received. All glassware was oven dried and experiments were performed using Schlenk line technique to avoid contact with ambient air when required. The high purity CO_2 ($\geq$ 99.995%) was used to avoid any hydrocarbon contamination.

4.2.2 Surface chemical modification of the photocatalysts with RuO_2

In this chapter, the templated materials with micro- and nano-architecture of the leaf photosystem are referred to as “artificial leaf” (AL). A previously employed procedure in the preparation of supported ruthenium oxide (RuO_2) catalysts was slightly modified to deposit ruthenium oxide onto the artificial leaf and commercial P25 TiO_2 (Ovoshchnikov et al., 2015). The solution of $RuCl_3 \cdot xH_2O$ (6.5 mg) in deionized water (2 mL) was added dropwise to TiO_2 (250 mg) dispersed in deionized water (5 mL). Solution of NaOH (150 mg) in deionized water (5 mL) was slowly added and the mixture was left stirring for 30 min. The solid was recovered by centrifugation, washed twice with deionized water (15 mL) and, in order to facilitate drying, with ethanol (15 mL) followed by diethyl ether (15 mL). The catalyst was dried under vacuum at room temperature and then calcined in convection oven preheated to 150 ºC for 30 min.

Before each catalytic reaction, portions of the catalyst were additionally calcined under the same conditions for 15 min.

The ruthenium content of the RuO_2/P25 and RuO_2/AL was measured using inductively coupled plasma-mass spectroscopy (ICP-MS) via acid pretreatment. The samples were treated with a mixture of HCl and HNO_3 (6:1, v/v) at 80 °C for 48 h. Then, the solid was removed via centrifugation, and the liquid, together with washings, was transferred to a volumetric flask and topped off with Milli-Q water. Ruthenium loading was measured via a standard measurement protocol using an ICP-MS Agilent 7500 cx.

4.2.3 Slurry system for photocatalytic reduction of CO_2 with H_2O

The photocatalytic reduction of carbon dioxide was carried out in a stirred batch annular reactor made from fused quartz with the internal volume of 155 ml and wall thickness of 5 mm (Figure 4-1). The hoop stress applied to the quartz tube is approximately 1.8×10^6 Pa at working pressure of 3×10^5 Pa. The equation 4-1 can approximate the hoop stress at ambient temperature:

$$S = \frac{pr}{t} \tag{4-1}$$

where S is hoop stress (Pa), p is working pressure (Pa), r is inside radius (mm), and t is wall thickness (mm). The practical maximum stress is approximately 7×10^6 Pa for fused quartz with good surface quality. However, the equation 4-1 is not applicable when internal pressure exceed 7×10^5 Pa in the blocked quartz vessels (*Momentive*).

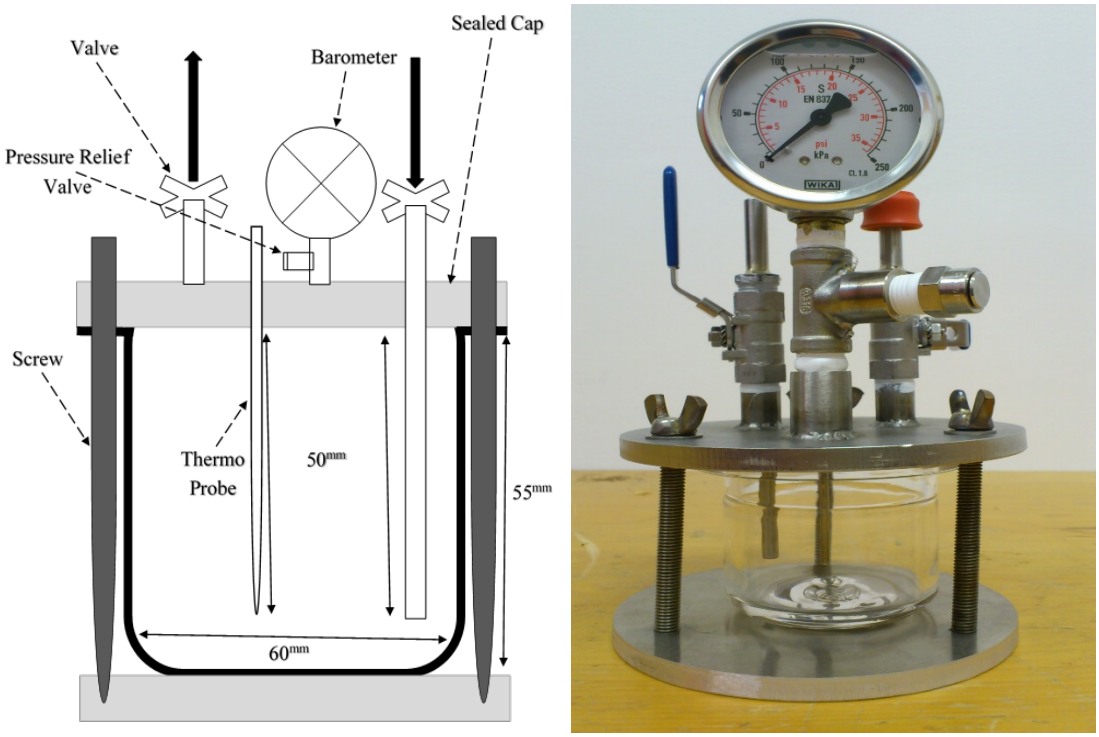

Figure 4-1. Annular photo-reactor made from fused quartz. Internal diameter = 60 mm, internal height = 55 mm, and wall thickness = 5 mm

An enclosed photocatalytic chamber equipped with two 50 W LEDs with maximum intensities at 370 nm (UV) and 515 nm (Green) was used in these experiments. The figure 4-2 illustrates the transmission curve of fused quartz tubing. The percent transmission of the 5 mm thick tubing is approximately 70% over a broad wavelengths (*ca*. 300 - 750 nm) using the equation 4-2 (*Momentive*) :

$$T = (1 - R)^2 \, e^{-at} \qquad (4\text{-}2)$$

where T is percent transmission expressed as a decimal, R is surface reflection loss for one surface, a is absorption coefficient (cm^{-1}), and t is the thickness (cm).

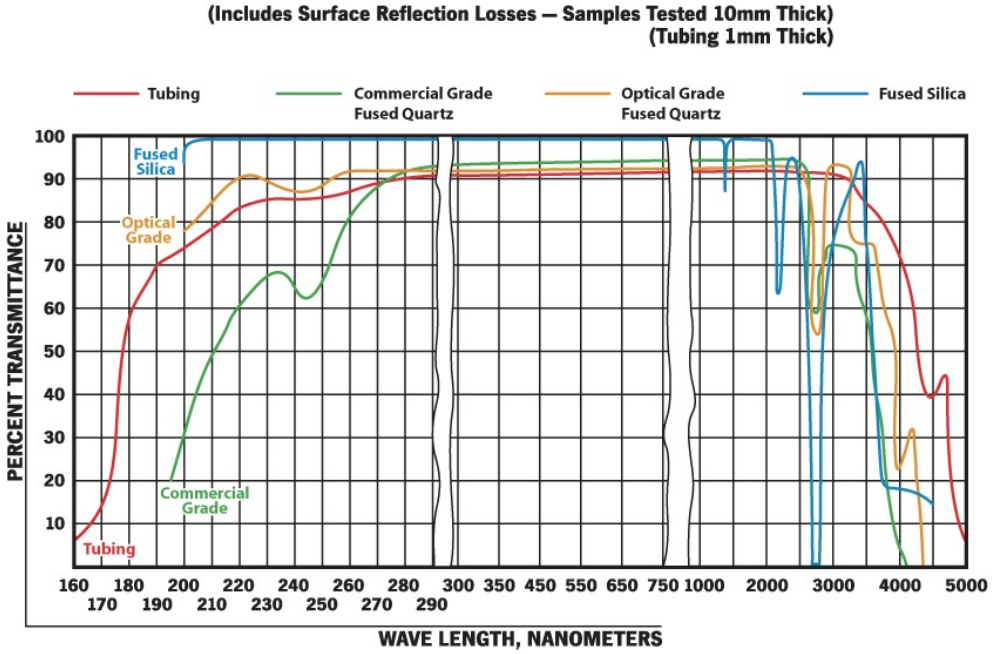

Figure 4-2. Fused quartz average transmittance curves (*Momentive*) .

The influence of the CO_2 pressure on formation of the products of the photocatalytic CO_2 reduction have been studied in many investigations (Kaneco et al., 1998; Kočí et al., 2008; Mizuno et al., 1996; Tseng et al., 2002). The solubility of CO_2 in water is very poor (0.034 mol/L (Carroll et al., 1991)), increasing the CO_2 pressure accelerates the reaction via increasing the concentration of dissolved CO_2. Tseng *et al.* (Tseng et al., 2002) observed the increase of the methane yield with increasing the CO_2 pressure. Mizuno *et al.* (Mizuno et al., 1996) reported high rate of liquid products formation at 1 MPa and higher CO_2 pressure.

The temperature can cause two effects in the CO_2 photoreduction slurry system. The high temperatures may help to overcome the thermodynamic barriers of the reaction. On the other hand, the high temperature determines the dissolved CO_2 equilibrium amount. Fox *et al.* (Fox & Dulay, 1993) revealed that the reaction of photocatalytic CO_2 reduction with H_2O is

not sensitive to small temperature variation. The temperature effect were studied in our preliminary experiments. The reaction medium was tempered to 323 K and then irradiated with UV LEDs. The results were same as the experiments done at the room temperature of 299 K.

The sufficient mixing is one of the most important requirements in order to overcome mass transfer limitations in slurry reactors. The volume of the reacting phase should be optimized to fulfil perfect mixing (Ballari et al., 2008a; Kočí et al., 2011). The high concentration of catalyst may cause the undesirable effects of light scattering, the catalyst loading should be below 1 g/L in order to have an efficient length of the light penetration (Ballari et al., 2008a,b). The use of NaOH solution as the reactant medium could increase the amount of dissolved CO_2 since the caustic NaOH solution dissolves more CO_2 than pure water (Yoo et al., 2013). The mechanism of CO_2 absorption in NaOH aqueous solution is illustrated in Table 4-1. In addition, the highly concentrated OH^- ions from NaOH in aqueous solution could act as strong hole-scavengers. Formation of $OH^{\cdot}$ radicals decreases the recombination rate of photoinduced electron-hole pairs (Kočí et al., 2010; Liu et al., 2007; Tseng et al., 2002; Zhao et al., 2007). The preliminary experiments were performed using 0.1, 0.2 and 0.3 M NaOH solutions to investigate the effect of the hole-scavenger concentration. The amount of photoreduced products was almost constant when the concentration exceeded 0.2 M.

Table 4-1. The reactions of CO_2 absorption in NaOH aqueous solution. Subscripts (aq), (g), and (l) present aqueous, gas and liquid, respectively.

Initial CO_2 absorption	$2NaOH(aq) + CO_2(g) \rightarrow Na_2CO_3(aq) + H_2O(l)$
Secondary CO_2 absorption	$Na_2CO_3(aq) + CO_2(g) + H_2O(l) \rightarrow 2NaHCO_3(aq)$
The net reaction	$NaOH(aq) + CO_2(g) \rightarrow NaHCO_3(aq)$

The catalyst powder (50 mg) was suspended in 50 ml of 0.2 M NaOH solutions for typical batches. The reaction solution was stirred (500 rpm) for 60 min to ensure that the catalyst was homogeneously dispersed before the reaction. Prior to the illumination, CO_2 was bubbled with a constant flow through the stirred suspension for another 60 min to purge the air and to saturate the solution. Saturation of liquid phase eliminates CO_2 diffusion limitation from the bulk through the reaction interface (Ballari et al., 2008a). The reactor was tightly closed and the CO_2 pressure was maintained at 250 kPa. Then the irradiation was started at the sealed photolysis chamber. The light flux was monitored to ensure that it was consistent across all experiments. A magnetic stirrer (250 rpm) at the bottom agitated the catalyst-suspended solution to prevent sedimentation of the catalyst. The temperature of the solution and the pressure of the gas phase were continuously monitored. The temperature of the solution raised up to 303 K during irradiation.

Gas sampling was performed using a gas-tight syringe (10 ml) and the samples were immediately analyzed. The gas phase samples were analyzed using a gas chromatograph equipped with methanizer FID and TCD detectors and Haysep-D column for hydrogen, carbon monoxide, carbon dioxide, methane, ethylene, and ethane quantification. Blank reactions were

performed to ensure that the hydrocarbons production was due to the photoreduction of CO_2. The first blank was UV illumination without the catalyst, the second was in the dark with the catalyst and CO_2 under the same experimental conditions and the third was over the illuminated photocatalyst in the absence of CO_2 (under inert gas). No hydrocarbons were detected in the above blank tests. Besides, the photocatalytic reforming of ethanol reactions were performed following the abovementioned experimental procedure under inert gas and in the presence of CO_2 (250 kPa). The 20% ethanoic solutions were used as the media in ethanol reforming reactions.

4.2.4 Kinetic modelling of the photocatalytic reduction of CO_2 over TiO_2

The details of the carbene pathway reactions (Scheme 4-1) for photocatalytic reduction of CO_2 with H_2O are shown in Table 2-1. Tan *et al.* (Tan et al., 2008) and Kočí *et al.* (K. Kočí, 2010) proposed a kinetic model for the photocatalytic reduction of CO_2 based on Langmuir-Hinshelwood mechanism. The kinetic equations of carbon dioxide reduction with water and the reverse reaction of oxidation of CO are inferred as equations 4-3 and 4-4, respectively:

$$r_{red} = k_1 \frac{ac_{CO_2} bc_{H_2O}}{(1+ac_{CO_2}+bc_{H_2O})^2} \quad (4\text{-}3)$$

where r_{red} is the rate of reduction, k_1 is the kinetic constant of reduction, a and b are the ratios of rate constants for adsorption and desorption of CO_2 and H_2O, respectively.

$$r_{ox} = k_2 \frac{mc_{CO}\sqrt{nc_{O_2}}}{(1+mc_{CO}+\sqrt{nc_{O_2}})^2} \quad (4\text{-}4)$$

where r_{ox} is the rate of oxidation, k_2 is the kinetic constant of oxidation, m and n are the ratios of rate constants for adsorption and desorption of CO and O_2, respectively.

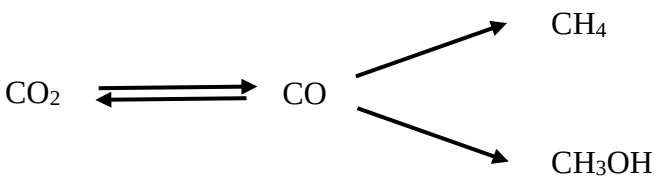

Scheme 4-1. The carbene pathway for photocatalytic reduction of CO_2 with H_2O.

Assuming that the CO molecules are strongly bound to the catalyst surface ($mC_{CO} \gg 1$), the net rate of CO_2 reduction ($r_{net\ red}$) could be expressed by:

$$r_{net\ red} = k_1 \frac{ac_{CO_2}\, bc_{H_2O}}{(mc_{CO})^2} - k_2 \frac{\sqrt{nc_{O_2}}}{mc_{CO}} \tag{4-5}$$

The concentration of carbon dioxide and water could be considered constant since they are in excess through the reaction. Hence, the equation 4-5 could be simplified to:

$$r_{net\ red} = k_3 \frac{1}{(mc_{CO})^2} - k_2 \frac{\sqrt{nc_{O_2}}}{mc_{CO}} \tag{4-6}$$

where $k_3 = ac_{CO_2}\, bc_{H_2O}$. The concentration of reactants in equation could be replaced by any given product according to the state of reduction. The equation 4-6 could be resolved as:

$$-\frac{dc}{dt} = \frac{k_4}{c^2} - \frac{k_5}{\sqrt{c}} \tag{4-7}$$

where c is the concentration of the given product, $k_4 = k_3/m^2$ and $k_5 = k_2 n^{(1/2)}/m$.

We have obtained the following equation after integration and resolving:

$$t = k_6 \ln(1 - k_7 c^{3/2}) + k_8 c^{3/2} \tag{4-8}$$

where k_6 is the kinetic constant related to the experimental conditions, $k_7 = k_5 / k_4$ and $k_8 = -2/3k_5$. See the details of integration in the appendix.

We also considered an alternative kinetic model based on the precondition that the running reactions are pseudofirst order ones. The formation rates of CO and CH_4 are reported to be pseudofirst order in several earlier studies (Ku et al., 2004; Lo et al., 2007). At low concentrations of the reactants, the formation equations could be inferred to:

$$r_{CO} = k_9 c_{CO_2} - k_{10} c_{CO} - k_{11} c_{CO} \tag{4-9}$$

$$r_{CH_4} = k_{11} c_{CO} \tag{4-10}$$

Where, k_9 relates to the direct reaction of CO_2 reduction to CO, k_{10} relates to the reverse reaction of oxidation of CO, and k_{11} relates to pathway where CO is converted to CH_4.

Given that concentration of CO_2 is assumed constant, the following expressions could be obtained after revision and integration:

$$c_{CO} = \frac{k_{9^*}}{k_{12}} (e^{tk_{12}} - 1) \tag{4-11}$$

$$c_{CH_4} = \frac{k_{9^*} k_{11}}{k_{12}} \left[\frac{1}{k_{12}} (e^{tk_{12}} - 1) - t\right] \tag{4-12}$$

where $k_{9^*} = k_9 c_{CO_2}$ and $k_{12} = -k_{10} - k_{11}$. See the details of integration in the appendix.

The kinetic models were validated by experimental data using a non-linear regression method. The sum of squares of the yields of residual products (observed minus calculated) was minimized (Press et al., 2007). The kinetic equations were processed under the form of $y = f(x_{1\text{-}a}, a_{0\text{-}m})$. Where $a_0, a_1, a_2, \ldots, a_m$ are the regression parameters, $x_1, x_2, \ldots, x_a$ are independent variables and y is a dependent variable.

4.3 Results and discussion

4.3.1 Catalyst characterization

Figure 4-3 shows the XRD patterns indicating that Art. Leaf consists of the anatase crystalline phase, whereas the P25 is a combination of anatase and rutile TiO_2 phases. See chapter 3 for experimental details. Commercial P25 TiO_2 is crystalline material consists of 80 wt % anatase and 20 wt % rutile (Hanaor & Sorrell, 2011). The electronic properties of TiO_2 are a function of the crystalline phase composition. Although antase is considered as the more active phase of titania, mixed anatase and rutile polymorph composites are revealed to have a better performance than any single-phase component. It has been proved that the synergistic effect of these two phases improve the electronic properties of TiO_2 significantly (Kho et al., 2010; Su et al., 2011). The XRD results of the RuO_2 deposited samples suggest that surface chemical modification does not affect the crystalline phase of the AL. Further peaks included in the pattern of the RuO_2/AL samples could be attributed to the RuO_2 content. The Scherrer equation was used to determine the average size of crystallites (Harold P. Klug, 1974). The average crystallites size of pure AL and the RuO_2/AL materials are approximately 15 nm which are smaller than the determined size of P25 TiO_2 crystallite (*ca*. 20 nm). The slightly larger size of P25 TiO_2 crystallite could be due to its synthesis approach, commercial P25 are formed by flame pyrolysis. The high temperature of combustion process favours the anatase to rutile phase transformation (Hanaor & Sorrell, 2011; Skandan et al., 1999).

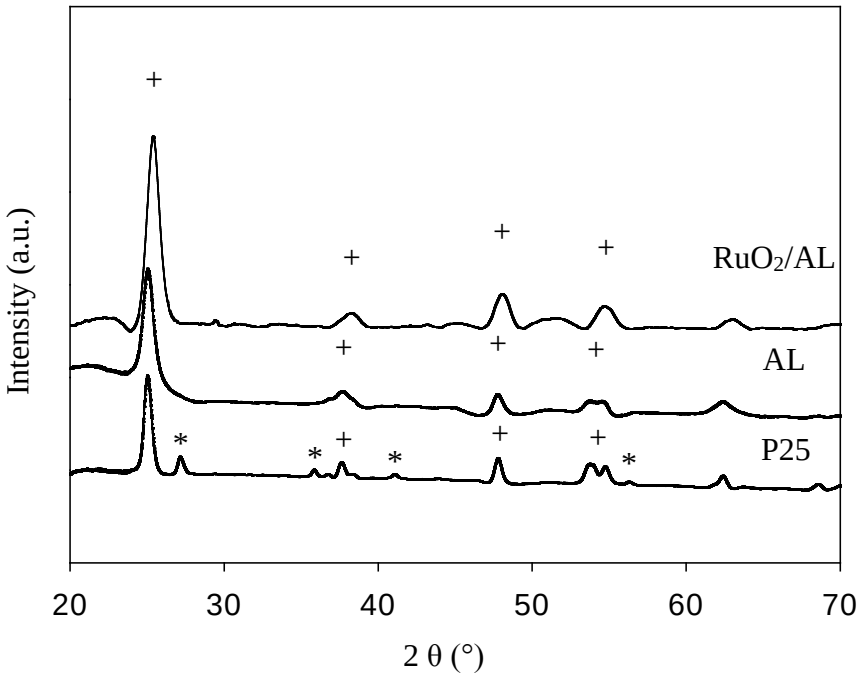

Figure 4-3. XRD patterns of the final catalysts. Corresponding peaks of the anatase phase and the rutile phase TiO_2 are marked by "+" and "*", respectively.

Nitrogen (N_2) physisorption measurements in Figure 4-4 show that the surface area of the AL and the reference P25 TiO_2 are 66.1 m^2/g and 51.7 m^2/g, respectively. The experimental details for such measurements are reported in chapter 3. According to the hysteresis observed in the adsorption isotherm, the artificial leaf sample possesses mesoporosity in its structure while the type of isotherm obtained for P25 showed it to be non-porous. The AL exhibited a H3 hysteresis loop indicating possible random pore network and irregular pore shape such as the "ink-bottle" geometry (Sing & Williams, 2004). The stepwise desorption observed at P/Po of 0.55 suggests the characteristic desorption mechanism *via* cavitation and, therefore, proves the presence of pore necks which are smaller than the critical size of N_2 (*ca*. 5 - 6 nm) at 77 K. The quantity of adsorbed N_2 (mmol/g) on the AL is much higher than that on the P25 (approximately 1.25 and 1.4 times higher at the relative pressures of 0.3 and 0.8, respectively). We hypothesised that the biotemplated layered nano-architecture derived from the thylakoid

membranes in chloroplasts present within the AL gives rise to the N_2 adsorption. Whereas the high surface area of the P25 TiO_2 could be attributed to its nano sized particles (Suttiponparnit et al., 2011; Viswanathan & Raj, 2009). Our measurements showed that the decoration of the surface of the TiO_2 by RuO_2 does not alter the surface area and N_2 physisorption so the data of RuO_2/AL and RuO_2/P25 are not included in the Figure 4-4.

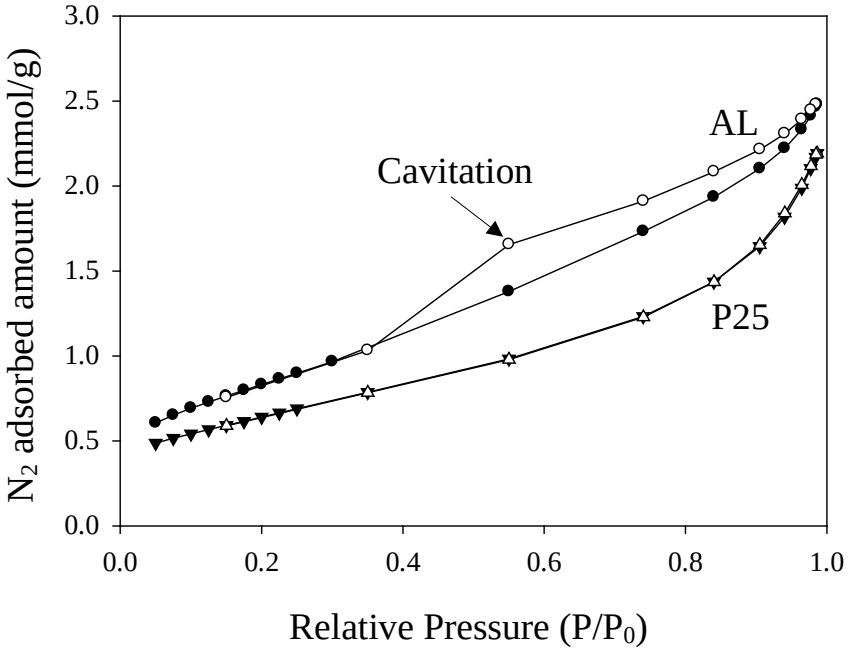

Figure 4-4. Nitrogen adsorption-desorption isotherm of the artificial leaf and the reference P25 TiO_2 catalysts.

The diffuse-reflectance UV-vis spectra are shown in Figure 4-5, see chapter 3 for experimental details. The absorption efficiency of pure TiO_2 antase is limited to the UV region whereas the smaller band gap of rutile phase in P25 catalyst extends the efficiency of light absorption into the visible range. Hurum *et al.* (Hurum et al., 2003) revealed that the electron transfer from rutile crystals to trapping sites of antase lattice leads to a stable charge separation in mixed-phase P25 under visible light illumination. The artificial leaf exhibits greater absorption efficiency over a broad UV-vis wavelength (*ca*. 350 - 600 nm) compared to the

reference P25 material. Such improved visible light absorbance could be imparted by the localized states within the compact layered nanostructure in the AL sample. Howe and Grätzel showed that photoinduced charge carriers in TiO_2 nanomaterials are present at different sites of the bulk defects, such as oxygen vacancies, and on the surface. The resulted additional electronic states within the TiO_2 band gap allow sub-band gap transitions (Howe & Grätzel, 1985,1987).

This finding is consistent with the results of other recent researches reporting that the effective wavelengths for light absorption red shifted in terms of titania nano-architectures (Sakai et al., 2004; Sato et al., 2003). In the spectrum of P25 and AL catalysts modified with the ruthenium oxide, the observed peak centred at *ca.* 450 nm could be attributed to RuO_2 content (Ohno et al., 1999; Sasirekha et al., 2006). The ruthenium content of 1.2±0.1 and 1.3±0.1 wt % was established using ICP-MS for the P25 and Al samples, respectively. The absorption of light by the RuO_2 /TiO_2 materials in the visible range is due to surface plasmon resonance.

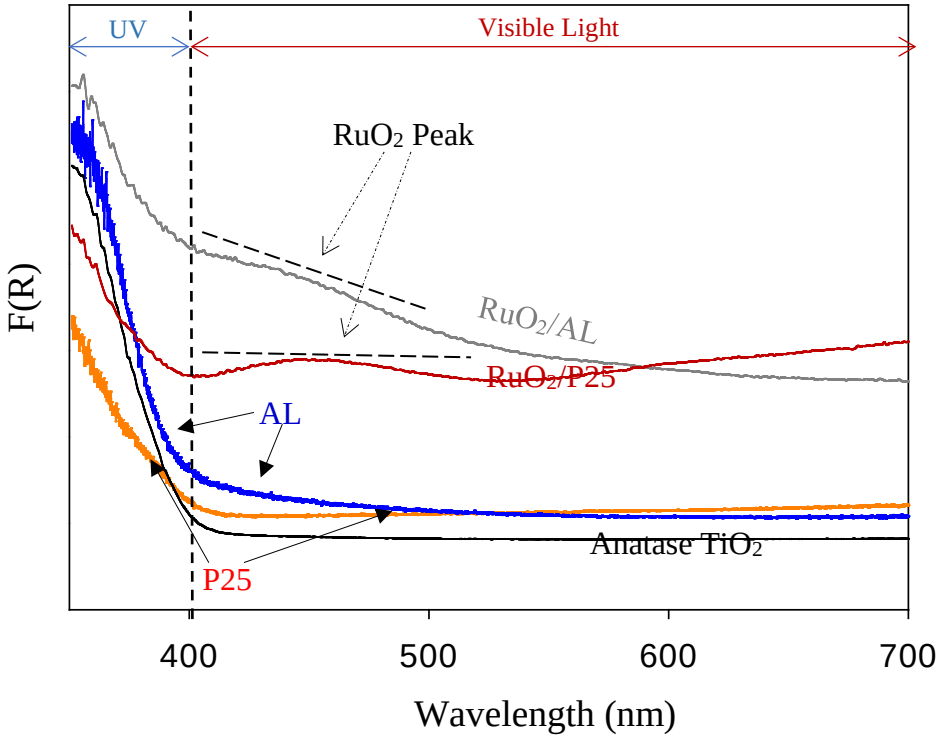

Figure 4-5. Diffuse-reflectance UV-Vis spectra of the final catalysts.

4.3.2 The morphological contribution of the bio-mimicked TiO_2 architectures towards photocatalytic reduction of CO_2

The results of photoreduction of CO_2 with water, after 20 h of irradiation under UV light (370 nm), are presented in Figure 4-6. The data from the 20 h reactions were used for the comparison because the yields of all products were the highest. The main product of the reactions catalysed by the porous artificial leaf materials is methane (3.8±0.6 μmol/g-cat.) whereas the reference nonporous TiO_2 commercial catalysts mostly yielded carbon monoxide (5.1±0.5 μmol/g-cat.). The multiple reduction is initiated by activation of carbon dioxide via interaction with surface atoms, and involves the transfer of up to eight electrons and protons (Habisreutinger et al., 2013). Although the AL possessed a slightly lower total conversion of CO_2, it shows higher selectivity to the CH_4. The efficiency of the photocatalytic reduction of CO_2 process depends on the transfer of electrons to the adsorbed molecules. The key factor which is responsible for the photocatalytic performance of the AL is their internal

interconnected nano-membrane structures (thylakoid membrane replicas). We hypothesised that prolonged residence time of the reactants within the unique hierarchical pore network of the stacked titania nano-sheets enhance reactant-catalyst contact through the artificial leaf photocatalyst body.

The high surface area of the AL (66.1 m^2/g) may offer a large proportion of surface atoms which could allow rapid transfer of the photogenerated electron/hole from bulk into both internal and external surfaces (Krishnan, 2007; Macdonald et al., 2012; Nowotny et al., 2008). One of the carriers is then captured on a localized state while the other one is free for reaction. As the net result of that, injection of the charge carriers to/from the reactants or reactive radical species is significantly accelerated by both the interface atoms and the defect points located within the volume of the AL 3D structure. This is consistent with the literature reporting improved mass transfer and superior charge transfer in titania nano-architectures (Chen & Mao, 2007). For example, Kar *et al.* (Kar et al., 2016) revealed the high adsorption capacity of CO_2 through TiO_2 nanotubes using temperature programmed desorption (TPD) experiments. Also, Reñones *et al.* (Reñones et al., 2016) showed that lower e-h recombination rate in TiO_2 nanofibres could give rise to higher selectivity to electron-demanding products of CO_2 photoreduction, such as methane. On the other hand, the 3D construction of the AL materials efficiently trap the incident light via multiple light scattering within the interconnected TiO_2 nanolayers (Mustárdy, 1996; Ruban et al., 2011; Rumak et al., 2010). Hence, the greater chance of the eventual photoexcitation events is resulted by a longer optical path of light travelling through the AL during the photocatalytic reaction. The improved light scattering properties and excitation behaviour of the 3D TiO_2 crystalline materials are also reported in other researches over the past few years (Cheng et al., 2012; Paramasivam et al., 2012; Waterhouse et al., 2008; Waterhouse & Waterland, 2007). For instance, Cargnello *et al.* (Cargnello et al., 2016) revealed

longer lifetimes of electron-hole pairs in TiO_2 nanorods by means of ultrafast transient absorption spectroscopy.

The slightly lower CO yield given by the commercial TiO_2 anatase (4.5±0.4 μmol/g-cat.) compared to reference P25 could be because of interaction between anatase and rutile in mixed phase P25 catalyst. Pure anatase phase is expected to have higher recombination rate of holes and electrons. The photoinduced electron-hole pairs within the semiconductor will recombine before being collected by the external reactants (Hao et al., 2002; Jiang et al., 2008; Lin et al., 2006). Kho *et al.* (Kho et al., 2010) studied the effect of the titania crystalline phase compositions on the photocatalytic evolution of hydrogen and observed higher activity of the mixed anatase/rutile TiO_2. The higher yield of CH_4 (4.3±0.35 μmol/g-cat.) given by the RuO_2/AL could be mainly due to the enhance charge transfer between metal-semiconductor heterojunction. The efficient charge separation at the RuO_2/TiO_2 heterostructures leads to higher surface charge density (Farsinezhad et al., 2015; Tan et al., 2016b). In addition, the ruthenium dioxide crystallites makes catalytic hot spots at the RuO_2/TiO_2 interface that could facilitate the charge injection to the reactants (Cargnello et al., 2013; Huang et al., 2014; Huang et al., 2015).

In the case of reactions catalysed by the pure artificial leaf and the RuO_2/AL samples formation of traces of ethane (C_2H_4) was also observed. The yields of C_2H_4 were not possible to quantify by our set up. Attempts to analyse liquid phase products failed because of the low yields of the products. According to the literature, the methanol yields are one order of magnitude lower than the yields of methane in slurry CO_2 photoreduction systems (Aresta et al., 2016; Hong et al., 2013). The results indicate that the RuO2/P25 catalysts also possess

higher selectivity to the CH_4. The lower photocatalytic activity given by the RuO_2/P25 is possibly because of lack of mesoporous channels for adsorption and desorption of the reactants.

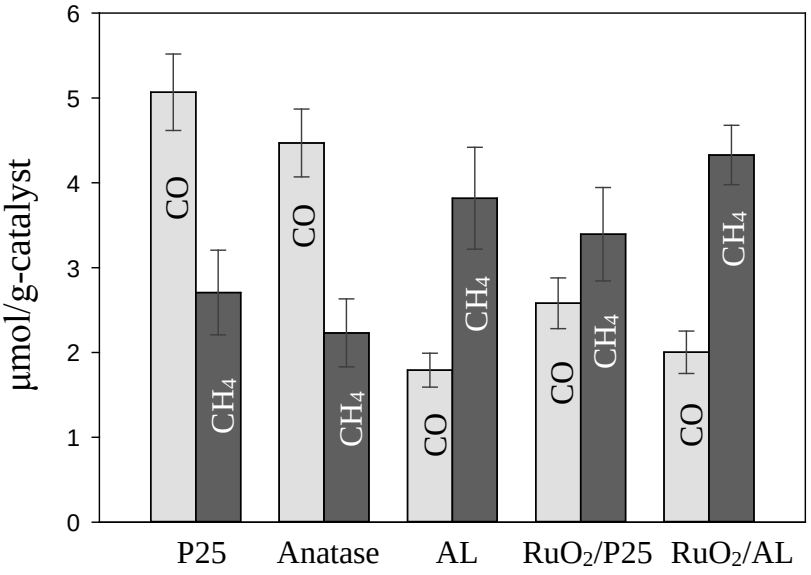

Figure 4-6. The product yields of the photocatalytic reduction of CO_2 with water under UV LEDs with a maximum intensity at 370 nm. The experimental conditions are 0.2 M NaOH solution, a catalyst loading of 1 g-cat/L, CO_2 pressure of 250 kPa, 20 h of irradiation, 30°C.

Moreover, photocatalytic reforming of ethanol reactions, under irradiation of UV light (370 nm) for 20 h, were employed to assist verifying photocatalytic performance of the biotemplated materials. The results (Figure 4-7) show that the selectivity of the reactions catalysed by the artificial leaf mesoporous catalysts differs from the reaction catalysed by the reference commercial catalysts. The ethanol reactions on TiO_2 catalysts are initiated by the oxidation of the adsorbed alcohol molecules to acetaldehyde and the two main overall reactions are (Chen et al., 2007; Muggli et al., 1998; Schneider & Bahnemann, 2013; Vaidya & Rodrigues, 2006):

$$C_2H_5OH \xrightarrow{\text{Dehydration}} C_2H_4 + H_2O$$

$$C_2H_5OH + H_2O \xrightarrow{\text{Decomposition}} CO_2/CO + CH_4 + 2H_2 + ½\ O_2$$

The observed product yields (μmol/g-cat.) order of the AL was CO_2 > H_2 > C2H4 > CH4 > CO whereas the selectivity of the reference nonporous TiO2 catalysts (pure anatase and P25) was $H_2 \geq CO_2 > CO > CH_4 > C_2H_4$. The AL TiO_2 materials increases the selectivity of the dehydration reaction possibly due to abstraction of the reactants in the different reaction sites on the surface of the catalyst (Nadeem et al., 2016). This finding and the results of CO_2 reduction reactions indicate that the efficiency and selectivity of the photocatalytic reactions can be potentially augmented by modifying the morphology of the photocatalyst without changing its overall chemical composition.

The RuO_2/AL produced the substantially higher carbon species (766.8±150 μmol/g-cat.) and hydrogen (3661.3±200 μmol/g-cat.) yields of the ethanol reforming. Tan *et al.* (Tan et al., 2016a) showed that the transition metal oxides/TiO_2 frameworks could enhance cleaving the C-C bond of ethanol. In addition, the presence of RuO_2 could prevent partial deactivation of the photocatalyst caused by stable byproduct formation on the catalyst surface. The 7.15±1 μmol/g-cat. and 3.25±0.35 μmol/g-cat. of ethane (C_2H_6) yields were observed in the reactions catalysed by RuO_2/P25 and RuO_2/AL samples, respectively. The C_2H_6 is likely produced via further hydrogenation of ethylene by RuO_2. The ruthenium dioxide is a well-known catalyst for hydrogenation reactions due to its unique properties (*e.g.*, the high electronic conductivity) (Over, 2012). The C_2H_6 yield of RuO_2/P25 catalyst is 2.2 times lower than that of the RuO_2/AL which is far greater than 1.3 times factor expected based on just surface area (the ruthenium wt % of P25 and AL samples are 1.2±0.1 and 1.3±0.1, respectively).

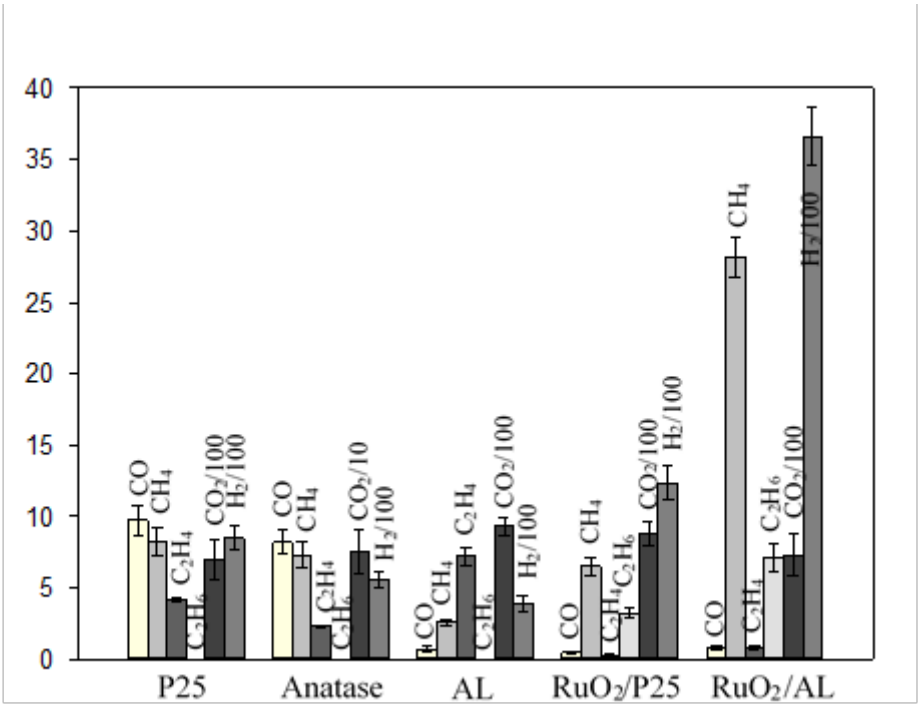

Figure 4-7. The product yields of the photocatalytic reforming of ethanol under UV LEDs with a maximum intensity at 370 nm. The experimental conditions are 20 v/v% ethanoic solution, a catalyst loading of 1 g-cat/L, 20 h of irradiation, 30°C.

Figure 4-8 shows the product yields of photoreduction of CO_2 with 20 v/v% ethanoic solution, after 20 h of irradiation under UV light (370 nm). The organic hole scavengers such as alcohols and oxalic acid have been used in some reports (Baran et al., 2016; Kaneco et al., 1998; Sasirekha et al., 2006). However, the exact reaction mechanism is still a matter of debate because of the possible interference with the products. The reduction reactions compete with the products formation by the sacrificial reagents oxidation. The results of the photocatalytic reforming of ethanol (Figure 4-7) could help to verify the pathway of the reaction. We hypothesised that the excess of CO_2 could decrease the rate of the ethanol oxidation reactions. For instance, the CO yield (24.9±2.6 µmol/g-cat.) given by the P25 is almost 2.5 times higher than that in absence of the CO_2. Attempts to analyse the yield of the CO_2 produced via decomposition of the ethanol failed because of the low yield of the CO_2 compared to the

amount of CO_2 already present in the reactor. On the other hand, the yield of the H_2 formed by the RuO_2/AL is notably reduced possibly due to the reduction reactions competing with one another on the reduction side. The **13**C labeled carbon dioxide ($^{13}CO_2$) and isotope labeled ethanol (CD_3CD_2OD) are required to verify the exact pathway of the reactions.

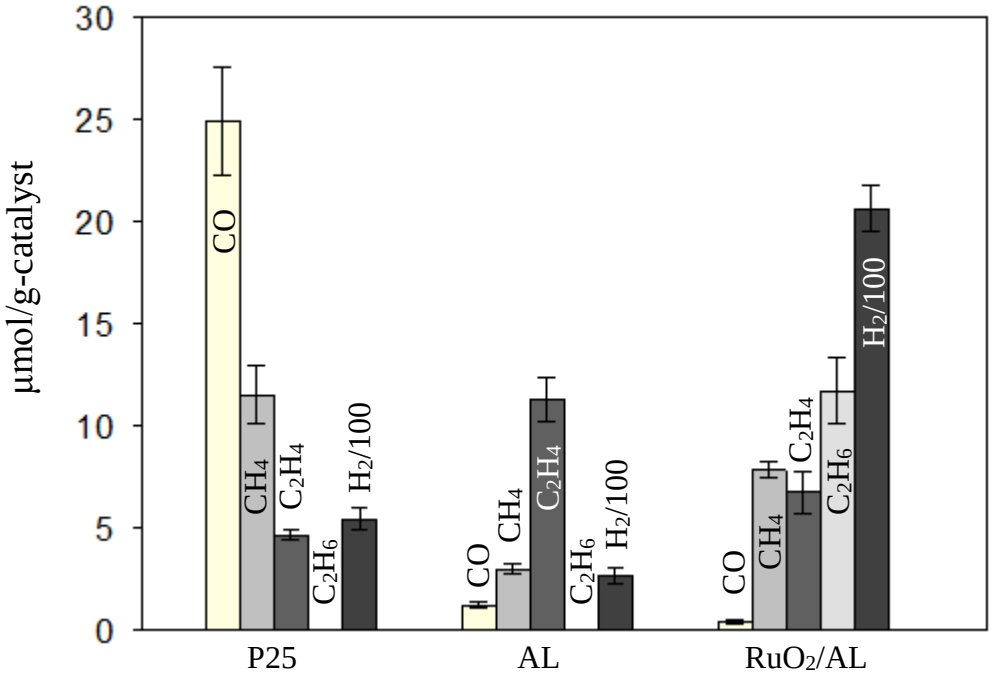

Figure 4-8. The product yields of the photocatalytic reduction of CO_2 with 20 v/v% ethanoic solution under UV LEDs with a maximum intensity at 370 nm. The experimental conditions are 20 v/v% ethanoic solution, a catalyst loading of 1 g-cat/L, CO_2 pressure of 250 kPa, 20 h of irradiation, 30°C. (i) the three catalysts that exhibited the best photocatalytic performance for reduction of CO_2 and reforming of ethanol (Figures 4-6 and 4-7), were tested here.

As shown in Figure 4-9, the total CO (0.5±0.1 µmol/g-cat.) and CH_4 (2.2±0.35 µmol/g-cat.) yields of the AL, under green light (515 nm) after 30 h, is almost 1.35 times higher than the yield of CO (2±0.5 µmol/g-cat.) given by P25. The small amount of methane was also formed by P25 the yield of which was not possible to quantify by our GC. In addition, the pure TiO_2 anatase exhibited no apparent photocatalytic activity in CO_2 reduction under green light

(not shown here). These results corroborate the diffuse-reflectance UV-vis spectra shown in Figure 4-5. The band gap of anatase crystals is 3.2 eV limiting the light absorption efficiency to wavelengths below 400 nm. The unique advantages of the morphology of the chloroplast-like structures in the AL samples clearly offset the theoretically low efficiency under the visible light region due to its predominantly pure anatase phase.

There are two types of localized centres in the 3D TiO_2 nanocrystalline which may lead to visible light absorbance: (a) the oxygen vacancies that can form Ti^{3+} defects in the crystal lattice. (b) the proportion of surface atoms in the AL is high relative to the total atoms due to the high surface area of such materials. Most of the surface/interface atoms could act as capture centres in the semiconductors (Abayev et al., 2007; Krishnan, 2007). These advanced optical properties and improved visible light activity of titania fabricated in the form of nanoplatfoprms, have been proved at many reports in recent years (Chen & Mao, 2007). The RuO_2/AL catalyst exhibited the significantly higher yield of CH_4 (3.15±0.35 μmol/g-cat.) than neat titania materials. The RuO_2 is capable of absorbing visible range wavelengths ($\geq 400\,nm$) (Over, 2012). The photo-excited electrons of RuO_2 have sufficient energy to overcome the Schottky barrier of TiO_2. The transfer of electrons from RuO_2 to conduction band of titania accelerate visible light absorption (Dvoranová et al., 2002; Litter, 1999). In the same manner, the RuO_2/P25 catalysts exhibited overall carbon dioxide conversion similar to that of the AL under visible light.

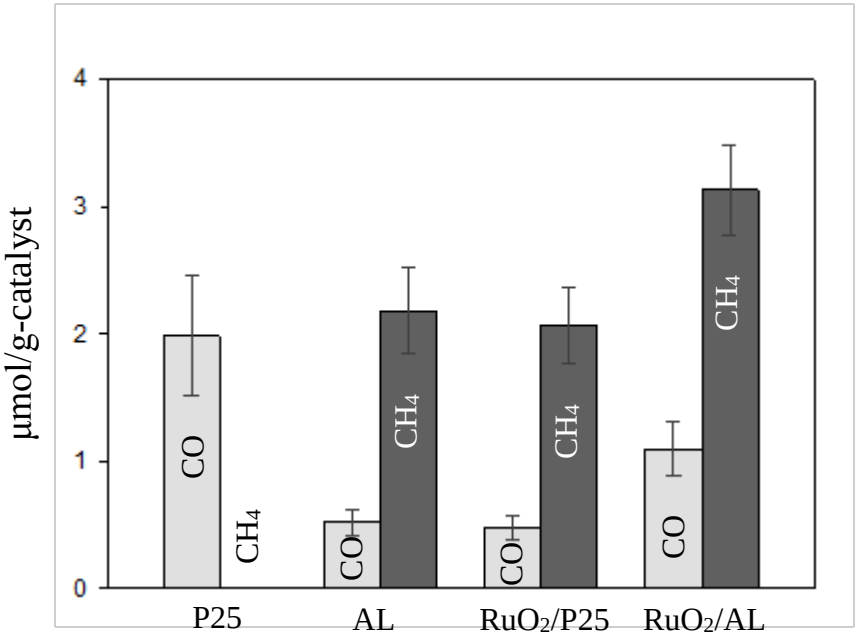

Figure 4-9. The product yields of the photocatalytic reduction of CO_2 with water under green LEDs with a maximum intensity at 515 nm. The experimental conditions are 0.2 M NaOH solution, a catalyst loading of 1 g-cat/L, CO_2 pressure of 250 kPa, 30 h of irradiation, 30°C. (i) much lower product yields were recorded here due to the use of a lower energy light source. (ii) the small amount of methane was also yielded by P25 (not detectable by our GC). (iii) the TiO_2 anatase exhibited no photocatalytic activity under green light (result not shown).

4.3.3 Mechanistic proposal for the CO_2 photoreduction based on the kinetic study

The effect of irradiation time on photocatalytic reduction the of CO_2 by the AL catalysts, over a period of 25 h with intervals of 5 h under UV light (370 nm), are illustrated in Figure 4-10. The formation of the products was negligible after the first 5 h of the reaction. The yield of the products did sharply rise after 10 h of irradiation. The highest yields of both CH_4 (3.8±0.6 µmol/g-cat.) and CO (1.8±0.2 µmol/g-cat.) were obtained after 20 h of the reaction. A steeper curve was recorded for the methane yields while the CO concentration profile is more moderate. A drop in product yields is observed after 20 h of irradiation. The reduction and oxidation half-reactions occur on similar or neighbouring sites on the surface of the TiO_2 (Dimitrijevic et al., 2012). The amount of the oxygen is expected to increase as product of water splitting in long reaction time span. Tseng *et al.* (Tseng et al., 2002) studied

the consequence of the oxygen generation for the CO_2 photoreduction. Their report showed that the higher ratio of molecular O_2 to the products could increase the risk of back reactions.

A few researchers studied the effect of irritation time on the formation of CO_2 photocatalytic reduction products in semiconductors powder suspended solutions (Indrakanti et al., 2009). Similar trends of yield-time dependency are reported for the TiO_2 catalysts (Kočí et al., 2010; Liu et al., 2007; Mizuno et al., 1996). However, it is difficult to compare the yields of a photocatalytic reaction between research reports because of the different experimental conditions. The efficiency of the reaction could be significantly changed under different UV wavelength and/or intensity, different reactor configuration and different reaction media.

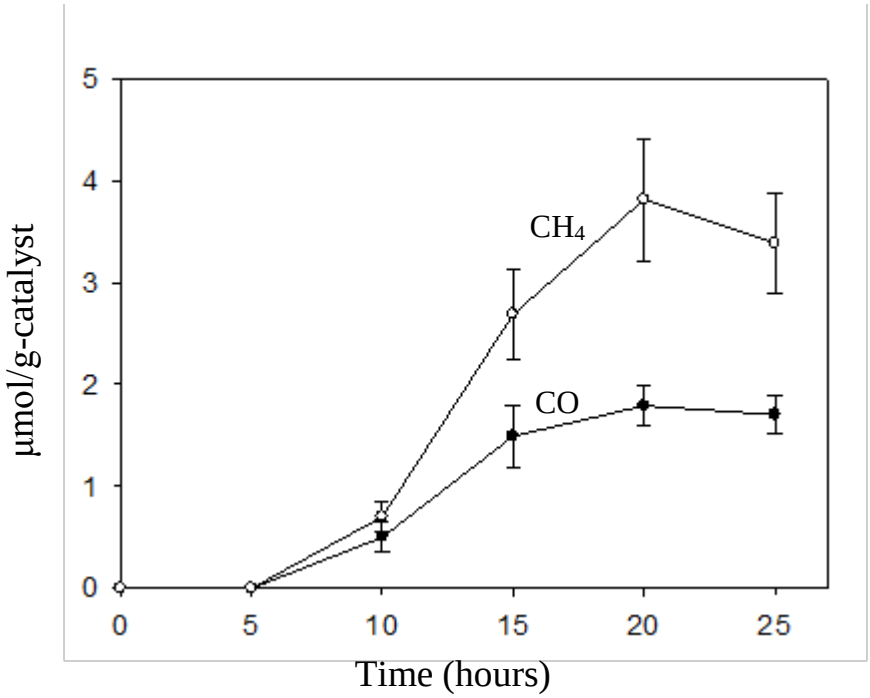

Figure 4-10. Time dependence of the product yields of the photocatalytic reduction of CO_2 with water over the TiO2 AL catalysts, under UV LEDs with a maximum intensity at 370 nm. The experimental conditions are 0.2 M NaOH solution, a catalyst loading of 1 g-cat/L, CO_2 pressure of 250 kPa, 30°C.

The obtained experimental data were compared with the data calculated using the both model equations. The comparison is demonstrated in Figure 4-11 a-d. The kinetic model developed based on pseudofirst order reactions fits well to the concentration profiles of CO and CH_4. The complex kinetic constants in the rate equations (4-11 and 4-12) are independent from the concentration of protons. This finding indicates that the formation of H^+ ions is not the rate limiting step of the reaction (Bartholomew & Farrauto, 2005). The electrons injection to CO_2 is likely limiting step and a severe obstacle to the multiple reduction reaction. Carbon dioxide molecules has a linear and symmetric geometry making them chemically stable with a closed-shell electronic configuration. The introducing of a free electron to the CO_2 molecule results in bending of the molecular structure. Therefore, the formation of $CO_2^{\cdot -}$ species has a very unfavourable energy balance of $E_0 = -1.90$ V (Freund & Roberts, 1996). The dissociation

of CO_2 (see the carbene pathway in Table 2-1) could proceed upon proton-assisted transfer of electrons (Indrakanti et al., 2009);

$$CO_2 + 2H^+ + 2e^- \longrightarrow CO + H_2O$$

The reduction potential of proton-assisted transfer of electron to CO_2 is less negative ($E_0 = -0.53$ V). However, there is little evidence of this multi-electron transfer process in literature (Habisreutinger et al., 2013). It is understood that the multiple reduction involves a series of one-electron steps. The interaction of adsorbed CO_2 molecules with surface atoms forms a partially charged $CO_2^{\delta.-}$ species. These adsorbates lose the linear symmetry of the free CO_2 molecules. Hence, the $CO_2^{\delta.-}$ radicals has lower barrier for accepting electrons (Dimitrijevic et al., 2011; Shkrob et al., 2012).

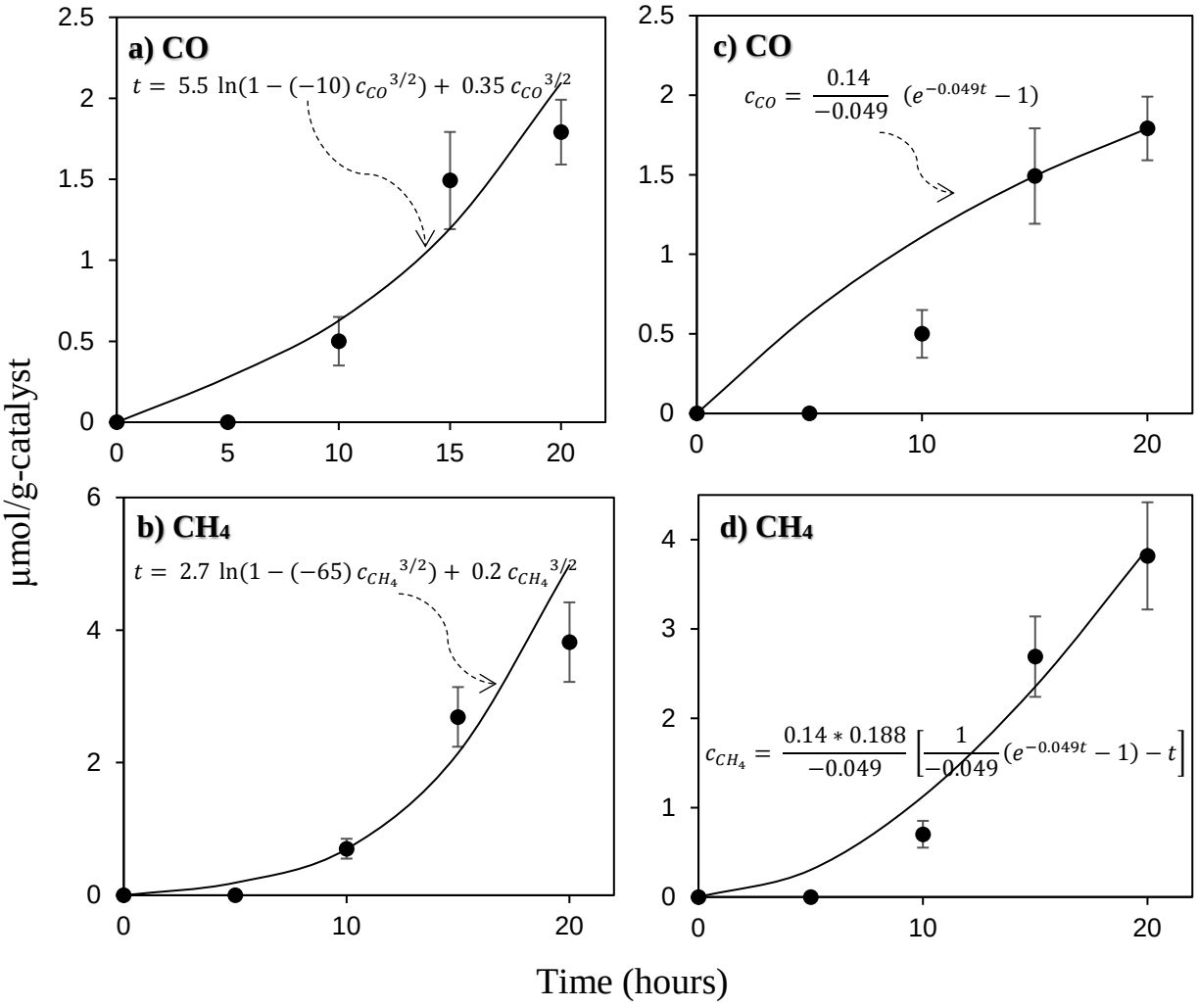

Figure 4-11. a-b) Comparison of the proposed kinetic model based on Langmuir-Hinshelwood mechanism with the empirical profiles of CO and CH_4 formation from photocatalytic reduction of CO_2 over the AL materials. c-d) Comparison of the proposed kinetic model based on pseudofirst order reactions with the experimental data of CO and CH_4 yields from photocatalytic reduction of CO_2 on the AL catalysts. The experimental conditions are 0.2 M NaOH solution, a catalyst loading of 1 g-cat/L, CO_2 pressure of 250 kPa, 30°C. (i) the data at 10 h measured for carbon monoxide were close to the determinableness limit of our set up (shown here but not included in model fitting).

4.4 Conclusions

In this chapter, we investigated the photocatalytic reduction of CO_2 with water in titania catalysts powder suspended solutions. The bio-mimicked titania nanoarchitecture referred to as the AL here, exhibited higher selectivity to methane under UV light. The artificial leaves also changed the selectivity of the photocatalytic reforming of the ethanol to the dehydration reaction. We hypothesised that the efficiency and selectivity of the photocatalytic reactions can be potentially augmented by modifying the morphology of the photocatalyst alone. The AL samples showed a greater visible light activity in photoreduction of CO_2 without a mixed phase (anatase and rutile) composition compared to the benchmark P25 titania. We attributed the improved light harvesting properties of the chloroplast-like 3-dimensional TiO_2 materials to its unique morphological contribution, such as enhance reactant-catalyst contact and the lattice defects. The deposition of ruthenium dioxide on the surface of the titania catalysts enhanced the photocatalytic activity in UV and visible wavelengths range. The highest products yield of the CO_2 photoreduction under UV and green lights have been obtained by the RuO_2/AL catalysts. Under UV light irritation, the charge transfer between RuO_2/TiO_2 heterojunction results in more efficient charge separation. In addition, the RuO_2 is capable of visible range wavelengths ($\geq 400\ nm$) absorption and electrons injection into TiO_2. The experimental data of the products concentration profiles have achieved an acceptable fit to the kinetic equations based on pseudofirst order reactions. This finding indicates that the reaction rate is independent from the rate of H^+ cations formation. The understanding of the morphological contribution of the photocatalyst provided in this study, could help to augment the efficiency and selectivity of the CO_2 photoreduction.

Chapter 5 – Enhancement of visible light activity of the bio-mimicked TiO_2 architectures

5.1 Introduction

Given that visible light with wavelengths longer than 400 nm makes up more than 95% of the solar spectrum, the visible light activity of photocatalysts could be extremely important for solar-assisted chemical reactions. The titania photocatalysts are inefficient for the utilization of sunlight because of their large band gap. Various methods are reported to broaden the spectrum of utilised light of semiconductors. Generally, mechanisms of enhancing visible light activity of TiO_2 photocatalysts could be categorized into two groups; (a) band gap modification via doping in order to provide mid-gap states. Photons can excite electrons from the valence band (VB) to mid-gap state or, from the mid-gap state to the conduction band (CB) if it lies below the Fermi level (Figure 5-1a). (b) surface chemical modification via coupling a sensitizer to TiO_2 materials. Such sensitizer absorbs visible light and injects electrons into the CB of TiO_2 (Figure 5-1b) (Rehman et al., 2009).

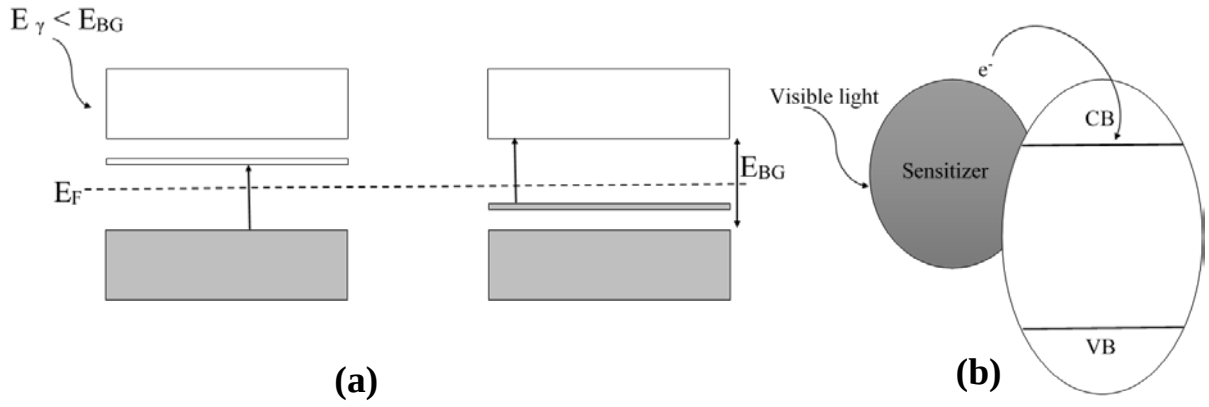

Figure 5-1. (a) Introducing mid-gap states to TiO_2 by doping. (b) Coupling a sensitizer TiO_2.

Band gap modification by doping with nonmetals could proceed via substitution for oxygen sites. The nonmetal atoms with a similar ionic radii (1.4 Å) to the O^{2-} could easily substitute for O atoms (Chen et al., 2008; Etacheri et al., 2015). Doping with sulfur (Ohno et al., 2004; Wang et al., 2008), nitrogen (Irie et al., 2003; Yang et al., 2007; Zhang et al., 2008), halogens (Long et al., 2007; Todorova et al., 2008), and carbon (Ren et al., 2007; Xu et al., 2006) in TiO_2 has been reported. On the other hand, various transition metals have been incorporated in titania lattice. The metal cations could substitute Ti^{4+} ions which are coordinated with O in TiO_2 lattice. Fe, Ni, Cu, and etc have been doped into the bulk of TiO_2 using chemical sol-gel and ion-implantation methods (Anpo & Takeuchi, 2003; Yamashita et al., 2003). The metal/nonmetal dopants generate localized states in the mid-gap of TiO_2.

The sensitizers include inorganic semiconductors with narrow band gap, metals, and organic dyes. The well-matched electronic structure of the transition metals to TiO_2 accelerates the electron transfer into the conduction band of TiO_2 (Etacheri et al., 2015; Rehman et al., 2009). Cu (Colón et al., 2006; Ganesh et al., 2014), Fe (Deng et al., 2009), Ru (Ohno et al., 1999; Sasirekha et al., 2006), Ag (Suwarnkar et al., 2014; Wen et al., 2005b) and etc, have shown promising results on increasing the visible light efficiency of TiO_2 photocatalysts.

Recently, the applications of localized surface plasmon resonance have also been at the centre of interest in regard to visible light absorption. Some metals cluster, *e.g.* gold nanoparticles, exhibited distinctive visible-light absorption (Etacheri et al., 2015; Rehman et al., 2009). The localized surface plasmon resonance is referred to interaction of the resonant electromagnetic energy (in the form of electric fields) with the collective motion of free charge carriers in a metallic nanoparticle. The energy is dissipated through the formation of energetic

charge carriers at the nanoparticle surface. The plasmon-induced hot carriers (hot being defined as having energy above the Fermi level) within optically excited plasmonic nanoparticles could transfer to the chemically attached semiconductor or medium (Mathew & Pradeep, 2014).

Ruthenium is a transition metal from platinum group metals. Although Ru is a relatively scarce metal, its price is still about 10 times lower than platinum. The ruthenium could adopt various oxidation states in chemical compounds giving interesting properties to this chemical element (Higgins, 2010). The ruthenium dioxide (RuO_2) reveals a complex oxidation/reduction surface chemistry, which makes it a versatile catalyst (Over, 2002). For example, the ruthenium dioxide is very well-known as the excellent catalyst for hydrogenation reactions. In recent years, various electrochemical reactions have been efficiently catalysed by RuO_2 (Over, 2012). The RuO_2 also possesses high metallic conductivity so can be coupled with semiconductors to form photocatalytic systems (Ryden et al., 1970; Uddin et al., 2013).

The efficiency of metal-semiconductor heterostructures depends on an effective charge carrier separation. The barrier heights of charge separation are governed by the work function of the metal. RuO_2 has a high work function which is above the valence band of TiO_2 (Mogyorósi et al., 2009). The RuO_2 is also very resistance to chemical attacks and poisoning (Kötz & Stucki, 1987; Suoranta et al., 2014). In addition, CO molecules could be absorbed on the surface of the RuO_2 quite strongly (Seitsonen et al., 2001). The efficient adsorption of CO is significant factor with respect to the mechanistic considerations of the CO_2 photoreduction (see earlier discussion in chapter 4).

In this chapter, the RuO_2 has been incorporated into the bulk of the bio-mimicked TiO_2 materials. The photocatalytic activity of the modified artificial TiO_2 leaves under visible light was studied through photoreduction of CO_2 with H_2O. The efficiency of band gap modification method in improving visible light activity was verified compared to the surface chemical modification strategy.

5.2 Incorporation of Ru into the bulk of bio-mimicked TiO_2 architectures

The sol-gel step of the previously explained chemical replication method was slightly modified to introduce the RuO_2 in titania lattice. The calculated amounts of $RuCl_3 \cdot xH_2O$ (required to achieve target ruthenium content of 1.25, 2 and 3 wt %) were added to the sol-gel precursor (the suspension of leaves and titanium isopropoxide in dry isopropanol) prior to addition of titanium isopropoxide. The other processes were as described in chapter 3. The artificial TiO_2 leaves modified with Ru via the doping method is referred to as Ru/TiO2 artificial leaf (Ru/AL). The experimental results of the neat artificial titania leaf (AL) and the surface decorated AL samples with RuO_2 (RuO_2/AL) from chapter 4 are used to assist the discussion.

5.3 Results and discussion

5.3.1 Catalyst characterization

The XRD patterns in Figure 5-2 show that the 1.25 and 2 wt % Ru/AL samples consist predominantly of the anatase, whereas the 3 wt % Ru/AL is a combination of anatase and rutile TiO_2 phases (see chapter 3 for experimental details). The relative concentrations of the crystalline phases were determined by analysis of the anatase and rutile primary peaks, using Spurr equation (Spurr & Myers, 1957). The 3 wt % Ru/AL is composed by approximately 90 % anatase and 10 % rutile. The results indicate that attempt to incorporate Ru into the lattice

of the biotemplated titania materials does not affect the crystalline phase formation till 2 wt % of ruthenium content. Mixed phases of anatase and rutile in the the 3 wt % Ru/AL could be caused by a high ratio between the Ru and Ti during heat treatment. The effects of the cationic dopants on the anatase to rutile transformation have been investigated in many studies (Hanaor & Sorrell, 2011). Doping of the cations of low valence (≤4) favours the anatase-to-rutile transformation at low temperatures. Substitution of the cations for Ti^{4+} ions accelerates the formation of Ti interstitials of lower valence (Hwang et al., 2006; Yang et al., 2004). Alternatively, interstitial solid solubility may occur rather than substitution. The dispersion of the cations in the structure results in the anatase-to-rutile transformation upon constriction of the lattice (Shannon, 1976).

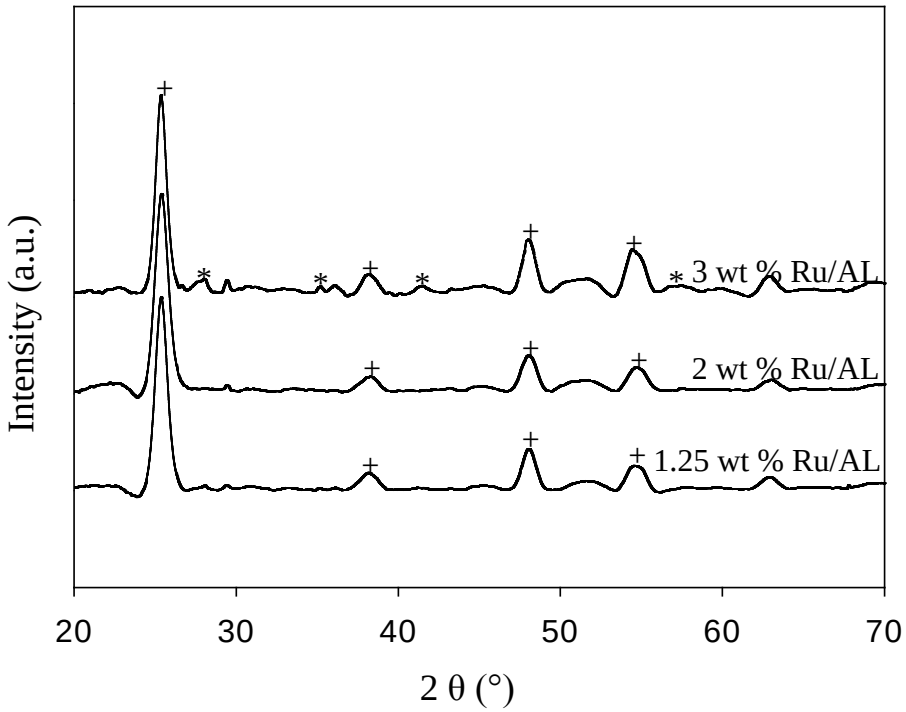

Figure 5-2. XRD patterns of the modified artificial TiO_2 leaves with Ru via the doping method. Corresponding peaks of the anatase phase and the rutile phase TiO_2 are marked by "+" and "*", respectively.

Fourier transform infrared (FTIR) spectra were recorded on a Bruker Alpha FTIR spectrometer. The Ru/AL samples containing whatever wt % of ruthenium exhibited the same feature by FTIR spectroscopy as the neat artificial TiO_2 leaf (Figure 5-3). This is consistent with the literature that focused on tuning the optical properties of modified TiO_2 with ruthenium (Sasirekha et al., 2006; Uddin et al., 2013). The absence of the band of Ri–O vibrations at 500 cm^{-1} (Khorasani-Motlagh et al., 2011), is because of overlapping of the two regions of the vibration frequencies of RuO_2 and TiO_2. The broad band at around 400 cm^{-1} corresponds to Ti–O vibrations and the band at *ca.* 1300 cm^{-1} is attributed to Ti–O–Ti vibrations (Sasirekha et al., 2006; Uddin et al., 2013). The weak band centred at *ca.* 1600 cm^{-1} resulted by stretching vibration band of adsorbed water molecules (Sasirekha et al., 2006). The band at around 2400 cm^{-1} is due to adventitious CO_2 stretching (Zhuiykov, 2009). In the same manner, the RuO_2/AL showed very similar FTIR spectrum.

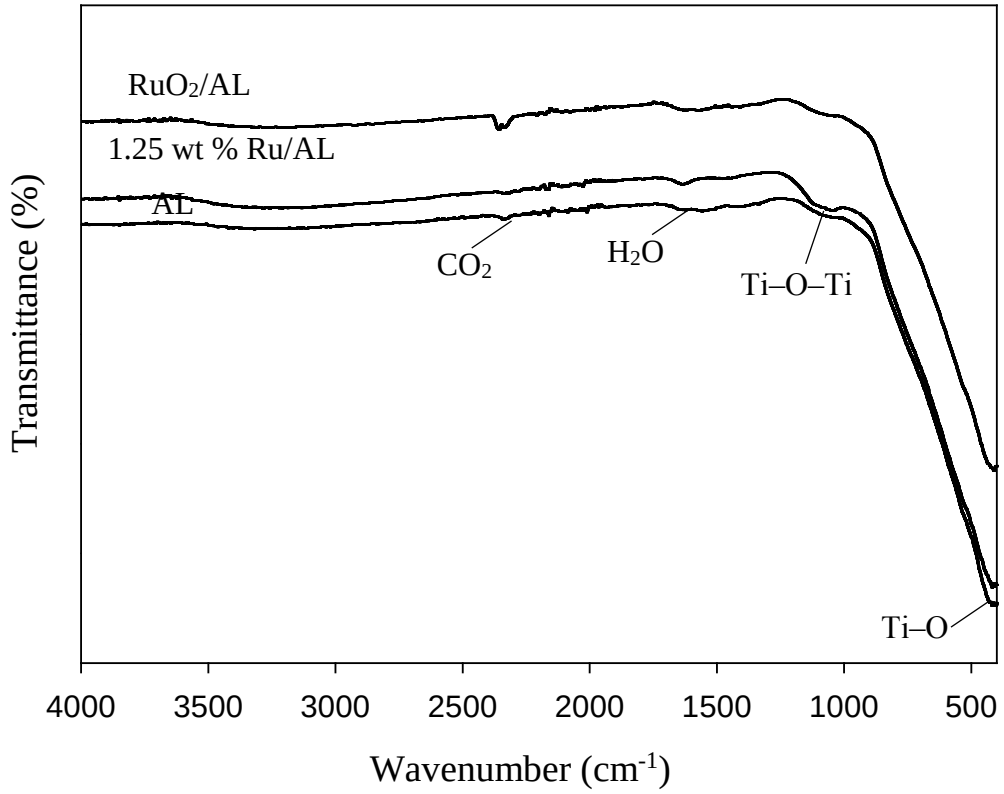

Figure 5-3. Fourier transform infrared (FTIR) spectra of the final catalysts. (i) the 2 and 3 wt % Ru/AL samples exhibited the same feature by FTIR spectroscopy as neat artificial TiO_2 leaf (not shown here).

The diffuse-reflectance UV-vis spectra are shown in Figure 5-4. See chapter 3 for experimental details. The peak centred at around 450 nm in the spectrum of the RuO_2/AL could be attributed to the role of RuO_2 (which is known to be plasmonic in some cases; see earlier discussion of visible light activity in chapter 5). Earlier publications of plasmonic RuO_2 reported similar bands observed around 450 nm (Ohno et al., 1999; Sasirekha et al., 2006). Comparison of the diffuse reflectance spectra of the Ru doped samples (Ru/AL) with the unmodified artificial TiO_2 leaf, showed that shape of the spectra remain almost unchanged. However, the overall light absorbance increases with Ru loading. This finding suggests the ultra fine dispersion of RuO_2 in the bulk of the Ru/AL materials. The metals with greater ionic radii than that of Ti^{4+} could not easily substitute at Ti sites in TiO_2 lattice (Zhao et al., 2008).

The ionic radii of Ti^{4+} and Ru^{4+} cations are 0.42 and 0.62 Å, respectively (Shannon, 1976). Doped Ru more likely was dispersed in the form of RuO_2 nanoparticles within the volume of the bulk TiO_2 (Rehman et al., 2009). Ion-implantation technique outclasses chemical sol-gel technique for doping transition metals ions into titania lattice (Anpo & Takeuchi, 2003; Yamashita et al., 2003).

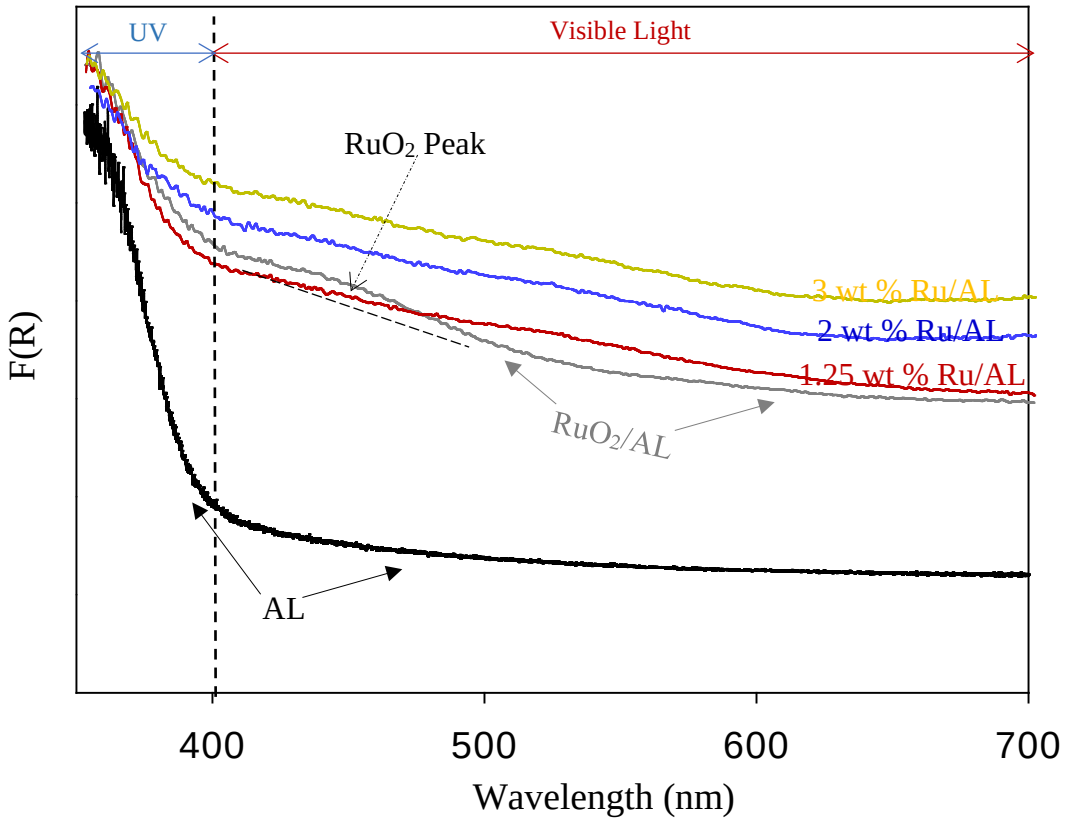

Figure 5-4. Diffuse-reflectance UV-Vis spectra of the modified and neat artificial TiO_2 leaf.

5.3.2 Enhanced product yields by photocatalytic reduction of CO_2 under visible light

The results of photoreduction of CO_2 with water, after 20 h of irradiation under UV light (370 nm), are shown in Figure 5-5. See chapter 4 for experimental details. The photoreduction reactions catalysed by the 1.25 wt % Ru/AL samples produced CO (1.75±0.2 µmol/g-cat.) and CH4 (3.65±0.45 µmol/g-cat.) yields similar to those obtained using the neat

AL under UV light. In the same manner, the product yields of the 2 wt % Ru/AL were similar to those observed when using pure AL (not shown here). The slightly lower product yields of the 3 wt % Ru/AL could be caused by high loading of Ru. The photocatalytic activity of titania materials doped with metals strongly depends on the doping ratio.

There is an optimal concentration of dopant for every transition metal (Bloh et al., 2012; Choi et al., 1994). As discussed in section 4.3.2 of the previous chapter, the dopant reduces the recombination rate under UV light via trapping the charge carriers. On the contrary, the recombination centres occur at a high doping ratio. The high concentration of dopant may also lead to blocking the active reaction sites of TiO_2 (Etacheri et al., 2015; Rehman et al., 2009). However, the highest product yields are resulted by the RuO_2/AL (1.3 wt % of Ru content) catalyst. We hypothesised that there is a correlation between the surface morphology of the RuO_2/AL photocatalyst and its better photocatalytic performance. The ruthenium dioxide crystallites form catalytic hot spots on structural defects, *e.g.* corners and edges (Figure 5-5 inset), at the RuO_2/TiO_2 interface (Cargnello et al., 2013; Huang et al., 2014; Huang et al., 2015).

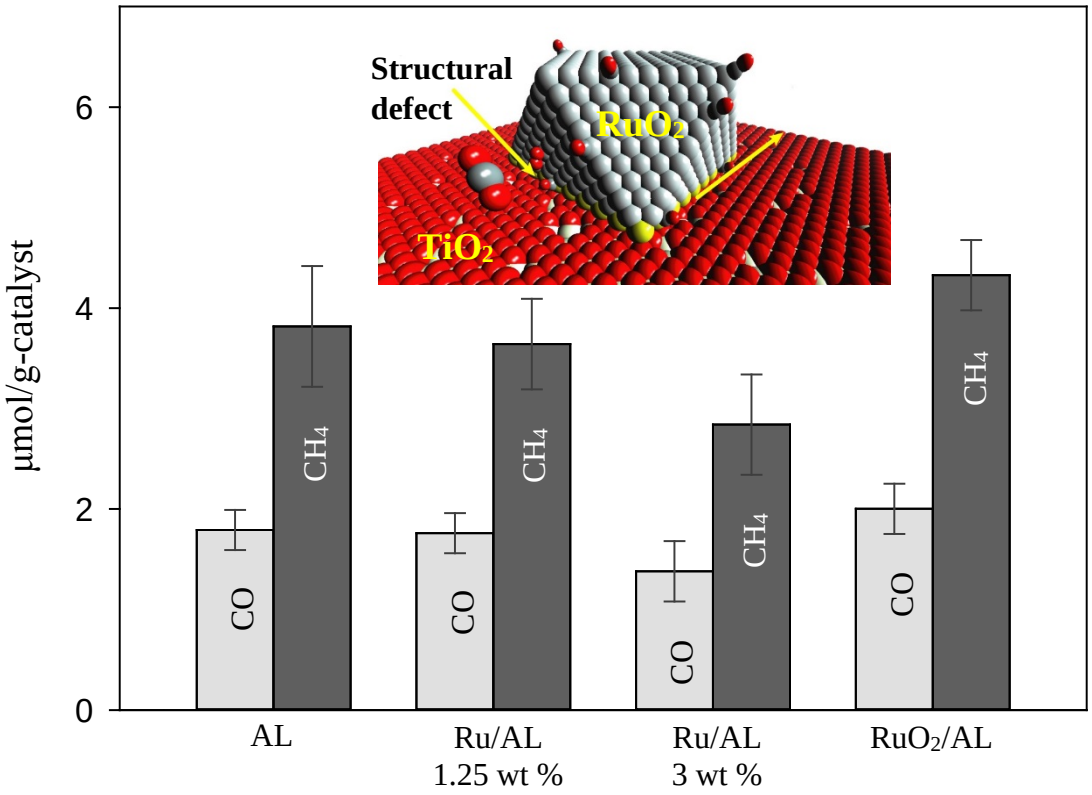

Figure 5-5. The product yields of the photocatalytic reduction of CO_2 with water under UV LEDs with a maximum intensity at 370 nm (Inset: Structural defects at the RuO_2/TiO_2 interface). The experimental conditions are 0.2 M NaOH solution, a catalyst loading of 1 g-cat/L, CO_2 pressure of 250 kPa, 20 h of irradiation, 30°C. (i) the photoreduction reactions catalysed by the 2 wt % Ru/AL samples showed product yields similar to that of the neat AL (not shown here).

Improving photocatalytic activity under visible light (*cf.* UV only) is one of the main areas of interest in this field. As shown in Figure 5-6, the total CO (1.1±0.2 µmol/g-cat.) and CH_4 (3.15±0.35 µmol/g-cat.) yields of the RuO_2/AL, under green light (515 nm) after 30 h, are almost 1.4 times higher than the total yields of CO (0.6±0.1 µmol/g-cat.) and CH_4 (2.5±0.35 µmol/g-cat.) given by 1.25 wt % Ru/AL. See chapter 4 for experimental details. The product yields of the 2 wt % Ru/AL were similar to those obtained using the 1.25 wt % Ru/AL (not shown here). This is consistent with the photocatalytic performance of the 1.25 and 2 wt % Ru/AL materials under UV light. In addition, the 3 wt % Ru/AL exhibited no apparent photocatalytic activity in CO_2 reduction under green light (not shown here). In the Ru/AL

materials, the RuO_2 nanoparticles are dispersed within the bulk of TiO_2 forming heterostructures. The localized states may act as recombination centres in case of deep doping (Etacheri et al., 2015; Rehman et al., 2009). The photocatalytic efficiency is determined by the competition between the photoinduced electron-hole pairs transfer rate to surface and the recombination rate. The charge carriers could not engage in the redox reactions on the surface if the recombination rate is high. However, the Ru/AL samples with up to 2 wt % of Ru content possessed a slightly higher total conversion of CO_2 under green light compared to that given by the neat AL.

On the other hand, the charge carriers are potogenerated at the surface of the RuO_2/AL coupled system. Under green light illumination, the hot electrons of RuO_2 tend to move to conduction band of TiO_2 and leave the holes behind in RuO_2 (Uddin et al., 2013). Hence, the photoinduced charge carriers could be separated effectively due Schottky barrier. This stable charges separation could result in higher surface charge density of the RuO_2/AL. The superior visible light activity of the surface decorated artificial TiO_2 leaf with RuO_2 (RuO_2/AL) could be attributed to the higher surface charge density. Higher recombination rate of the photoinduced electron-hole pairs is expected in the materials modified via incorporation of RuO_2 into the bulk of titania (Ru/AL). Noteworthy, the difference in CO_2 photoreduction yields of the 1.25 wt % Ru/AL and 1.3 wt % RuO_2/AL photocatalysts is far greater than the dopant contents difference of these materials.

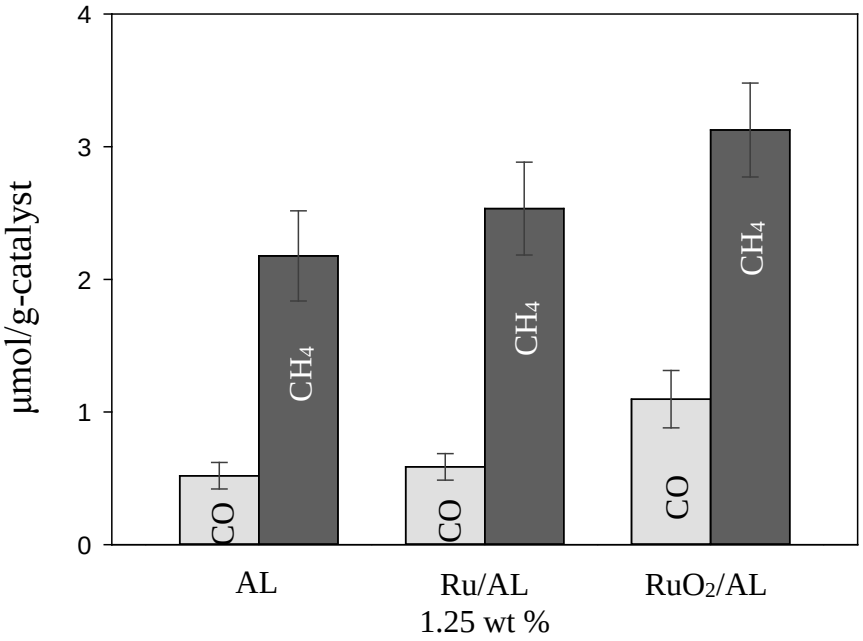

Figure 5-6. The product yields of the photocatalytic reduction of CO_2 with water under green LEDs with a maximum intensity at 515 nm. The experimental conditions are 0.2 M NaOH solution, a catalyst loading of 1 g-cat/L, CO_2 pressure of 250 kPa, 30 h of irradiation, 30°C. (i) much lower product yields were recorded here due to the use of a lower energy light source. (ii) the product yields of the 2 wt % Ru/AL were similar to that of the 1.25 wt % Ru/AL. The 3 wt % Ru/AL exhibited no photocatalytic activity under green light (results not shown).

5.4 Conclusions

In this chapter, the two most reported strategies in literature were used to enhance the visible light activity of the biotemplated TiO_2 photocatalyst. The previously explained sol-gel step was slightly modified to intercorporate the RuO_2 into bulk of the titania. On the other hand, the surface of the artificial TiO_2 leaf were modified with RuO_2 using a previously reported method in literature. We hypothesised that the Ru^{4+} cations could not substitute in TiO_2 lattice because of the much greater ionic radii compared to Ti^{4+}. We conclude that the Ru is likely to be dispersed in the form of ultra small RuO_2 nanoparticles within the volume of the Ru/AL photocatalysts. The Ru/AL samples exhibited lower efficiency in photoreduction of CO_2 under UV and visible lights compared to that of the RuO_2/AL. This finding could be

attributed to the high recombination rate of the electron-hole pairs within the bulk of the Ru/AL. We demonstrated the advantage of the surface modification strategy (on example of RuO_2/AL) for improving the visible light activity of the titania materials. The photocatalytic efficiency under wavelengths longer than 400 nm, which makes up more than 95% of the solar spectrum, could be extremely attractive for solar-assisted reduction of CO_2 with H_2O.

Chapter 6 - Conclusion, recommendations and future study

6.1 Summary of the work

In this thesis, a systematic study was carried out on the effects of the reaction variables on the photocatalytic reduction of CO_2 with H_2O. The main findings of the study are generally detailed as:

Firstly, an improved chemical replication method was developed to replicate the full architecture of the leaf photosystem with TiO_2. Scanning and transmission electron microscopy images of the final products confirmed that the detailed microscale framework and nanostructures, such as the chloroplast and the thylakoids were well replicated. The novel TiO_2 architecture produced from biotemplating, has highly porous network. The synthesis method reported in this work provides a reliable and promising procedure to synthesize TiO2 hierarchical structures which could overcome the issues in controlling the structure and crystallinity of end product associated with conventional procedures.

Secondly, the biotemplated titania materials, referred to as artificial leaf in this work, exhibited a substantially improved photocatalytic activity under visible light. The unique advantages of the layered TiO_2 nanostructure were confirmed in the preliminary photocatalytic tests. The improved visible light photocatalytic performance could be a result of overall morphological contribution given by the 3-D nanostructured light-harvesting system, derived from the thylakoid membranes of the natural leaves. This finding is consistent with the literature reporting the advanced optical properties of other titania nano-architectures. We

hypothesised that the extrinsic excitation behaviour of TiO_2 photocatalyst can potentially be augmented by modifying its morphology without changing its composition.

Later on, the biotemplated photocatalyst with the unique pore network was employed to catalyse the photocatalytic reduction of CO_2 with water. The non-porous commercial titania catalysts, pure anatase and well-known P25, were used as benchmark. Although the artificial TiO_2 leaves showed a slightly lower product yields of CO_2 photoreduction compared to commercial catalysts under UV light (370 nm), it increases the selectivity of the methane. The bio-mimicked nanostructured framework also showed a higher selectivity to dehydration reaction in the photocatalytic reforming of ethanol under UV light. Moreover, the chloroplast-like 3-D TiO_2 materials leaves outperformed the product yields of P25 titania under visible light (515 nm) more than 1.35 times. These results confirm that there is a strong correlation between the morphology of the inorganic artificial leaves made of TiO2 and their photocatalytic performance. We hypothesised that modifying the morphology of the photocatalysts could alter the pathway and selectivity of the photocatalytic reactions. The understanding of morphological contribution of the photocatalyst provided in this study, could help to augment the efficiency and selectivity of the CO_2 photoreduction.

Two kinetic models, that incorporate the coupled reduction and oxidation effect of the adsorptive photocatalytic reduction of CO_2 with water, were also validated by the products concentration profiles. The experimental data have obtained a very good fit to the kinetic model developed based on pseudofirst order reactions. The rate equations are independent from the concentration of hydrogen. This finding indicates that the formation of H^+ cations is not the rate limiting step of the reaction.

Finally, the effects of modification of titania catalysts with the ruthenium dioxide were investigated. The surface modified artificial leaves, referred to as RuO_2/artificial leaf in this work, possessed the highest activity in the reduction of CO_2 under UV and visible lights. The lower photocatalytic efficiency of bulk modified biotemplated materials could be assigned to the high recombination rate of the electron-hole pairs within their volume. We demonstrated the advantage of the surface modification strategy for improving the visible light activity of the titania materials. Given that visible light with wavelengths longer than 400 nm makes up more than 95% of the solar spectrum, the superior photocatalytic efficiency under visible light could be extremely attractive for solar assisted chemical reactions.

6.2 Recommendations and future study

6.2.1 TiO_2 photocatalysts

The study of the trapping phenomena is essential for semiconductor materials. The spin-dependent recombination (SDR) method is suitable to obtain information about the trap centres of the nanostructured semiconductors (Adams et al., 2003). Electron paramagnetic resonance (EPR) spectroscopy could be used to investigate the trapping-detrapping phenomena in the artificial titania leaf. In addition, stability and recyclability of the catalyst is a key requirement for possible industrial applications. Further work on the reported new biotemplated photocatalyst could be the cycling reuse experiments. The artificial TiO_2 leaf should be recycled and reused several times without significant loss of efficiency.

This study demonstrated the importance of the morphological contribution of the 3-D layered nanostructure of the bio-mimicked TiO_2 photocatalysts in the catalytic performance. The advantages of TiO_2 nanostructures over conventional TiO_2-based flat platfroms would promote the efforts to address energy and environmental issues. The high surface/volume ratio

of the number of atoms in TiO_2 nanomaterials play a major role in their superior light harvesting features. Among TiO_2 nanostructures, the highest surface area has been recorded from titania aerogels (Malinowska et al., 2003; Shao et al., 2013). Yang *et al.* (Yang et al., 1999) reported TiO_2 aerogels with a BET surface area of >200 m^2/g (Figure 6-1). The large specific surface area increases the number of surface/interface atoms. A similar systematic study could be performed on the photocatalytic performance of the TiO_2 aerogels. The results should corroborate the findings of our research.

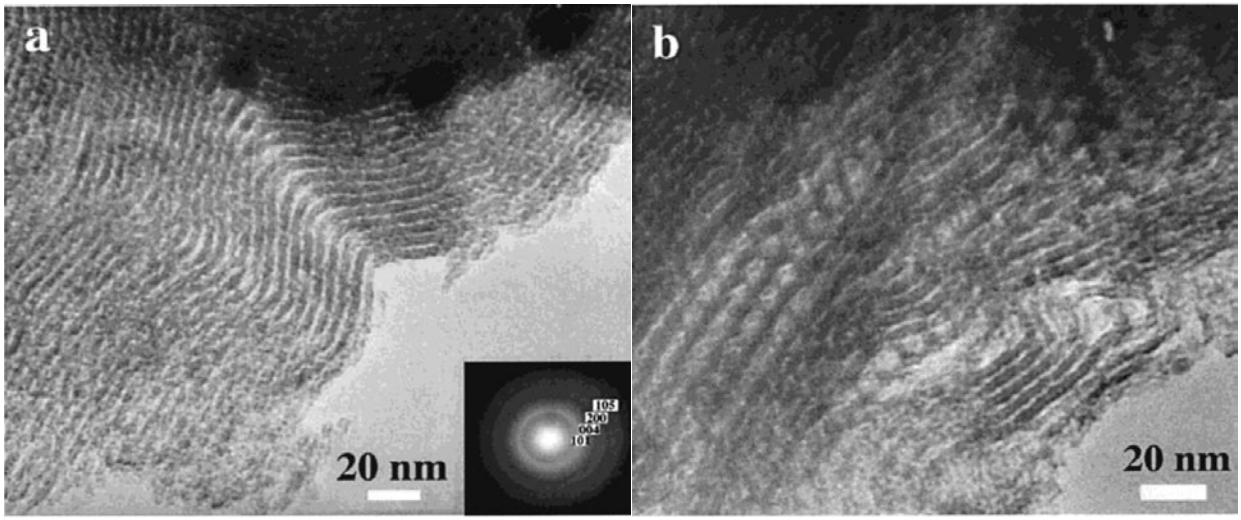

Figure 6-1. TEM images of cubic mesoporous TiO_2, reprinted from Yang *et al.*, 1999.

The effects of modification of the TiO_2 materials with RuO_2 were investigated in previous chapter. Further work in this area could focus on the decoration of the surface of the artificial titania leaf with the noble metals cluster. Some metals cluster, *e.g.* gold nanoparticles, exhibit distinctive visible-light absorption due to surface plasmon resonance. However, the effects of metal cluster strongly depend upon the particle size. The main issue facing the deposition methods of metal cluster is controlling the particles size and distribution on the surface of the semiconductor materials (Mathew & Pradeep, 2014).

6.2.2 Photocatalytic reduction of CO_2 with H_2O

The CO_2 photoreduction is thought to proceed through several intermediate reactions. An understanding of underlying mechanism could help to increase the overall efficiency of CO_2 reduction via minimizing the relevant barriers of intermediate reactions. Many analytical developments have been carried out in the area of *in-situ* analysis of photocatalytic reactions in recent years. Diffuse Reflection Infrared Spectroscopy (DRIFTS) technique, is extremely useful for identifying and quantifying intermediate species formation (Armaroli et al., 2004). The *in-situ* DRIFTS analysis approach could be used to probe the surface of the photocatalysts so as to achieve a detailed description of the exact mechanism pertaining photoreduction of CO_2 on the titania semiconductors.

As discussed in the section 4.3.2 of chapter 4, interference of the products may occur in case of photoreduction of CO_2 with organic hole scavengers. Hence, the ^{13}C labeled carbon dioxide ($^{13}CO_2$) and isotope labeled ethanol (CD_3CD_2OD) should be used to investigate the detailed underlying mechanism. On the other hand, the efficiency of photocatalytic reforming of ethanol using TiO_2 suspensions was demonstrated in this study. We recommend the application of the proposed slurry system for photocatalytic oxidation of other alcohols in the

area of green chemistry and engineering. The selective oxidation of glycerol is worthy of special mention. The commercial use of biodiesel has been rapidly expanding over the last 10 years. Glycerol plays a very important role as the major by-product (produced at a rate of about 10 wt. % of total biodiesel) toward the price trend of biodiesel. Thus, research attempts for the conversion of glycerol into value-added substances have received enormous efforts (Ayoub & Abdullah, 2012).

The slurry reactor is the most straightforward set up for photocatalytic reduction of CO_2 with H_2O. However, the formation rate of CO_2 photoreduction products in semiconductors powder suspended solutions is still far away from commercial application. The main issue facing the photocatalytic reduction of CO_2 in slurry system is the mass transfer limitations of the three-phase systems. The gas phase reaction has been investigated to improve the efficiency of CO_2 photoreduction (Reñones et al., 2016; Zhao et al., 2016). Although higher product yields are reported for photoreduction of CO_2 with water vapour, the photocatalysts have to be immobilized for gas-solid interface reactions. This may decrease the accessible area for both photons and reactants (Habisreutinger et al., 2013). A less-explored approach is using fluidized-bed photoreactor (Figure 6-2). The fluidized-bed set up significantly facilitates tuning up of the reactants, products and photocatalyst materials. The external and internal mass transfer limitations of photocatalyst particles could be eliminated in the fluidized-bed reactor operated under fully developed turbulent flow (Jing et al., 2013).

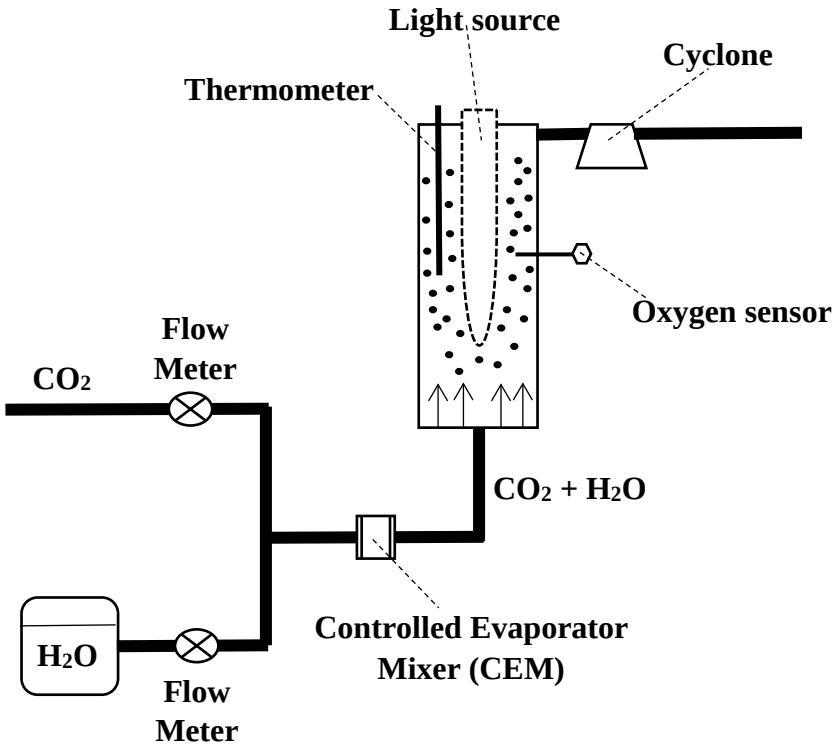

Figure 6-2. The recommended fluidized-bed photoreactor for photocatalytic reduction of CO_2 with water vapour.

Appendix

Kinetic models integrations

The equation 4-7 could be resolved as follows:

$$-dt = \frac{c^2}{k_4 - k_5 c^{3/2}}\, dc$$

$$\int dt = -\int \frac{c^2}{k_4 - k_5 c^{3/2}}\, dc$$

Let $u=\sqrt{c}$, $k_4=a$ and $k_5=b$. Then $du = \frac{1}{2\sqrt{c}} dc$ and we have that $\frac{dc}{\sqrt{c}} = 2du$. Integral can be rewritten as:

$$\int \frac{c^2}{k_4 - k_5 c^{3/2}}\, dc = -2 \int \frac{u^5}{-a + bu^3}\, du$$

Simplify integrand:

$$-2 \int -\frac{u^5}{a - bu^3}\, du = 2 \int \frac{u^5}{a - bu^3}\, du = 2 \int \frac{au^2}{b(a - bu^3)} - \frac{u^2}{b}\, du$$

Integrate term by term:

$$2 \int \frac{au^2}{b(a - bu^3)} - \frac{u^2}{b}\, du = -2 \int \frac{u^2}{b}\, du + 2 \int \frac{au^2}{b(a - bu^3)}$$

Apply constant multiple rule:

$$-2\int \frac{u^2}{b}\,du + 2\int \frac{au^2}{b(a-bu^3)} = -2\frac{1}{b}\int u^2\,du + 2\frac{a}{b}\int \frac{u^2}{(a-bu^3)}$$

Applying power rule $\int u^n\,du = \frac{u^{n+1}}{n+1}$ *(n ≠ -1)* with *n = 2*:

$$2\frac{a}{b}\int \frac{u^2}{(a-bu^3)}\,du - \frac{2}{b}\int u^2\,du = 2\frac{a}{b}\int \frac{u^2}{(a-bu^3)}\,du - \frac{2u^3}{3b}$$

Let $v = a\text{-}bu^3$ and then we have that $u^2du = -\frac{dv}{3b}$:

$$2\frac{a}{b}\int \frac{u^2}{(a-bu^3)}\,du - \frac{2u^3}{3b} = -\frac{2a}{3b^2}\int \frac{1}{v}\,dv - \frac{2u^3}{3b}$$

Integral of $\int \frac{1}{v}\,dv$ is *ln (v)*:

$$-\frac{2a}{3b^2}\int \frac{1}{v}\,dv - \frac{2u^3}{3b} = -\frac{2a}{3b^2}\,ln\,(v) - \frac{2u^3}{3b}$$

Recall, that $v = a\text{-}bu^3$:

$$-\frac{2a}{3b^2}\,ln\,(v) - \frac{2u^3}{3b} = -\frac{2a}{3b^2}\,ln\,(a-bu^3) - \frac{2u^3}{3b}$$

Recall, that $u=\sqrt{c}$, $k_4=a$ and $k_5=b$:

$$\int \frac{c^2}{k_4 - k_5 c^{3/2}}\, dc = -\frac{2k_4}{3{k_5}^2}\, ln\left(k_4 - k_5 c^{3/2}\right) - \frac{2c^{3/2}}{3k_5}$$

Therefore:

$$t = -\int_{c_0}^{c} \frac{c^2}{k_4 - k_5 c^{3/2}}\, dc = \int_{c}^{c_0} -\frac{2k_4}{3{k_5}^2}\, ln\left(k_4 - k_5 c^{3/2}\right) - \frac{2c^{3/2}}{3k_5}$$

Given that $c_0 = 0$ the integration could be resolved as follows:

$$t = -\frac{2k_4}{3{k_5}^2}\, ln\left(k_4 - k_5 c^{3/2}\right) - \frac{2c^{3/2}}{3k_5} + \frac{2k_4}{3{k_5}^2} ln\, k_4$$

Simplify:

$$t = -\frac{2k_4}{3{k_5}^2}\, ln\, k_4 \left(\frac{k_4 - k_5 c^{3/2}}{k_4}\right) - \frac{2c^{3/2}}{3k_5} + \frac{2k_4}{3{k_5}^2} ln\, k_4$$

Applying $ln\, ab = ln\, a + ln\, b$:

$$t = -\frac{2k_4}{3{k_5}^2}\, ln\left(1 - \frac{k_5}{k_4} c^{3/2}\right) - \frac{2c^{3/2}}{3k_5} - \frac{2k_4}{3{k_5}^2} ln\, k_4 + \frac{2k_4}{3{k_5}^2} ln\, k_4$$

$$t = -\frac{2k_4}{3{k_5}^2}\, ln\left(1 - \frac{k_5}{k_4} c^{3/2}\right) - \frac{2c^{3/2}}{3k_5}$$

The above expression could be rewritten as equation 4-8:

$$t = k_6 \ln(1 - k_7 c^{3/2}) + k_8 c^{3/2}$$

where $k_6 = -2k_4/3k_5^2$,$k_7 = k_5 / k_4$ and $k_8 = -2/3k_5$.

On the other hand, the equation 4-9 could be rewritten as:

$$r_{CO} = k_9^* + k_{12} c_{CO}$$

where $k_{9^*} = k_9 c_{CO_2}$ and $k_{12} = -k_{10} - k_{11}$.

Therefore:

$$-dt = \frac{dc}{k_9^* + k_{12} c_{CO}}$$

$$\int dt = -\int \frac{dc}{k_9^* + k_{12} c_{CO}}$$

Let $c_{CO} = x$, $k_9^* = b$ and $k_{12} = a$. Integral can be rewritten as:

$$\int \frac{dc}{k_9^* + k_{12} c_{CO}} = \int \frac{dx}{ax + b}$$

Integral of $\int \frac{dx}{ax+b}\ dv$ is $\frac{1}{a}\ ln\ (ax+b)$:

$$\int \frac{dc}{k_9^* + k_{12} c_{CO}} = \frac{1}{k_{12}} ln(k_9^* + k_{12} c_{CO})$$

Therefore:

$$t = -\int_{c_0}^{c} \frac{1}{k_{12}} ln(k_9^* + k_{12}c_{CO}) = \int_{c}^{c_0} \frac{1}{k_{12}} ln(k_9^* + k_{12}c_{CO})$$

Given that $c_0 = 0$ the integration could be resolved as follows:

$$t = \frac{1}{k_{12}} ln(k_9^* + k_{12}c_{CO}) - \frac{1}{k_{12}} ln(k_9^*) = \frac{ln(k_9^* + k_{12}c_{CO}) - ln(k_9^*)}{k_{12}}$$

$$k_{12}t = ln(k_9^* + k_{12}c_{CO}) - ln(k_9^*)$$

Applying *ln a/b = ln a - ln b*:

$$k_{12}t = ln\frac{(k_9^* + k_{12}c_{CO})}{k_9^*}$$

Simplify:

$$e^{k_{12}t} = \frac{(k_9^* + k_{12}c_{CO})}{k_9^*}$$

$$\frac{k_{12}c_{CO}}{k_9^*} + 1 = e^{k_{12}t}$$

Therefore, the formation rate of CO could be expressed as equation 4-11:

$$c_{CO} = \frac{k_9^*}{k_{12}}(e^{tk_{12}} - 1)$$

Replacing equation the 4-11 in equation 4-10, the formation rate of CH_4 could be expressed as equation 4-12.

References

Abayev, I, Zaban, A, Kytin, VG, Danilin, AA, Garcia-Belmonte, G & Bisquert, J 2007, 'Properties of the electronic density of states in TiO_2 nanoparticles surrounded with aqueous electrolyte', *Journal of Solid State Electrochemistry*, vol. 11, no. 5, pp. 647-653.

Abbott, D 2010, 'Keeping the Energy Debate Clean: How Do We Supply the World's Energy Needs?', *Proceedings of the IEEE*, vol. 98, no. 1, pp. 42-66.

Abu Bakar, F, Ruzicka, J-Y, Nuramdhani, I, Williamson, BE, Holzenkaempfer, M & Golovko, VB 2015, 'Investigation of the Photodegradation of Reactive Blue 19 on P-25 Titanium Dioxide: Effect of Experimental Parameters', *Australian Journal of Chemistry*, vol. 68, no. 3, pp. 471-480.

Adachi, S 1999, *Optical Properties of Crystalline and Amorphous Semiconductors*, Kluwer Academic Publishers, Norwell MA.

Adams, DM, Brus, L, Chidsey, CED, Creager, S, Creutz, C, Kagan, CR, Kamat, PV, Lieberman, M, Lindsay, S, Marcus, RA, Metzger, RM, Michel-Beyerle, ME, Miller, JR, Newton, MD, Rolison, DR, Sankey, O, Schanze, KS, Yardley, J & Zhu, X 2003, 'Charge Transfer on the Nanoscale: Current Status', *The Journal of Physical Chemistry B*, vol. 107, no. 28, pp. 6668-6697.

Anpo, M & Takeuchi, M 2003, 'The design and development of highly reactive titanium oxide photocatalysts operating under visible light irradiation', *Journal of Catalysis,* vol. 216, no. 1–2, pp. 505-516.

Anpo, M, Yamashita, H, Ichihashi, Y & Ehara, S 1995, 'Photocatalytic reduction of CO_2 with H_2O on various titanium oxide catalysts', *Journal of Electroanalytical Chemistry,* vol. 396, no. 1, pp. 21-26.

Aresta, M, Dibenedetto, A & Quaranta, E 2016, 'State of the art and perspectives in catalytic processes for CO_2 conversion into chemicals and fuels: The distinctive contribution of chemical catalysis and biotechnology', *Journal of Catalysis,* vol. 343, pp. 2-45.

Armaroli, T, Bécue, T & Gautier, S 2004, 'Diffuse Reflection Infrared Spectroscopy (Drifts): Application to the in Situ Analysis of Catalysts', *Oil & Gas Science and Technology - Rev. IFP,* vol. 59, no. 2, pp. 215-237.

Asahi, R, Morikawa, T, Ohwaki, T, Aoki, K & Taga, Y 2001, 'Visible-Light Photocatalysis in Nitrogen-Doped Titanium Oxides', *Science,* vol. 293, no. 5528, pp. 269-271.

Ayoub, M & Abdullah, AZ 2012, 'Critical review on the current scenario and significance of crude glycerol resulting from biodiesel industry towards more sustainable renewable energy industry', *Renewable and Sustainable Energy Reviews,* vol. 16, no. 5, pp. 2671-2686.

Bae, S, Kim, S, Lee, S & Choi, W 2014, 'Dye decolorization test for the activity assessment of visible light photocatalysts: Realities and limitations', *Catalysis Today,* vol. 224, pp. 21-28.

Ballari, MdlM, Brandi, R, Alfano, O & Cassano, A 2008a, 'Mass transfer limitations in photocatalytic reactors employing titanium dioxide suspensions. I. Concentration profiles in the bulk', *Chemical Engineering Journal,* vol. 136, no. 1, pp. 50-65.

Ballari, MdlM, Brandi, R, Alfano, O & Cassano, A 2008b, 'Mass transfer limitations in photocatalytic reactors employing titanium dioxide suspensions. II. External and internal particle constrains for the reaction', *Chemical Engineering Journal,* vol. 136, no. 2-3, pp. 242-255.

Baran, T, Wojtyła, S, Dibenedetto, A, Aresta, M & Macyk, W 2016, 'Photocatalytic Carbon Dioxide Reduction at p-Type Copper(I) Iodide', *ChemSusChem,* vol. 9, no. 20, pp. 2933-2938.

Bartholomew, CH & Farrauto, RJ 2005, 'Front Matter', in *Fundamentals of Industrial Catalytic Processes*, John Wiley & Sons, Inc., pp. 1-64.

Battiston, GA, Gerbasi, R, Gregori, A, Porchia, M, Cattarin, S & Rizzi, GA 2000, 'PECVD of amorphous TiO2 thin films: effect of growth temperature and plasma gas composition', *Thin Solid Films,* vol. 371, no. 1–2, pp. 126-131.

Bavykin, DV, Gordeev, SN, Moskalenko, AV, Lapkin, AA & Walsh, FC 2005, 'Apparent Two-Dimensional Behavior of TiO_2 Nanotubes Revealed by Light Absorption and Luminescence', *The Journal of Physical Chemistry B,* vol. 109, no. 18, pp. 8565-8569.

Beltrán, A, Gracia, L & Andrés, J 2006, 'Density Functional Theory Study of the Brookite Surfaces and Phase Transitions between Natural Titania Polymorphs', *The Journal of Physical Chemistry B,* vol. 110, no. 46, pp. 23417-23423.

Bloh, JZ, Dillert, R & Bahnemann, DW 2012, 'Designing Optimal Metal-Doped Photocatalysts: Correlation between Photocatalytic Activity, Doping Ratio, and Particle Size', *The Journal of Physical Chemistry C,* vol. 116, no. 48, pp. 25558-25562.

Bone, RA, Lee, DW & Norman, JM 1985, 'Epidermal cells functioning as lenses in leaves of tropical rain-forest shade plants', *Applied Optics,* vol. 24, no. 10, pp. 1408-1412.

Burda, C, Lou, Y, Chen, X, Samia, ACS, Stout, J & Gole, JL 2003, 'Enhanced Nitrogen Doping in TiO_2 Nanoparticles', Nano Letters, vol. 3, no. 8, pp. 1049-1051.

Calliari, L, Fanchenko, S & Filippi, M 2007, 'Plasmon features in electron energy loss spectra from carbon materials', *Carbon,* vol. 45, no. 7, pp. 1410-1418.

Caporali, S, Bardi, U & Lavacchi, A 2006, 'X-ray photoelectron spectroscopy and low energy ion scattering studies on 1-buthyl-3-methyl-imidazolium bis(trifluoromethane) sulfonimide', *Journal of Electron Spectroscopy and Related Phenomena,* vol. 151, no. 1, pp. 4-8.

Cargnello, M, Doan-Nguyen, VVT, Gordon, TR, Diaz, RE, Stach, EA, Gorte, RJ, Fornasiero, P & Murray, CB 2013, 'Control of Metal Nanocrystal Size Reveals Metal-Support Interface Role for Ceria Catalysts', *Science,* vol. 341, no. 6147, pp. 771-773.

Cargnello, M, Montini, T, Smolin, SY, Priebe, JB, Delgado Jaén, JJ, Doan-Nguyen, VVT, McKay, IS, Schwalbe, JA, Pohl, M-M, Gordon, TR, Lu, Y, Baxter, JB, Brückner, A, Fornasiero, P & Murray, CB 2016, 'Engineering titania nanostructure to tune and improve its photocatalytic activity', *Proceedings of the National Academy of Sciences,* vol. 113, no. 15, pp. 3966-3971.

Carroll, JJ, Slupsky, JD & Mather, AE 1991, 'The Solubility of Carbon Dioxide in Water at Low Pressure', *Journal of Physical and Chemical Reference Data,* vol. 20, no. 6, pp. 1201-1209.

Centi, G & Perathoner, S 2009, 'Opportunities and prospects in the chemical recycling of carbon dioxide to fuels', *Catalysis Today,* vol. 148, no. 3–4, pp. 191-205.

Chen, A, Qian, J, Chen, Y, Lu, X, Wang, F & Tang, Z 2013, 'Enhanced sunlight photocatalytic activity of porous TiO_2 hierarchical nanosheets derived from petal template', *Powder Technology,* vol. 249, no. 0, pp. 71-76.

Chen, G, Li, S, Jiao, F & Yuan, Q 2007, 'Catalytic dehydration of bioethanol to ethylene over TiO_2/γ-Al2O3 catalysts in microchannel reactors', *Catalysis Today,* vol. 125, no. 1–2, pp. 111-119.

Chen, J, Zhang, G, Luo, B, Sun, D, Yan, X & Xue, Q 2011, 'Surface amorphization and deoxygenation of graphene oxide paper by Ti ion implantation', *Carbon,* vol. 49, no. 9, pp. 3141-3147.

Chen, X, Glans, P-A, Qiu, X, Dayal, S, Jennings, WD, Smith, KE, Burda, C & Guo, J 2008, 'X-ray spectroscopic study of the electronic structure of visible-light responsive N-, C- and S-doped TiO_2', *Journal of Electron Spectroscopy and Related Phenomena,* vol. 162, no. 2, pp. 67-73.

Chen, X & Mao, SS 2007, 'Titanium dioxide nanomaterials: Synthesis, properties, modifications and applications', *Chemical Reviews,* vol. 107, no. 7, pp. 2891-2959.

Cheng, C, Karuturi, SK, Liu, L, Liu, J, Li, H, Su, LT, Tok, AIY & Fan, HJ 2012, 'Quantum-Dot-Sensitized TiO_2 Inverse Opals for Photoelectrochemical Hydrogen Generation', *Small*, vol. 8, no. 1, pp. 37-42.

Cheng, H, Wang, J, Zhao, Y & Han, X 2014, 'Effect of phase composition, morphology, and specific surface area on the photocatalytic activity of TiO_2 nanomaterials', *RSC Advances*, vol. 4, no. 87, pp. 47031-47038.

Choi, W, Termin, A & Hoffmann, MR 1994, 'The Role of Metal Ion Dopants in Quantum-Sized TiO_2: Correlation between Photoreactivity and Charge Carrier Recombination Dynamics', *The Journal of Physical Chemistry*, vol. 98, no. 51, pp. 13669-13679.

Colombo, DP & Bowman, RM 1996, 'Does Interfacial Charge Transfer Compete with Charge Carrier Recombination? A Femtosecond Diffuse Reflectance Investigation of TiO2 Nanoparticles', *The Journal of Physical Chemistry*, vol. 100, no. 47, pp. 18445-18449.

Colón, G, Maicu, M, Hidalgo, MC & Navío, JA 2006, 'Cu-doped TiO_2 systems with improved photocatalytic activity', *Applied Catalysis B: Environmental*, vol. 67, no. 1–2, pp. 41-51.

Cong, Y, Zhang, J, Chen, F & Anpo, M 2007, 'Synthesis and Characterization of Nitrogen-Doped TiO_2 Nanophotocatalyst with High Visible Light Activity', *The Journal of Physical Chemistry C*, vol. 111, no. 19, pp. 6976-6982.

Corma, A, de la Torre, O, Renz, M & Villandier, N 2011, 'Production of High-Quality Diesel from Biomass Waste Products', *Angewandte Chemie International Edition*, vol. 50, no. 10, pp. 2375-2378.

Corma, A & Garcia, H 2013, 'Photocatalytic reduction of CO_2 for fuel production: Possibilities and challenges', *Journal of Catalysis*, vol. 308, no. 0, pp. 168-175.

Deng, L, Wang, S, Liu, D, Zhu, B, Huang, W, Wu, S & Zhang, S 2009, 'Synthesis, Characterization of Fe-doped TiO_2 Nanotubes with High Photocatalytic Activity', *Catalysis Letters*, vol. 129, no. 3, pp. 513-518.

Dey, GR 2007, 'Chemical Reduction of CO_2 to Different Products during Photo Catalytic Reaction on TiO_2 under Diverse Conditions: an Overview', *Journal of Natural Gas Chemistry*, vol. 16, no. 3, pp. 217-226.

Dimitrijevic, NM, Shkrob, IA, Gosztola, DJ & Rajh, T 2012, 'Dynamics of Interfacial Charge Transfer to Formic Acid, Formaldehyde, and Methanol on the Surface of TiO2 Nanoparticles and Its Role in Methane Production', *The Journal of Physical Chemistry C*, vol. 116, no. 1, pp. 878-885.

Dimitrijevic, NM, Vijayan, BK, Poluektov, OG, Rajh, T, Gray, KA, He, H & Zapol, P 2011, 'Role of Water and Carbonates in Photocatalytic Transformation of CO_2 to CH_4 on Titania', *Journal of the American Chemical Society,* vol. 133, no. 11, pp. 3964-3971.

Drnovšek, N, Daneu, N, Rečnik, A, Mazaj, M, Kovač, J & Novak, S 2009, 'Hydrothermal synthesis of a nanocrystalline anatase layer on Ti6A_4V implants', *Surface and Coatings Technology,* vol. 203, no. 10–11, pp. 1462-1468.

Drzewiecka-Matuszek, A, Skalna, A, Karocki, A, Stochel, G & Fiedor, L 2005, 'Effects of heavy central metal on the ground and excited states of chlorophyll', *JBIC Journal of Biological Inorganic Chemistry,* vol. 10, no. 5, pp. 453-462.

Dvoranová, D, Brezová, V, Mazúr, M & Malati, MA 2002, 'Investigations of metal-doped titanium dioxide photocatalysts', *Applied Catalysis B: Environmental,* vol. 37, no. 2, pp. 91-105.

Ellis, JR & Leech, RM 1985, 'Cell size and chloroplast size in relation to chloroplast replication in light-grown wheat leaves', *Planta,* vol. 165, no. 1, pp. 120-125.

Etacheri, V, Di Valentin, C, Schneider, J, Bahnemann, D & Pillai, SC 2015, 'Visible-light activation of TiO_2 photocatalysts: Advances in theory and experiments', *Journal of Photochemistry and Photobiology C: Photochemistry Reviews,* vol. 25, pp. 1-29.

Farsinezhad, S, Sharma, H & Shankar, K 2015, 'Interfacial band alignment for photocatalytic charge separation in TiO_2 nanotube arrays coated with CuPt nanoparticles', *Physical Chemistry Chemical Physics*, vol. 17, no. 44, pp. 29723-29733.

Fort, CI, Pap, Z, Indrea, E, Baia, L, Danciu, V & Popa, M 2014, 'Pt/N–TiO_2 Aerogel Composites Used for Hydrogen Production Via Photocatalysis Process', *Catalysis Letters*, vol. 144, no. 11, pp. 1955-1961.

Fox, MA & Dulay, MT 1993, 'Heterogeneous photocatalysis', *Chemical Reviews*, vol. 93, no. 1, pp. 341-357.

Freund, HJ & Roberts, MW 1996, 'Surface chemistry of carbon dioxide', *Surface Science Reports*, vol. 25, no. 8, pp. 225-273.

Furube, A, Asahi, T, Masuhara, H, Yamashita, H & Anpo, M 1999, 'Charge Carrier Dynamics of Standard TiO_2 Catalysts Revealed by Femtosecond Diffuse Reflectance Spectroscopy', *The Journal of Physical Chemistry B*, vol. 103, no. 16, pp. 3120-3127.

Ganesh, I, Kumar, PP, Annapoorna, I, Sumliner, JM, Ramakrishna, M, Hebalkar, NY, Padmanabham, G & Sundararajan, G 2014, 'Preparation and characterization of Cu-doped TiO_2 materials for electrochemical, photoelectrochemical, and photocatalytic applications', *Applied Surface Science*, vol. 293, pp. 229-247.

Gattrell, M, Gupta, N & Co, A 2006, 'A review of the aqueous electrochemical reduction of CO_2 to hydrocarbons at copper', *Journal of Electroanalytical Chemistry*, vol. 594, no. 1, pp. 1-19.

Górska, P, Zaleska, A, Kowalska, E, Klimczuk, T, Sobczak, JW, Skwarek, E, Janusz, W & Hupka, J 2008, 'TiO_2 photoactivity in vis and UV light: The influence of calcination temperature and surface properties', *Applied Catalysis B: Environmental*, vol. 84, no. 3–4, pp. 440-447.

Gupta, SM & Tripathi, M 2011, 'A review of TiO_2 nanoparticles', *Chinese Science Bulletin*, vol. 56, no. 16, pp. 1639-1657.

György, E, Pérez del Pino, A, Serra, P & Morenza, JL 2003, 'Depth profiling characterisation of the surface layer obtained by pulsed Nd:YAG laser irradiation of titanium in nitrogen', *Surface and Coatings Technology*, vol. 173, no. 2–3, pp. 265-270.

Habisreutinger, SN, Schmidt-Mende, L & Stolarczyk, JK 2013, 'Photocatalytic reduction of CO_2 on TiO_2 and other semiconductors', *Angew Chem Int Ed Engl*, vol. 52, no. 29, pp. 7372-7408.

Halmann, M 1983, '15 - Photochemical Fixation of Carbon Dioxide A2 - Grätzel, Michael', in *Energy Resources Through Photochemistry and Catalysis*, Academic Press, pp. 507-534.

Hanaor, DAH & Sorrell, CC 2011, 'Review of the anatase to rutile phase transformation', *Journal of Materials Science,* vol. 46, no. 4, pp. 855-874.

Hao, WC, Zheng, SK, Wang, C & Wang, TM 2002, 'Comparison of the photocatalytic activity of TiO_2 powder with different particle size', *Journal of Materials Science Letters,* vol. 21, no. 20, pp. 1627-1629.

Harold P. Klug, LEA 1974, *X-Ray Diffraction Procedures: For Polycrystalline and Amorphous Materials*, Wiley, London.

He, H, Zapol, P & Curtiss, LA 2012, 'Computational screening of dopants for photocatalytic two-electron reduction of CO_2 on anatase (101) surfaces', *Energy & Environmental Science,* vol. 5, no. 3, pp. 6196-6205.

He, Z, Que, W & He, Y 2013, 'Synthesis and characterization of bioinspired hierarchical mesoporous TiO_2 photocatalysts', *Materials Letters,* vol. 94, pp. 136-139.

Higgins, S 2010, 'Regarding ruthenium', *Nat Chem,* vol. 2, no. 12, pp. 1100-1100.

Hong, J, Zhang, W, Ren, J & Xu, R 2013, 'Photocatalytic reduction of CO_2: a brief review on product analysis and systematic methods', *Analytical Methods,* vol. 5, no. 5, pp. 1086-1097.

Hörtensteiner, S & Kräutler, B 2011, 'Chlorophyll breakdown in higher plants', *Biochimica et Biophysica Acta (BBA) - Bioenergetics*, vol. 1807, no. 8, pp. 977-988.

Howe, RF & Grätzel, M 1985, 'EPR observation of trapped electrons in colloidal TiO2', *Journal of Physical Chemistry*, vol. 89, no. 21, pp. 4495-4499.

Howe, RF & Grätzel, M 1987, 'EPR study of hydrated anatase under UV irradiation', *Journal of Physical Chemistry*, vol. 91, no. 14, pp. 3906-3909.

Huang, X, Zhao, Z, Chen, Y, Chiu, C-Y, Ruan, L, Liu, Y, Li, M, Duan, X & Huang, Y 2014, 'High Density Catalytic Hot Spots in Ultrafine Wavy Nanowires', *Nano Letters*, vol. 14, no. 7, pp. 3887-3894.

Huang, Y, Kannan, P, Zhang, L, Rong, Y, Dai, L, Huang, R & Chen, T 2015, 'Close-packed assemblies of discrete tiny silver nanoparticles on triangular gold nanoplates as a high performance SERS probe', *RSC Advances*, vol. 5, no. 115, pp. 94849-94854.

Huber, GW & Corma, A 2007, 'Synergies between Bio- and Oil Refineries for the Production of Fuels from Biomass', *Angewandte Chemie International Edition*, vol. 46, no. 38, pp. 7184-7201.

Hurum, DC, Agrios, AG, Gray, KA, Rajh, T & Thurnauer, MC 2003, 'Explaining the Enhanced Photocatalytic Activity of Degussa P25 Mixed-Phase TiO_2 Using EPR', *The Journal of Physical Chemistry B,* vol. 107, no. 19, pp. 4545-4549.

Hwang, DS, Lee, NH, Lee, DY, Song, JS, Shin, SH & Kim, SJ 2006, 'Phase transition control of nanostructured TiO_2 powders with additions of various metal chlorides', *Smart Materials and Structures,* vol. 15, no. 1, p. S74.

Ikeue, K, Nozaki, S, Ogawa, M & Anpo, M 2002, 'Characterization of self-standing Ti-containing porous silica thin films and their reactivity for the photocatalytic reduction of CO_2 with H_2O', *Catalysis Today,* vol. 74, no. 3–4, pp. 241-248.

Ikeue, K, Yamashita, H, Anpo, M & Takewaki, T 2001, 'Photocatalytic Reduction of CO_2 with H_2O on Ti−β Zeolite Photocatalysts: Effect of the Hydrophobic and Hydrophilic Properties', *The Journal of Physical Chemistry B,* vol. 105, no. 35, pp. 8350-8355.

Indrakanti, VP, Kubicki, JD & Schobert, HH 2009, 'Photoinduced activation of CO_2 on Ti-based heterogeneous catalysts: Current state, chemical physics-based insights and outlook', *Energy & Environmental Science,* vol. 2, no. 7, pp. 745-758.

Inoue, T, Fujishima, A, Konishi, S & Honda, K 1979, 'Photoelectrocatalytic reduction of carbon dioxide in aqueous suspensions of semiconductor powers', *Nature,* vol. 277, no. 5698, pp. 637-638.

Irie, H, Watanabe, Y & Hashimoto, K 2003, 'Nitrogen-Concentration Dependence on Photocatalytic Activity of $TiO_{2-x}N_x$ Powders', *The Journal of Physical Chemistry B,* vol. 107, no. 23, pp. 5483-5486.

Jiang, J, Oberdörster, G, Elder, A, Gelein, R, Mercer, P & Biswas, P 2008, 'Does Nanoparticle Activity Depend upon Size and Crystal Phase?', *Nanotoxicology,* vol. 2, no. 1, pp. 33-42.

Jing, D, Jing, L, Liu, H, Yao, S & Guo, L 2013, 'Photocatalytic Hydrogen Production from Refinery Gas over a Fluidized-Bed Reactor I: Numerical Simulation', *Industrial & Engineering Chemistry Research,* vol. 52, no. 5, pp. 1982-1991.

Kaneco, S, Shimizu, Y, Ohta, K & Mizuno, T 1998, 'Photocatalytic reduction of high pressure carbon dioxide using TiO_2 powders with a positive hole scavenger', *Journal of Photochemistry and Photobiology A: Chemistry,* vol. 115, no. 3, pp. 223-226.

Kar, P, Farsinezhad, S, Mahdi, N, Zhang, Y, Obuekwe, U, Sharma, H, Shen, J, Semagina, N & Shankar, K 2016, 'Enhanced CH_4 yield by photocatalytic CO_2 reduction using TiO_2 nanotube

arrays grafted with Au, Ru, and ZnPd nanoparticles', *Nano Research,* vol. 9, no. 11, pp. 3478-3493.

Kho, YK, Iwase, A, Teoh, WY, Mädler, L, Kudo, A & Amal, R 2010, 'Photocatalytic H_2 Evolution over TiO_2 Nanoparticles. The Synergistic Effect of Anatase and Rutile', *The Journal of Physical Chemistry C,* vol. 114, no. 6, pp. 2821-2829.

Khorasani-Motlagh, M, Noroozifar, M & Yousefi, M 2011, 'A Simple New Method to Synthesize Nanocrystalline Ruthenium Dioxide in the Presence of Octanoic Acid As Organic Surfactant', *International Journal of Nanoscience and Nanotechnology,* vol. 7, no. 4, pp. 167-172.

Kisch, H 2013, 'Semiconductor Photocatalysis—Mechanistic and Synthetic Aspects', *Angewandte Chemie International Edition,* vol. 52, no. 3, pp. 812-847.

K. Kočí, LO, O. ŠOLCOVÁ 2010, 'Kinetic study of photocatalytic reduction of CO_2 over TiO_2', *Chemical and Process Engineering,* vol. Vol. 31, no. z. 3, pp. 395--407.

Kočí, K, Matějů, K, Obalová, L, Krejčíková, S, Lacný, Z, Plachá, D, Čapek, L, Hospodková, A & Šolcová, O 2010, 'Effect of silver doping on the TiO_2 for photocatalytic reduction of CO_2', *Applied Catalysis B: Environmental,* vol. 96, no. 3–4, pp. 239-244.

Kočí, K, Obalová, L, Matějová, L, Plachá, D, Lacný, Z, Jirkovský, J & Šolcová, O 2009, 'Effect of TiO_2 particle size on the photocatalytic reduction of CO_2', *Applied Catalysis B: Environmental,* vol. 89, no. 3–4, pp. 494-502.

Kočí, K, Obalová, L, Plachá, D & Lacný, Z 2008, 'Effect of temperature, pressure and volume of reacting phase on photocatalytic CO_2 reduction on suspended nanocrystalline TiO_2', *Collection of Czechoslovak Chemical Communications,* vol. 73, no. 8-9, pp. 1192-1204.

Kočí, K, Reli, M, Kozák, O, Lacný, Z, Plachá, D, Praus, P & Obalová, L 2011, 'Influence of reactor geometry on the yield of CO_2 photocatalytic reduction', *Catalysis Today,* vol. 176, no. 1, pp. 212-214.

Kötz, ER & Stucki, S 1987, 'Ruthenium dioxide as a hydrogen-evolving cathode', *Journal of Applied Electrochemistry,* vol. 17, no. 6, pp. 1190-1197.

Krishnan, R 2007, 'Fundamentals of Semiconductor Electrochemistry and Photoelectrochemistry', in *Encyclopedia of Electrochemistry*, vol. 6, Wiley-VCH Verlag GmbH & Co. KGaA, pp. 34-39.

Ku, Y, Lee, W-H & Wang, W-Y 2004, 'Photocatalytic reduction of carbonate in aqueous solution by UV/TiO_2 process', *Journal of Molecular Catalysis A: Chemical,* vol. 212, no. 1–2, pp. 191-196.

Küpper, H, Küpper, F & Spiller, M 1998, 'In situ detection of heavy metal substituted chlorophylls in water plants', *Photosynthesis Research,* vol. 58, no. 2, pp. 123-133.

Lang, J-w, Yan, X-b, Liu, W-w, Wang, R-t & Xue, Q-j 2012, 'Influence of nitric acid modification of ordered mesoporous carbon materials on their capacitive performances in different aqueous electrolytes', *Journal of Power Sources,* vol. 204, pp. 220-229.

Lei, M, Sakae, T, Shoichi, T, Kenji, K & Masaki, T 2004, 'Fabrication and Photoluminescence of Rutile-TiO_2 Nanorods', *Japanese Journal of Applied Physics,* vol. 43, no. 10R, p. 7342.

Li, X, Fan, T, Zhou, H, Chow, SK, Zhang, W, Zhang, D, Guo, Q & Ogawa, H 2009, 'Enhanced light-harvesting and photocatalytic properties in morph-TiO_2 from green-leaf biotemplates', *Advanced Functional Materials,* vol. 19, no. 1, pp. 45-56.

Li, XH, Liu, WM & Li, HL 2005, 'Template synthesis of well-aligned titanium dioxide nanotubes', *Applied Physics A,* vol. 80, no. 2, pp. 317-320.

Lin, H, Huang, CP, Li, W, Ni, C, Shah, SI & Tseng, Y-H 2006, 'Size dependency of nanocrystalline TiO_2 on its optical property and photocatalytic reactivity exemplified by 2-chlorophenol', *Applied Catalysis B: Environmental,* vol. 68, no. 1–2, pp. 1-11.

Litter, MI 1999, 'Heterogeneous photocatalysis: Transition metal ions in photocatalytic systems', *Applied Catalysis B: Environmental,* vol. 23, no. 2–3, pp. 89-114.

Liu, G, Wang, L, Yang, HG, Cheng, H-M & Lu, GQ 2010, 'Titania-based photocatalysts-crystal growth, doping and heterostructuring', *Journal of Materials Chemistry*, vol. 20, no. 5, pp. 831-843.

Liu, J, Ren, Z, Alfantazi, A & Asselin, E 2016, 'Turning Bulk Titanium into Rutile Nanorods in One Step: Synthesis, Mechanism, and Application', *Crystal Growth & Design*, vol. 16, no. 3, pp. 1583-1590.

Liu, S, Zhao, Z & Wang, Z 2007, 'Photocatalytic reduction of carbon dioxide using sol-gel derived titania-supported CoPc catalysts', *Photochemical and Photobiological Sciences*, vol. 6, no. 6, pp. 695-700.

Lo, C-C, Hung, C-H, Yuan, C-S & Wu, J-F 2007, 'Photoreduction of carbon dioxide with H_2 and H_2O over TiO_2 and ZrO_2 in a circulated photocatalytic reactor', *Solar Energy Materials and Solar Cells*, vol. 91, no. 19, pp. 1765-1774.

Long, M, Cai, W, Chen, H & Xu, J 2007, 'Preparation, characterization and photocatalytic activity of visible light driven chlorine-doped TiO_2', *Frontiers of Chemistry in China*, vol. 2, no. 3, pp. 278-282.

Lu, AH & Schüth, F 2006, 'Nanocasting: a versatile strategy for creating nanostructured porous materials', *Advanced Materials*, vol. 18, no. 14, pp. 1793-1805.

Macdonald, IR, Rhydderch, S, Holt, E, Grant, N, Storey, JMD & Howe, RF 2012, 'EPR studies of electron and hole trapping in titania photocatalysts', *Catalysis Today,* vol. 182, no. 1, pp. 39-45.

MacWan, DP, Dave, PN & Chaturvedi, S 2011, 'A review on nano-TiO_2 sol-gel type syntheses and its applications', *Journal of Materials Science,* vol. 46, no. 11, pp. 3669-3686.

Maginn, EJ 2010, 'What to Do with CO_2', *The Journal of Physical Chemistry Letters,* vol. 1, no. 24, pp. 3478-3479.

Malinowska, B, Walendziewski, J, Robert, D, Weber, JV & Stolarski, M 2003, 'Titania aerogels: Preparation and photocatalytic tests', *International Journal of Photoenergy,* vol. 5, no. 3, pp. 147-152.

Mathew, A & Pradeep, T 2014, 'Noble Metal Clusters: Applications in Energy, Environment, and Biology', *Particle & Particle Systems Characterization,* vol. 31, no. 10, pp. 1017-1053.

Mikkelsen, M, Jorgensen, M & Krebs, FC 2010, 'The teraton challenge. A review of fixation and transformation of carbon dioxide', *Energy & Environmental Science,* vol. 3, no. 1, pp. 43-81.

Milczarek, G, Ciszewski, A & Stepniak, I 2011, 'Oxygen-doped activated carbon fiber cloth as electrode material for electrochemical capacitor', *Journal of Power Sources,* vol. 196, no. 18, pp. 7882-7885.

Mizuno, T, Adachi, K, Ohta, K & Saji, A 1996, 'Effect of CO_2 pressure on photocatalytic reduction of CO_2 using TiO_2 in aqueous solutions', *Journal of Photochemistry and Photobiology A: Chemistry,* vol. 98, no. 1, pp. 87-90.

Mogyorósi, K, Kmetykó, Á, Czirbus, N, Veréb, G, Sipos, P & Dombi, A 2009, 'Comparison of the substrate dependent performance of Pt-, Au- and Ag-doped TiO_2 photocatalysts in H_2-production and in decomposition of various organics', *Reaction Kinetics and Catalysis Letters,* vol. 98, no. 2, p. 215.

Momentive, viewed 2017, <https://www.momentive.com/en-US/categories/quartz/pressure-determination/#.>.

Mori, K, Yamashita, H & Anpo, M 2012, 'Photocatalytic reduction of CO_2 with H_2O on various titanium oxide photocatalysts', *RSC Advances,* vol. 2, no. 8, pp. 3165-3172.

Muggli, DS, McCue, JT & Falconer, JL 1998, 'Mechanism of the Photocatalytic Oxidation of Ethanol on TiO_2', *Journal of Catalysis,* vol. 173, no. 2, pp. 470-483.

Mustárdy, L 1996, *Oxygenic Photosynthesis: The Light Reactions*, Kluwer Academic Publishers, Dordrecht, Netherlands.

Mutin, PH & Vioux, A 2009, 'Nonhydrolytic Processing of Oxide-Based Materials: Simple Routes to Control Homogeneity, Morphology, and Nanostructure', *Chemistry of Materials*, vol. 21, no. 4, pp. 582-596.

Nadeem, MA, Waterhouse, GIN & Idriss, H 2016, 'A study of ethanol reactions on O_2-treated Au/TiO_2. Effect of support and metal loading on reaction selectivity', *Surface Science*, vol. 650, pp. 40-50.

Nelson, N & Ben-Shem, A 2004, 'The complex architecture of oxygenic photosynthesis', *Nat Rev Mol Cell Biol*, vol. 5, no. 12, pp. 971-982.

Ni, M, Leung, MKH, Leung, DYC & Sumathy, K 2007, 'A review and recent developments in photocatalytic water-splitting using for hydrogen production', *Renewable and Sustainable Energy Reviews*, vol. 11, no. 3, pp. 401-425.

Niinemets, Ü & Sack, L 2006, 'Structural determinants of leaf light-harvesting capacity and photosynthetic potentials', in K Esser, U Lüttge, W Beyschlag & J Murata (eds), *Progress in Botany*, Springer Berlin Heidelberg, Berlin, Heidelberg, pp. 385-419.

Nishimura, M, Graham, D & Akazawa, T 1976, 'Isolation of Intact Chloroplasts and Other Cell Organelles from Spinach Leaf Protoplasts', *Plant Physiology,* vol. 58, no. 3, pp. 309-314.

Nowotny, MK, Sheppard, LR, Bak, T & Nowotny, J 2008, 'Defect Chemistry of Titanium Dioxide. Application of Defect Engineering in Processing of TiO_2-Based Photocatalysts', *The Journal of Physical Chemistry C,* vol. 112, no. 14, pp. 5275-5300.

Ohno, T, Akiyoshi, M, Umebayashi, T, Asai, K, Mitsui, T & Matsumura, M 2004, 'Preparation of S-doped TiO_2 photocatalysts and their photocatalytic activities under visible light', *Applied Catalysis A: General,* vol. 265, no. 1, pp. 115-121.

Ohno, T, Tanigawa, F, Fujihara, K, Izumi, S & Matsumura, M 1999, 'Photocatalytic oxidation of water by visible light using ruthenium-doped titanium dioxide powder', *Journal of Photochemistry and Photobiology A: Chemistry,* vol. 127, no. 1–3, pp. 107-110.

Ohwada, M, Kimoto, K, Mizoguchi, T, Ebina, Y & Sasaki, T 2013, 'Atomic structure of titania nanosheet with vacancies', *Scientific Reports,* vol. 3, p. 2801.

Okada, K, Yamamoto, N, Kameshima, Y, Yasumori, A & MacKenzie, KJD 2001, 'Effect of Silica Additive on the Anatase-to-Rutile Phase Transition', *Journal of the American Ceramic Society,* vol. 84, no. 7, pp. 1591-1596.

Over, H 2002, 'Ruthenium dioxide, a fascinating material for atomic scale surface chemistry', *Applied Physics A,* vol. 75, no. 1, pp. 37-44.

Over, H 2012, 'Surface Chemistry of Ruthenium Dioxide in Heterogeneous Catalysis and Electrocatalysis: From Fundamental to Applied Research', *Chemical Reviews,* vol. 112, no. 6, pp. 3356-3426.

Ovoshchnikov, DS, Donoeva, BG & Golovko, VB 2015, 'Visible-Light-Driven Aerobic Oxidation of Amines to Nitriles over Hydrous Ruthenium Oxide Supported on TiO_2', *ACS Catalysis,* vol. 5, no. 1, pp. 34-38.

Paramasivam, I, Jha, H, Liu, N & Schmuki, P 2012, 'A Review of Photocatalysis using Self-organized TiO_2 Nanotubes and Other Ordered Oxide Nanostructures', *Small,* vol. 8, no. 20, pp. 3073-3103.

Paszkiewicz, M, Łuczak, J, Lisowski, W, Patyk, P & Zaleska-Medynska, A 2016, 'The ILs-assisted solvothermal synthesis of TiO_2 spheres: The effect of ionic liquids on morphology and photoactivity of TiO_2', *Applied Catalysis B: Environmental,* vol. 184, pp. 223-237.

Peng, C, Lang, J, Xu, S & Wang, X 2014, 'Oxygen-enriched activated carbons from pomelo peel in high energy density supercapacitors', *RSC Advances,* vol. 4, no. 97, pp. 54662-54667.

Poulson, ME & Vogelmann, TC 1990, 'Epidermal focussing and effects upon photosynthetic light-harvesting in leaves of Oxalis', *Plant, Cell & Environment,* vol. 13, no. 8, pp. 803-811.

Press, WH, Teukolsky, SA, Vetterling, WT & Flannery, BP 2007, *Numerical Recipes 3rd Edition: The Art of Scientific Computing*, Cambridge University Press.

Rehman, S, Ullah, R, Butt, AM & Gohar, ND 2009, 'Strategies of making TiO_2 and ZnO visible light active', *Journal of Hazardous Materials,* vol. 170, no. 2–3, pp. 560-569.

Ren, W, Ai, Z, Jia, F, Zhang, L, Fan, X & Zou, Z 2007, 'Low temperature preparation and visible light photocatalytic activity of mesoporous carbon-doped crystalline TiO_2', *Applied Catalysis B: Environmental,* vol. 69, no. 3–4, pp. 138-144.

Reñones, P, Moya, A, Fresno, F, Collado, L, Vilatela, JJ & de la Peña O'Shea, VA 2016, 'Hierarchical TiO2 nanofibres as photocatalyst for CO2 reduction: Influence of morphology and phase composition on catalytic activity', *Journal of CO_2 Utilization,* vol. 15, pp. 24-31.

Robinson, SP 1983, 'Isolation of intact chloroplasts with high CO_2 fixation capacity from sugarbeet leaves containing calcium oxalate', *Photosynthesis Research,* vol. 4, no. 3, pp. 281-287.

Roy, SC, Varghese, OK, Paulose, M & Grimes, CA 2010, 'Toward Solar Fuels: Photocatalytic Conversion of Carbon Dioxide to Hydrocarbons', *ACS Nano,* vol. 4, no. 3, pp. 1259-1278.

Ruban, AV, Johnson, MP & Duffy, CDP 2011, 'Natural light harvesting: principles and environmental trends', *Energy & Environmental Science,* vol. 4, no. 5, pp. 1643-1650.

Rudowska, Ł, Gieczewska, K, Mazur, R, Garstka, M & Mostowska, A 2012, 'Chloroplast biogenesis — Correlation between structure and function', *Biochimica et Biophysica Acta (BBA) - Bioenergetics,* vol. 1817, no. 8, pp. 1380-1387.

Rumak, I, Gieczewska, K, Kierdaszuk, B, Gruszecki, WI, Mostowska, A, Mazur, R & Garstka, M 2010, '3-D modelling of chloroplast structure under (Mg^{2+}) magnesium ion treatment. Relationship between thylakoid membrane arrangement and stacking', *Biochimica et Biophysica Acta (BBA) - Bioenergetics,* vol. 1797, no. 10, pp. 1736-1748.

Ruzicka, J-Y, Bakar, FA, Thomsen, L, Cowie, BC, McNicoll, C, Kemmitt, T, Brand, HEA, Ingham, B, Andersson, GG & Golovko, VB 2014, 'XPS and NEXAFS study of fluorine modified TiO_2 nano-ovoids reveals dependence of Ti^{3+} surface population on the modifying agent', *RSC Advances,* vol. 4, no. 40, pp. 20649-20658.

Ryden, WD, Lawson, AW & Sartain, CC 1970, 'Electrical Transport Properties of IrO_2 and RuO_2, *Physical Review B,* vol. 1, no. 4, pp. 1494-1500.

Sakai, N, Ebina, Y, Takada, K & Sasaki, T 2004, 'Electronic Band Structure of Titania Semiconductor Nanosheets Revealed by Electrochemical and Photoelectrochemical Studies', *Journal of the American Chemical Society,* vol. 126, no. 18, pp. 5851-5858.

Sanchez, C, Arribart, H & Giraud Guille, MM 2005, 'Biomimetism and bioinspiration as tools for the design of innovative materials and systems', *Nat Mater,* vol. 4, no. 4, pp. 277-288.

Sasaki, T, Ebina, Y, Kitami, Y, Watanabe, M & Oikawa, T 2001, 'Two-Dimensional Diffraction of Molecular Nanosheet Crystallites of Titanium Oxide', *The Journal of Physical Chemistry B,* vol. 105, no. 26, pp. 6116-6121.

Sasirekha, N, Basha, SJS & Shanthi, K 2006, 'Photocatalytic performance of Ru doped anatase mounted on silica for reduction of carbon dioxide', *Applied Catalysis B: Environmental,* vol. 62, no. 1–2, pp. 169-180.

Sato, H, Ono, K, Sasaki, T & Yamagishi, A 2003, 'First-Principles Study of Two-Dimensional Titanium Dioxides', *The Journal of Physical Chemistry B,* vol. 107, no. 36, pp. 9824-9828.

Schiavello, M 1997, *Heterogeneous Photocatalysis*, Wiley, pp. 117-125.

Schneider, J & Bahnemann, DW 2013, 'Undesired Role of Sacrificial Reagents in Photocatalysis', *The Journal of Physical Chemistry Letters,* vol. 4, no. 20, pp. 3479-3483.

Seitsonen, AP, Kim, YD, Knapp, M, Wendt, S & Over, H 2001, 'CO adsorption on the reduced RuO_2(110) surface: Energetics and structure', *Physical Review B,* vol. 65, no. 3, p. 035413.

Shannon, R 1976, 'Revised effective ionic radii and systematic studies of interatomic distances in halides and chalcogenides', *Acta Crystallographica Section A,* vol. 32, no. 5, pp. 751-767.

Shao, X, Lu, W, Zhang, R & Pan, F 2013, 'Enhanced photocatalytic activity of TiO_2-C hybrid aerogels for methylene blue degradation', *Scientific Reports,* vol. 3, p. 3018.

Sharma, SD, Singh, D, Saini, KK, Kant, C, Sharma, V, Jain, SC & Sharma, CP 2006, 'Sol–gel-derived super-hydrophilic nickel doped TiO_2 film as active photo-catalyst', *Applied Catalysis A: General,* vol. 314, no. 1, pp. 40-46.

Shimoni, E, Rav-Hon, O, Ohad, I, Brumfeld, V & Reich, Z 2005, 'Three-Dimensional Organization of Higher-Plant Chloroplast Thylakoid Membranes Revealed by Electron Tomography', *The Plant Cell,* vol. 17, no. 9, pp. 2580-2586.

Shin, H, Jung, HS, Hong, KS & Lee, J-K 2005, 'Crystal phase evolution of TiO_2 nanoparticles with reaction time in acidic solutions studied via freeze-drying method', *Journal of Solid State Chemistry,* vol. 178, no. 1, pp. 15-21.

Shkrob, IA, Dimitrijevic, NM, Marin, TW, He, H & Zapol, P 2012, 'Heteroatom-Transfer Coupled Photoreduction and Carbon Dioxide Fixation on Metal Oxides', *The Journal of Physical Chemistry C*, vol. 116, no. 17, pp. 9461-9471.

Sing, K & Williams, R 2004, 'Physisorption hysteresis loops and the characterization of nanoporous materials', *Adsorption Science & Technology*, vol. 22, no. 10, pp. 773-782.

Skandan, G, Chen, YJ, Glumac, N & Kear, BH 1999, 'Synthesis of oxide nanoparticles in low pressure flames', *Nanostructured Materials*, vol. 11, no. 2, pp. 149-158.

Skoog, DA, Holler, FJ & Crouch, SR 2017, *Principles of instrumental analysis*, Cengage learning.

Smirnova, N, Eremenko, A, Gayvoronskij, V, Petrik, I, Gnatyuk, Y, Krylova, G, Korchev, A & Chuiko, A 2004, 'Sol–Gel Processed Functional Nanosized TiO_2 and SiO_2-Based Films for Photocatalysts and Other Applications', *Journal of Sol-Gel Science and Technology*, vol. 32, no. 1, pp. 357-362.

Somani, M, Liauw, MA & Luss, D 1996, 'Hot spot formation on a catalyst', *Chemical Engineering Science*, vol. 51, no. 18, pp. 4259-4269.

Spurr, RA & Myers, H 1957, 'Quantitative Analysis of Anatase-Rutile Mixtures with an X-Ray Diffractometer', *Analytical Chemistry,* vol. 29, no. 5, pp. 760-762.

Stechel, EB & Miller, JE 2013, 'Re-energizing CO_2 to fuels with the sun: Issues of efficiency, scale, and economics', *Journal of CO_2 Utilization,* vol. 1, pp. 28-36.

Su, R, Bechstein, R, Sø, L, Vang, RT, Sillassen, M, Esbjörnsson, B, Palmqvist, A & Besenbacher, F 2011, 'How the Anatase-to-Rutile Ratio Influences the Photoreactivity of TiO_2', *The Journal of Physical Chemistry C,* vol. 115, no. 49, pp. 24287-24292.

Subrahmanyam, M, Kaneco, S & Alonso-Vante, N 1999, 'A screening for the photo reduction of carbon dioxide supported on metal oxide catalysts for C1–C3 selectivity', *Applied Catalysis B: Environmental,* vol. 23, no. 2–3, pp. 169-174.

Suoranta, T, Niemelä, M & Perämäki, P 2014, 'Comparison of digestion methods for the determination of ruthenium in catalyst materials', *Talanta,* vol. 119, pp. 425-429.

Suttiponparnit, K, Jiang, J, Sahu, M, Suvachittanont, S, Charinpanitkul, T & Biswas, P 2011, 'Role of Surface Area, Primary Particle Size, and Crystal Phase on Titanium Dioxide Nanoparticle Dispersion Properties', *Nanoscale Research Letters,* vol. 6, no. 1, pp. 27-27.

Suwarnkar, MB, Dhabbe, RS, Kadam, AN & Garadkar, KM 2014, 'Enhanced photocatalytic activity of Ag doped TiO_2 nanoparticles synthesized by a microwave assisted method', *Ceramics International*, vol. 40, no. 4, pp. 5489-5496.

Takahashi, Y & Matsuoka, Y 1988, 'Dip-coating of TiO_2 films using a sol derived from Ti(O-i-Pr)4-diethanolamine-H2O-i-PrOH system', *Journal of Materials Science*, vol. 23, no. 6, pp. 2259-2266.

Tan, SS, Zou, L & Hu, E 2008, 'Kinetic modelling for photosynthesis of hydrogen and methane through catalytic reduction of carbon dioxide with water vapour', *Catalysis Today*, vol. 131, no. 1–4, pp. 125-129.

Tan, TH, Scott, J, Ng, YH, Taylor, RA, Aguey-Zinsou, K-F & Amal, R 2016a, 'C–C Cleavage by Au/TiO_2 during Ethanol Oxidation: Understanding Bandgap Photoexcitation and Plasmonically Mediated Charge Transfer via Quantitative in Situ DRIFTS', *ACS Catalysis*, vol. 6, no. 12, pp. 8021-8029.

Tan, TH, Scott, J, Ng, YH, Taylor, RA, Aguey-Zinsou, K-F & Amal, R 2016b, 'Understanding Plasmon and Band Gap Photoexcitation Effects on the Thermal-Catalytic Oxidation of Ethanol by TiO_2-Supported Gold', *ACS Catalysis*, vol. 6, no. 3, pp. 1870-1879.

Tayade, RJ, Natarajan, TS & Bajaj, HC 2009, 'Photocatalytic Degradation of Methylene Blue Dye Using Ultraviolet Light Emitting Diodes', *Industrial & Engineering Chemistry Research,* vol. 48, no. 23, pp. 10262-10267.

Teoh, WY, Scott, JA & Amal, R 2012, 'Progress in Heterogeneous Photocatalysis: From Classical Radical Chemistry to Engineering Nanomaterials and Solar Reactors', *The Journal of Physical Chemistry Letters,* vol. 3, no. 5, pp. 629-639.

Testino, A, Bellobono, IR, Buscaglia, V, Canevali, C, D'Arienzo, M, Polizzi, S, Scotti, R & Morazzoni, F 2007, 'Optimizing the Photocatalytic Properties of Hydrothermal TiO_2 by the Control of Phase Composition and Particle Morphology. A Systematic Approach', *Journal of the American Chemical Society,* vol. 129, no. 12, pp. 3564-3575.

Todorova, N, Giannakopoulou, T, Romanos, G, Vaimakis, T, Yu, J & Trapalis, C 2008, 'Preparation of Fluorine-Doped Photocatalysts with Controlled Crystalline Structure', *International Journal of Photoenergy,* vol. 2008, p. 9.

Tseng, IH, Chang, W-C & Wu, JCS 2002, 'Photoreduction of CO_2 using sol–gel derived titania and titania-supported copper catalysts', *Applied Catalysis B: Environmental,* vol. 37, no. 1, pp. 37-48.

Uddin, MT, Nicolas, Y, Olivier, C, Toupance, T, Müller, MM, Kleebe, H-J, Rachut, K, Ziegler, J, Klein, A & Jaegermann, W 2013, 'Preparation of RuO_2/TiO_2 Mesoporous Heterostructures and Rationalization of Their Enhanced Photocatalytic Properties by Band Alignment Investigations', *The Journal of Physical Chemistry C,* vol. 117, no. 42, pp. 22098-22110.

Vaidya, PD & Rodrigues, AE 2006, 'Insight into steam reforming of ethanol to produce hydrogen for fuel cells', *Chemical Engineering Journal,* vol. 117, no. 1, pp. 39-49.

Varghese, OK, Paulose, M, LaTempa, TJ & Grimes, CA 2009, 'High-Rate Solar Photocatalytic Conversion of CO_2 and Water Vapor to Hydrocarbon Fuels', *Nano Letters,* vol. 9, no. 2, pp. 731-737.

Viswanathan, B & Raj, KJA 2009, 'Effect of surface area, pore volume and particle size of P25 titania on the phase transformation of anatase to rutile', *Indian Journal of Chemistry - Section A Inorganic, Physical, Theoretical and Analytical Chemistry,* vol. 48, no. 10, pp. 1378-1382.

Vogelmann, TC, Bornman, JF & Yates, DJ 1996, 'Focusing of light by leaf epidermal cells', *Physiologia Plantarum,* vol. 98, no. 1, pp. 43-56.

Vogelmann, TC & Martin, G 1993, 'The functional significance of palisade tissue: penetration of directional versus diffuse light', *Plant, Cell & Environment,* vol. 16, no. 1, pp. 65-72.

Wang, Y, Li, J, Peng, P, Lu, T & Wang, L 2008, 'Preparation of S-TiO_2 photocatalyst and photodegradation of L-acid under visible light', *Applied Surface Science,* vol. 254, no. 16, pp. 5276-5280.

Waterhouse, GIN, Metson, JB, Idriss, H & Sun-Waterhouse, D 2008, 'Physical and Optical Properties of Inverse Opal CeO_2 Photonic Crystals', *Chemistry of Materials,* vol. 20, no. 3, pp. 1183-1190.

Waterhouse, GIN & Waterland, MR 2007, 'Opal and inverse opal photonic crystals: Fabrication and characterization', *Polyhedron,* vol. 26, no. 2, pp. 356-368.

Wen, B-M, Liu, C-Y & Liu, Y 2005a, 'Solvothermal synthesis of ultralong single-crystalline TiO_2 nanowires', *New Journal of Chemistry,* vol. 29, no. 7, pp. 969-971.

Wen, B, Liu, C & Liu, Y 2005b, 'Bamboo-Shaped Ag-Doped TiO_2 Nanowires with Heterojunctions', *Inorganic Chemistry*, vol. 44, no. 19, pp. 6503-6505.

Xia, F & Jiang, L 2008, 'Bio-inspired, smart, multiscale interfacial materials', *Advanced Materials,* vol. 20, no. 15, pp. 2842-2858.

Xu, C, Killmeyer, R, Gray, ML & Khan, SUM 2006, 'Photocatalytic effect of carbon-modified n-TiO_2 nanoparticles under visible light illumination', *Applied Catalysis B: Environmental*, vol. 64, no. 3–4, pp. 312-317.

Xue, G, Dai, Q & Jiang, S 1988, 'Chemical reactions of imidazole with metallic silver studied by the use of SERS and XPS techniques', *Journal of the American Chemical Society*, vol. 110, no. 8, pp. 2393-2395.

Yamashita, H, Harada, M, Misaka, J, Takeuchi, M, Neppolian, B & Anpo, M 2003, 'Photocatalytic degradation of organic compounds diluted in water using visible light-responsive metal ion-implanted TiO_2 catalysts: Fe ion-implanted TiO2', *Catalysis Today*, vol. 84, no. 3–4, pp. 191-196.

Yang, H, Xu, Z, Fan, M, Gupta, R, Slimane, RB, Bland, AE & Wright, I 2008a, 'Progress in carbon dioxide separation and capture: A review', *Journal of Environmental Sciences*, vol. 20, no. 1, pp. 14-27.

Yang, HG, Sun, CH, Qiao, SZ, Zou, J, Liu, G, Smith, SC, Cheng, HM & Lu, GQ 2008b, 'Anatase TiO_2 single crystals with a large percentage of reactive facets', *Nature*, vol. 453, no. 7195, pp. 638-641.

Yang, K, Dai, Y & Huang, B 2007, 'Study of the Nitrogen Concentration Influence on N-Doped TiO_2 Anatase from First-Principles Calculations', *The Journal of Physical Chemistry C,* vol. 111, no. 32, pp. 12086-12090.

Yang, P, Zhao, D, Margolese, DI, Chmelka, BF & Stucky, GD 1999, 'Block Copolymer Templating Syntheses of Mesoporous Metal Oxides with Large Ordering Lengths and Semicrystalline Framework', *Chemistry of Materials,* vol. 11, no. 10, pp. 2813-2826.

Yang, Y, Li, X-j, Chen, J-t & Wang, L-y 2004, 'Effect of doping mode on the photocatalytic activities of Mo/TiO_2', *Journal of Photochemistry and Photobiology A: Chemistry,* vol. 163, no. 3, pp. 517-522.

Yao, B, Chan, Y, Zhang, X, Zhang, W, Yang, Z & Wang, N 2003, 'Formation mechanism of TiO_2 nanotubes', *Applied physics letters,* vol. 82, no. 2, pp. 281-283.

Yao, J & Wang, C 2010, 'Decolorization of Methylene Blue with TiO_2 Sol via UV Irradiation Photocatalytic Degradation', *International Journal of Photoenergy,* vol. 2010

Ye, X, Yang, Q, Zheng, Y, Mo, W, Hu, J & Huang, W 2014, 'Biotemplate synthesis of carbon nanostructures using bamboo as both the template and the carbon source', *Materials Research Bulletin,* vol. 51, no. 0, pp. 366-371.

Yoo, M, Han, SJ & Wee, JH 2013, 'Carbon dioxide capture capacity of sodium hydroxide aqueous solution', *Journal of Environmental Management,* vol. 114, pp. 512-519.

Youngblood, WJ, Lee, S-HA, Maeda, K & Mallouk, TE 2009, 'Visible Light Water Splitting Using Dye-Sensitized Oxide Semiconductors', *Accounts of Chemical Research,* vol. 42, no. 12, pp. 1966-1973.

Yu, J, Zhao, X & Zhao, Q 2000, 'Effect of surface structure on photocatalytic activity of TiO_2 thin films prepared by sol-gel method', *Thin Solid Films,* vol. 379, no. 1–2, pp. 7-14.

Yuan, J, Yuan, D, Tan, X, Zou, F & Xiao, S 2015, 'Correlation between Selenium and Heavy Metal Content in Camellia oleifera in Hainan, China', *Open Biotechnology Journal,* vol. 9, pp. 170-177.

Zhang, J, Wang, Y, Jin, Z, Wu, Z & Zhang, Z 2008, 'Visible-light photocatalytic behavior of two different N-doped TiO_2', *Applied Surface Science,* vol. 254, no. 15, pp. 4462-4466.

Zhang, Y, Li, G, Jin, Y, Zhang, Y, Zhang, J & Zhang, L 2002, 'Hydrothermal synthesis and photoluminescence of TiO_2 nanowires', *Chemical Physics Letters,* vol. 365, no. 3, pp. 300-304.

Zhao, H, Xu, J, Liu, L, Rao, G, Zhao, C & Li, Y 2016, 'CO_2 photoreduction with water vapor by Ti-embedded MgAl layered double hydroxides', *Journal of CO_2 Utilization,* vol. 15, pp. 15-23.

Zhao, Y, Li, C, Liu, X, Gu, F, Du, HL & Shi, L 2008, 'Zn-doped TiO_2 nanoparticles with high photocatalytic activity synthesized by hydrogen–oxygen diffusion flame', *Applied Catalysis B: Environmental,* vol. 79, no. 3, pp. 208-215.

Zhao, Z-H, Fan, J-M & Wang, Z-Z 2007, 'Photo-catalytic CO_2 reduction using sol–gel derived titania-supported zinc-phthalocyanine', *Journal of Cleaner Production,* vol. 15, no. 18, pp. 1894-1897.

Zhao, Z, Jiao, X & Chen, D 2009, 'Preparation of TiO_2 aerogels by a sol-gel combined solvothermal route', *Journal of Materials Chemistry,* vol. 19, no. 19, pp. 3078-3083.

Zhao, Z, Shan, W, Zhang, Y, Li, X, Ma, J & Yan, Y 2012, 'Fabrication and properties of degradable poly(amino acid)/nano hydroxyapatite bioactive composite', *Journal of Applied Polymer Science,* vol. 125, no. 4, pp. 2502-2509.

Zhou, H, Fan, T & Zhang, D 2011, 'Biotemplated materials for sustainable energy and environment: current status and challenges', *ChemSusChem,* vol. 4, no. 10, pp. 1344-1387.

Zhuiykov, S 2009, 'In situ FTIR study of oxygen adsorption on nanostructured RuO_2 thin-film electrode', *Ionics,* vol. 15, no. 4, pp. 507-512.